A study of decadal scale glacier changes of the Lunana glacier system in Bhutan, Himalaya, with considerations to glacial lake outburst floods (GLOFs)

Master thesis in physical geography

Written by: Ole-Gunnar Turøy Skjolddal

Department of Geography

University of Bergen

Spring 2020

Abstract

This study assesses changes in glacier area, velocity, and geodetic mass balance for a selection of glaciers in the Lunana glacier system of Bhutan, Himalaya. It takes considerations to Glacial Lake Outburst Floods (GLOFs) by creating a glacial lake inventory of two important potential dangerous glacial lakes, Raphstreng Tsho and Luggye Tsho. Bhutan is located in the eastern parts of the HKH region and is known for its earlier GLOF events. The precipitation in Bhutan is driven by the Indian monsoon resulting in 60% annual precipitation, the high amount of rainfall results in rockfalls that covers large valley glacier tongues with debris. I studied the glacier area changes between 1976, 1996 and 2018 using freely available Landsat satellite imagery, SAR Sentinel 1&2, the SRTM Digital Elevation Model (DEM) and HMA DEM. The geodetic mass balance was calculated between 1976, 2000 and 2018/9 (for selected glaciers) using DEM constructed from high-resolution stereo images, Pléiades and SPOT, granted from the European Space Agency, as well as using the already accessed SRTM DEM and a Hexagon DEM courtesy of King, et al. (2019). The glacier velocity was generated using SAR TerraSAR-X data from 2016 and shows an average yearly displacement over the Lunana glacier system. The glacial lake time series for Raphstreng Tsho and Luggye Tsho where studied between 1993 and 2018 using a stack of freely available Landsat imagery. The results of this study, show a variety of decadal glacial changes over Lunana glacier system, with glaciers lowering on an average by 0.48± 0.08 m a^{-1} between 1976 and 2018/9 which calculates to a geodetic mass balance of -0.41 ± 0.068 m w.e. a^{-1}. The system had a total average of 12.73% area of reduction for all glaciers, between the same time period. The Lunana glacier system consists of both debris-covered glaciers in the south and debris-free glaciers in the north, and as a result, the glacier changes vary between the two regions. Between 1976 – 2018/9 the southern region had an average surface melt of 0.76 ± 0.07 m a^{-1} which calculates to a geodetic mass balance of -0.65 ± 0.06 m w.e. a^{-1} and a 12.65% area of reduction. For the Northern region, the average surface melt was measured to be 1.26 ± 0.07 m a^{-1} which calculates to a geodetic mass balance of 1.07 ± 0.06 m w.e. a^{-1} and a 12.80% area of reduction. The glacier velocity was calculated to be at average of 3.05 ± 0.73 m a^{-1} over the south region and 3.78 ± 0.73 m a^{-1} over the north region.

The Luggye glacier 1, located in the southern parts of Lunana glacier system, is the main input source for glacier meltwater to Luggye Tsho an ice-moraine dam proglacial lake which outburst in 1994 due to hydrostatic pressure. Between 1976 and 2019, the Luggye glacier 1 has had a considerable loss in surface elevation by 1.19 ± 0.07 m a^{-1} which calculates to a

geodetic mass balance of 1.01 ± 0.069 m w.e. a^{-1}. The 1994 GLOF event discharged over 18 million m^3 of water, destroying infrastructure, flooding villages and houses which killed 21 humans. Today, Luggye Tsho is classified to yield over 1.41 km^2 of water, an increase from its former state of 1.12 km^2 in 1993, just before the event. This study cannot affirm if PDGLs such as Luggye Tsho is to outburst in the future, but it does affirm its growth in lake area and its input source from glacier melt over Luggye glacier from the past 40 years, and that it should be monitored in case of potential outbreak. This can be done by doing repeated analysis of glacier velocity and calculation of glacier mass balance, as this would calculate the input source amount of meltwater to the lake, as well as keep monitoring the areal growth of Luggye Tsho.

Acknowledgments

I would like to pay my special regards to my supervisor Benjamin Aubrey Robson, postdoc at the geography department at the University of Bergen, for his contribution to my thesis and this study. His aid in the completion of this study was quite critical, as he contributed with knowledge of general remote sensing and the different methods that were used in this study, as well as his contribution towards editing my thesis and his general encouragement. Without his persistent help, this study would not have been completed. I would like to acknowledge the academic crew of the geographic department at the University of Bergen, which helped me in completing the studies and classes needed to assess my master thesis. I wish to show my gratitude the European Space Agency for their contribution of the stereo data that were used in this study. I wish to express my deepest gratitude to Tobias Bolch, whose contribution with the Hexagon DEM from King, et al. (2019) was most needed to calculate a large decadal geodetic mass balance change over the Lunana glacier system. I wish to acknowledge the support of my loving girlfriend, Amalie. Which kept me going and encouraged me to work hard as this would not have been possible without her contribution.

Table of Contents

Chapter 1: Introduction

This study revolves around the study of glacier changes in Himalaya and their connections to glacial natural hazards such as glacial lake outburst floods (GLOFs). This chapter is introducing the relevance of monitoring glaciers and why it is important to do so, as well as gives an influence on the story of Himalaya and the usefulness of using remote sensing to monitor such glacial mountain ranges.

1.1 Importance of monitoring glaciers

Glaciers are known to be a strong and important natural resource for both power and electricity for certain countries and regions, like the Himalayas. Glaciers provide insight to regional global climate change, as they work as indicators due to their influential response to temperature fluxes and precipitation (Karpilo, et al. 2009). Monitoring of these glaciers provides therefore information of the conditions of the local, regional, and global environment, and how to understand climate change and learn about the past, present, and future conditions of these environments. This gives influence to local and regional authority and provides them with data and information on how to operate a responsible land management (Karpilo, et al. 2009), as well as help certain facilities make predictions on how glacier changes impacts the environment. An example could be: if the glacier melts increases exponentially due to an increase in global warmth climate, there is a high risk that local hydrologic systems will experience an increase in water flow and will not be able to sustain the seasonal variability[1] (Fountain and Tangborn 1985; Gill and Niller 1973), and as a result the sea level would rise. Monitoring glacier changes can also further study on how glacial hazards operates. Hazards like e.g. glacial lake outburst floods (GLOFs) and jökulhlaups are known for their destructive effects on infrastructure and civilizations, and operates through sudden outburst of waters and are often released due to failure moraine damn (Emmer 2017; Yuanfang, et al. 2002: p. 57 - 63). Other glacial hazards like, glacier icebergs known as tidewater glaciers which are known for their destruction on oceanic infrastructure, such as drilling platforms and passing ships (Karpilo, et al. 2009; Lawrence 2012).

[1] Seasonal variability: is the expected change in streamflow which follows throughout the year. This includes the seasonal of snow, snowmelt, rainfall, and dry periods (Gill and Niller, 1973).

1.2 Relevance of Himalayan glaciers

The Hindu Kush- Himalayan (HKH) region is the highest mountain region on earth and is ranging from Afghanistan and to Bhutan, covered by 60 000 km^2 of glaciers (Dyurgerov and Meier 2005). The region includes 14 of the world's biggest mountain tops (peaks over 8000 meters), this includes the world's biggest mountain Mount Everest (8848 m a.s.l), and trends east-west and extends for over 2900 km, including the Tibetan plateau (Coenraads, et al. 2008). The Himalayas was formed approximately 40-50 million years ago, when the Indian tectonic plate collided with the Eurasian plate resulting in an uplift of metamorphic processed rocks from the Tehtys ocean, building up the mountain range known as the Himalayas. The rising process is still on going by more than 1 cm a year and are resulting in great seismic activities (Coenraads, et al. 2008). These forces are resulting in eroding powers which can later result in other different catastrophic phenomena's, e.g. glacial lake outburst floods (GLOFs). These outbursts of water can lead to catastrophic damage on villages and infrastructure nearby and can easily be triggered by e.g. earthquakes (**Fig. 1.1**), like the one in Kashmir in 2005. More than a thousand proglacial- and supraglacial lakes have been developed in the HKH region and increased in area these last few decades due to glacial retreat (Ives, et al. 2010). Which makes it one of the world greatest freshwater resources as water from the snow, ice and the monsoons enrichen the great river system. These water sources are used as drinking water for the villages and to drive several hydropower stations used to provide electricity and heat to the same villages. As an example, in Bhutan there are five major hydropower projects, according to IHA (2016), that are operational and in 2013-14 these stations provided over 4,9 GWh wort of power to India, as the domestic demand for electricity and powers are quite low in Bhutan. Even though the glacial landscape provides with feasible water resources they do also provide with extreme and dangerous glacial hazards, e.g. GLOFs. Due to climate change, high mountain glacier has had an increase in glacier melt leading to an increase in supraglacial and proglacial lake area in the HKH (Maurer, et al. 2019). The HKH region is scattered with proglacial lakes, and in 2011 these numbers where counted to be almost 1700 lakes calculated cover over 80 km^2 of water surfaces (Gardelle, et al. 2011).

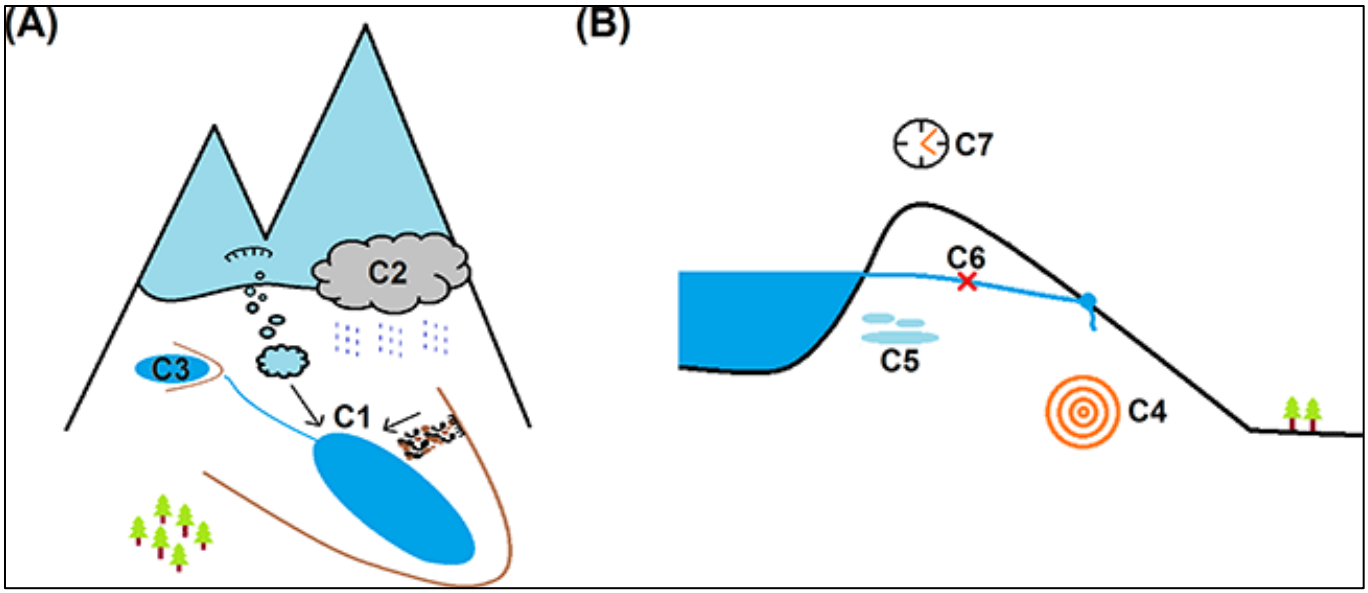

(C1) Rapid slope movement into the lake
(C2) Heavy rainfall/snowmelt
(C3) Cascading processes (flood from a lake situated upstream)
(C4) Earthquake
(C5) Melting of ice incorporated in dam/forming the dam (including volcanic activity-triggered jökulhlaups)
(C6) Blocking of subsurface outflow tunnels (applies only to lakes without surface outflow or lakes with a combination of surface and subsurface outflow)
(C7) Long-term dam degradation.

Fig 1.1: GLOF causes. **(A)** causes relevant for all glacial lake subtypes and part **(B)** a longitudinal section of a dam, relevant for only a certain number of subtypes. Source: (Emmer 2017).

1.3 Use of remote sensing for studying glaciers

Remote sensing is a way to process and monitor the physical characteristic of an area. This is done by using satellites or aircrafts with cameras to detect and measure the radiation that an environment is reflecting and emitting (Clark 2001). The uses for remote sensing are abundant, but the main pro factors for remote sensing are, large area coverage and repetitive coverage. Remote sensing allows for very large area coverages, which enables regional surveys and classification. Kääb, et al. (2012) studied mass changes and glacier thickness over the Hindu Kush-Karakoram-Himalaya (HKKH) region by combining two elevation data sets (DEMs). Gardelle, et al. (2011) focuses on evolution of glacial lakes along the Hindu Kush Himalaya mountain range between 1990 and 2009, and Bajracharya, et al. (2014) which focuses on decadal change of glaciers in Bhutan from the 1980s to 2010 based on satellite data, both covers a large time period of decades. Not to mention, there are methods which uses high-resolution imagery for a more local approach on glacier changes. Hubbard, et al. (2000) determined the glacier mass balance of the Haut Glacier d'Arolla in Valais, Switzerland, by comparing two DEM data created by analytic photogrammetry using 20 m high-resolution images. Berthier, et al. (2007) determined the glacier mass balance in the Himachal Pradesh, Western Himalaya, India, by comparing a 2004 DEM to the 2000 SRTM (Shuttel Radar Topgraphic) DEM. The 2004 DEM was calculated from two high-resolution SPOT5 optical images using the PCI-Geomatica software. These remote sensing methods can be processed fast using a computer and by using the needed software's, and the same data can be used for a variety of remote sensing methods. Remote sensing optical imagery are usually free to download if one is not using high-resolution images such as SPOT or Pléiades images. Satellites provide regular sampled scenes which can be utilized to give almost daily updates of glacier changes. Not to mention that sampled areas, such as the Himalayas, are difficult areas to excavate field work from and hard to get to. Remote sensing gives any user the ability to survey these areas from their own computer, making it extremely more viable to survey. As the time moves forward, processing is becoming more and more automated which means users can study even larger scale areas in less amount of time (Gardelle, et al. 2011; Kääb, et al. 2012). However, there are some limitations to remote sensing. One of the biggest struggles with remote sensing and its image analyzing is the interference by other variables such as weather conditions and sun oscillation which results in shadowing. These variables will cause distortion in optical images and can lead to faulty imagery. This problem can be dealt with by using radar images instead of optical (Clark 2001), and can also be acquired free of charge.

1.4 Study area

The field of study is in the north-western part of Bhutan, Himalaya called Lunana, a region north of the main capital called Thimpu close to the Masang Kang mountain (**Fig. 1.1**), and is located on the border with the Tibetan plateau, China. The glacier environment is mainly consisting of both debris-covered glaciers in the south and clean ice in the north. The Lunana glacier system is therefore consisting of both southern glaciers within the north western part of Bhutan, and northern glaciers located within the south western part of China. For this study, nine glaciers within the Lunana glacier system will be individually picked based on their glacial characteristic and their location to two glacial lakes, the Luggye Tsho- and Raphtreng Tsho proglacial lakes (**Fig. 1.2**). The different glaciers consist of either just clean ice, or a combination of both clean ice and debris-covered glaciers. The southern glaciers terminate into a basin that is derived by a river called Pho Chhu river. The northern region is contains over 640 km^2 of glaciers (Bajracharya, et al. 2014),which is a huge source of meltwater and results in fast flowing rivers which the hydropower relies on (Williams, et al. 2016). There are five hydropower projects that are currently operational in Bhutan and are located in the south western part of Bhutan. In 2015 a total of 1,615 MW of hydropower was already installed and had generated 7,780 GWh of power. The glaciers of the Lunana system is connected to the Pho Chhu river, which of runs down towards Gasa a town located in northwestern Bhutan. The meltwater that these glaciers produce is essential for the generation of hydropower from the power stations that are located further down the stream in south western Bhutan.

In Bhutan, the precipitation are driven by the Indian monsoon, occurring from June to September (Bohner 2006), resulting in 60% of annual precipitation (Dorji, et al. 2016). Also, that is the season when ablation and accumulation is at its highest (Fujita 2008), leading to massive cloud cover during this season.

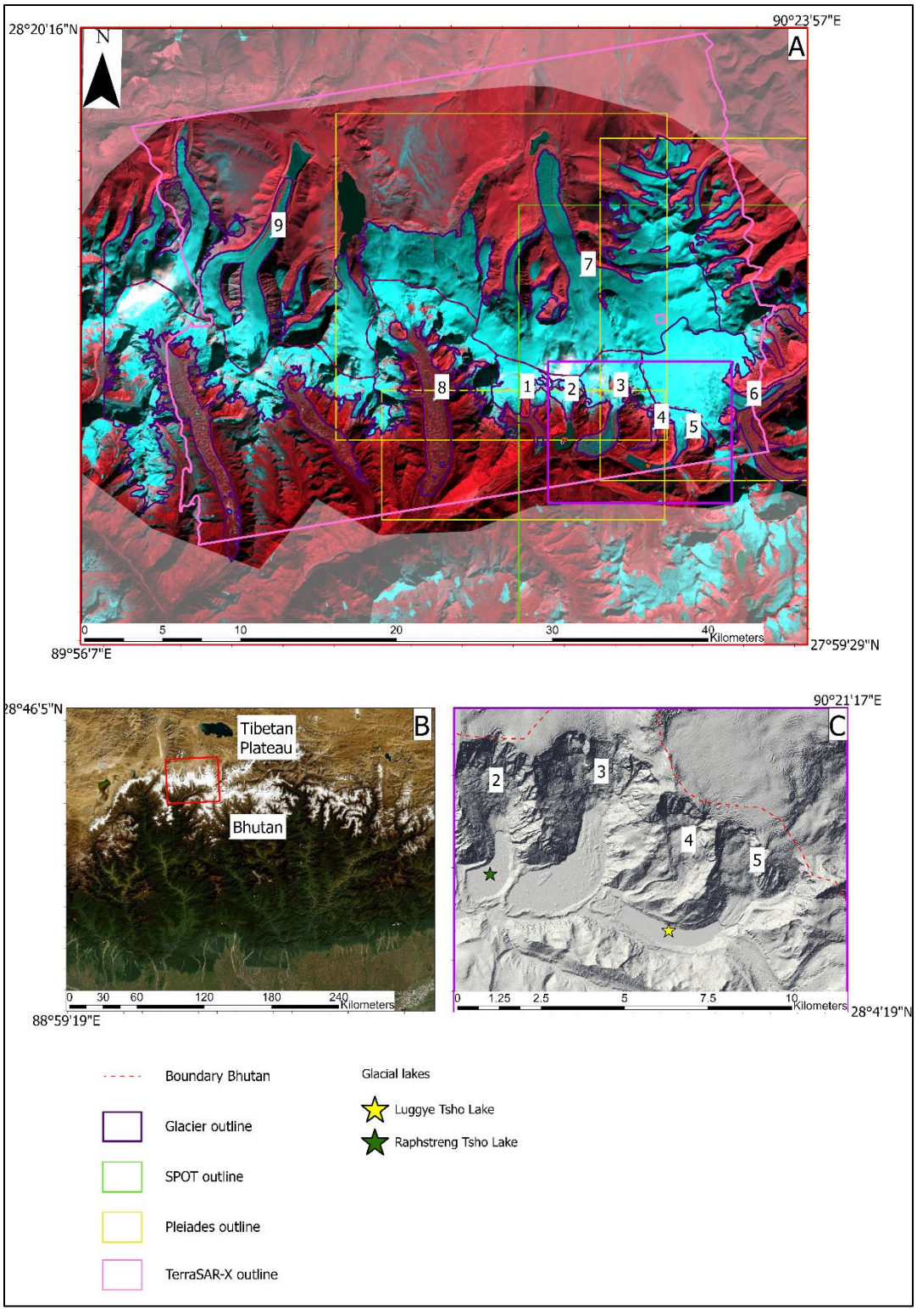

Fig. 1.2: **(A)** Overview map of the study area in Bhutan, outlines of the glacier are derived from the glacial area classification. **(A)** The study area is fully covered by the Landsat datasets used, as well as SRTM and Hexagon DEM. **(A)** The PLÉIADES datasets are shown by the yellow polyline indicators, the SPOT data is shown by the green outline and the TerraSAR-X data is shown by the pink outline. **(A)** 1 - Bechung glacier, 2 – Raphstreng glacier, 3 – Thorthormi glacier, 4 – Luggye glacier 2, 5 – Luggye glacier 1, 6 – Lianggang glacier, 7 – Zeng glacier, 8 - G090157E28136N, 9 – Shimo glacier. **(B)** Overview map of South Asia, overviewing Bhutan, the Tibeatan Plateau, and parts of central Himalya. **(B)** The study area is marked with a purple outline. **(C)** A hillshade model (marked in pink on image **(A)**) of the Raphstreng Tsho, glacial and Luggye Tsho glacial lake. Background image **(A)**: Landsat 8 false color composition (13.12.2018).

1.5 Objectives

The objectives of this thesis are to study how glacier parameters, such as volume, area, and velocity changes, can be extracted from remote sensing and how to use them to assess and study GLOF risks.

- Could glacial inventories extracted from remote sensing be used to better understand the temporal and spatial dynamics of GLOF events?
- Can a combination of optical- and SAR data be used to effectively identify debris-covered ice?
- In what way does a debris-cover effect the glacier?
    - Will the glacier melt rate be affected by the debris-covers?
    - Is there any connection between the melt rate and the glacier velocity?
- How have Luggye Tsho- and Raphstreng Tsho glacial lake developed to over the last 25 years?

Chapter 2: Background

The background for this study is comprised of studies regarding the use of remote sensing for studying Himalayan glaciers and what methods can be used to create a glacier inventory as well as the methods to study glacial lakes change in physical state. This chapter will also include former GLOF events that has occurred in the Himalayas with focus on Bhutan.

2.1 Use of remote sensing for studying Himalayan glaciers

Remote sensing has long been a sought-out way to monitor the glacier changes over the world and is mostly used for the places that are way more complicated to collect ground truth data from. Places like the Himalaya mountains, which contains over 24 000 km^2 of glacier ice (Gardelle, et al. 2011) with a mean altitude of over 5500 m, which is making it difficult to engage field surveys and collect good ground data from. There is a lack of in-situ data when it comes to the studying of Himalayan glaciers, due to it being remote and hard to access (Bolch, et al. 2012), and the data that does exist are mostly bias towards small, debris-free glaciers (Berthier, et al. 2007). Remote sensing has the potential to cover these large areas in a systematic way.

While there are certain studies revolving around identifying glacier structures and glacier surfaces manually (Kulkarni and Bahuguna 2002; Nuimura, et al. 2015), there are also studies doing this automatically. Automatic classification methods are often using algorithms to identify and classify pixels with certain spatial values. Gupta, et al. (2005) used remote sensing data to identify and classify dry- and wet snow in the Gangotri glacier, located in the Uttarkashi District in India. The project used IRS – LISS – III multispectral data and a digital elevation model. The classification used an algorithm called Normalized-Difference Snow Index (NDSI) as a main parameter for the spectral reflectance classification of snow-covered areas and use the Near-Infrared band (NIR) to differentiate between dry- and wet snow areas. NDSI utilizes the spectral characteristics from snow and ice, which is characterized with a high reflectance value in the visible spectrum (usually green band, 0.5-0.7 μm) and a high absorption in the short-wave infrared (SWIR) spectrum (1.0 – 3.5 μm) (Gupta, et al. 2005; Hall, et al. 1995). They unified a threshold value for the NIR classification between dry- (≥ 0.5) and wet (< 0.5) snow and conclude that based on IRS-LISS-III sensor data it is possible to classify and differentiate between wet- and dry snow areas.

2.2 GLOFs in the Himalayas

Glacial lake outburst floods (GLOFs) is a huge problem in Hindu Kush Himalayan (HKH) region and has shaped the major valley trains of the Himalaya for the last thousand years (Korup and Tweed 2007). A GLOF commonly occurs through sudden emptying of glacial lakes and are often released through faulty moraine dams. GLOFs have taken several hundreds of lives these past decades and destroyed infra structures and damaged hydropower stations and livestock in many villages (Kuensel 1994a; Kuensel 1994b), and research shows that Bhutan and Nepal may have suffered the most from GLOF events when looking at the socio economic impact[2] (Carrivick and Tweed 2016). These GLOFs are known to transport millions of cubic meters of water and sediments within hours, and is considered one of the most dangerous glacial hazards known to mankind (Richardson and Reynolds 2000). Table 2.1 provides a list of some of the former GLOF events that has occurred in the HKH region with general information on how great their collateral damage was as well as their outburst volume.

Earlier GLOF events have been studied and observed in the north-western area of Bhutan, Himalaya. On 6 - 7 October 1994 there was an outburst flood in the Luggye Tsho glacial lake. A moraine dammed glacial lake that is in the upper valley of the East Pho Chhu, Lunana, south west from Thanza. The lake was, according to Bhutan's daily newspaper, ranging of a depth between 60-100 meters (Kuensel 2011). According to (Fountain, et al. 2000: pp. 169) the outburst was caused by a failure of the moraine dam by a sudden expansion of a small gap at the lower end of the western lateral moraine of Luggye glacier 1. This led to an expansion of the outlet channel to Luggye Tsho and cause a sudden outburst of water draining parts of the lake. The outburst created a chain reaction, where the water from Luggye Tsho lake flooded down towards another lake just downstream, Tshopdak Tsho, which collapsed as a result. The discharged from Luggye Tsho was calculated to be around 23 m (Kuensel 1994a) and a total water amount of around 18 million cubic meters (WWF 2009). The flooding resulted in several houses in Chozo village (at 4000 m) was laid to ruins and the village of Thanza & Tenchey (at 4100 m) were flooded and cut off from each other because the bridge where destroyed (Kuensel 1994b). The outburst also resulted in an increase in area of the channel path to the Pho Chu river and caused damage to the moraine wall that is currently damming Raphstreng Tsho glacial lake. The flooding event carried lots of debris through the

[2] Socio-economic impact: tells about the advantages and disadvantages of a certain object or proposal and see how it impacts a society (Carrivick and Tweed 2016).

channel of Pho Chu river. The debris deposited in the same channel path shows a distinct light tone that is located along the drainage channel and banks, this is because of the bank erosion and the deposition along the river, from the GLOF event. After the event Luggye Tsho reduced in size, with the western end of the lake being receded by almost 500 m (Fountain, et al. 2000: pp. 169), and became less hazardous because of this great loss of water after the event (Kuensel 2012). Research has theorized that the Luggye Tsho lake could have another outburst in the future, if the outlet channel of the lake where to become block and the water level where to rise (Fountain, et al. 2000: pp. 169). At the same time the lake is located at a higher altitude and in a very close vicinity of the western located glacial lake Raphstreng Tsho and the small supra glacial lakes located on the far end of Thorthormi glacier tongue. If Luggye Tsho where the outburst in the future there could be a possibility of the outbursting water flooding the supraglacial lakes on Thorthormi glacier and cascading down into Raphstreng Tsho leading to a catastrophic chain GLOF event. (Fountain, et al. 2000: pp. 169-170).

To prevent that such an event to ever happen again in the future the government of Bhutan invited experts from several countries to investigate the conditions of the glacial lakes and conclude with some resilience to prevent similar events in the future (Ahmed, et al. 2020; Singh 2009). As a result, the experts conclude with a set of risk reduction measures which consist of structural interventions: such as repairing the moraine wall dam of Raphstreng Tsho which were damaged by the 1994 GLOF event, building set of gabion-toe structure walls along the Pho Chhu river to provide surface roughness to the river channel, and lowering the water level of Luggye Tsho and other adjacent lakes in the area. The drainage was provided to reduce the hydrostatic pressure of the lake, and therefore reduce the risk of causing another fault in the moraine dam of Luggye Tsho. These structural interventions where accompanied by other long-term actions such as: safeguards against earthquakes, vegetation plantings to strengthen slope stability against debris fall, and set up surveillance and monitoring stations (Mool, et al. 2001). *The Raphstreng Tsho Outburst Flood Mitigation Project* was a project initiated in 1996 as a counterattack for the 1994 GLOF event, ensuring structural mitigation of the Raphstreng Tsho lake as well as drainage of glacial lakes surrounding Luggye Tsho. Where they were able to lower the glacial lakes water level by four meters in just a couple of years (Singh 2009).

After the 1994 GLOF event, downstream valleys like Thimphu have become more and more populated and several hydroplants have been constructed as a result of the increase in

production of glacier meltwater due to the climate change-induced glacial melt (Singh 2009). As a consequence, this increase in population and infrastructure can lead to a more devastating outcome if a new GLOF event would originate from the Lunana glacier system. A similar event like the one in 1994 could lead to 10 times more fatalities and damage (Brauner, et al. 2003).

Another event, more present to time, took place in 2015 in the Lemthang Tsho glacial lake, a supra glacial lake located north west from Thimphu. The lake outburst as a result of 2 days of continuing rainfall, that breached the vertical wall of glacier that was damming the lake up, emptying 0.37 million m^3 of water streaming at a velocity of 7.14-7.57 m/s 30 km downstream from the lake (Deo Raj, et al. 2017).

Table 2.1: Documented GLOF events between 1964 and 2016 in the Himalayas. Source: (Ashraf, et al. 2010; Daisuke, et al. 2012; Deo Raj, et al. 2017; Govindha Raj K 2009; Kuensel 1994a; Kuensel 1994b; Li, et al. 2017: pp. 397; Mei, et al. 2020; Mool, et al. 2001; Vuichard and Zimmermann 1987; Watanbe and Rothacher 1996; WWF 2009).

Year	Lake	River Basin/ Area	Country affected	Cause of GLOF	Outburst volume (m^3)	Note
September 1964	Gelhaipuco	Purn Qu / Arun	China and Nepal	Glacier surge	Unknown	Destroyed one highway and 12 trucks.
September 1977	Nare	Dudh Koshi	Nepal	Moraine collapse	Unknown	Human lives taken and bridges destroyed.
June 1980	Nagma Pokhari	Tamor	Nepal	Moraine collapse	Unknown	Villages destroyed 71 km downstream.
July 1981	Zhangzangbo	Boqu / Sun Koshi	China and Nepal	Glacier surge	0.2 million m^3	Damaged friendship bridge China-Nepal highway. Destroyed Koshi power station and caused serious economic loss.
August 1985	Dig Tsho	Lagmoche valley	Nepal	Ice avalanche	5 million m^3	New hydroplant, livestock, houses, trails, and bridges destroyed.
October 1994	Luggye Tsho	Pho Chhu	Bhutan	Moraine collapse	18 million m^3	21 people died.
2008	Ghulkin Glacier lake	Karakoram	Pakistan	Moraine collapse	Unknown	Flooded 4 times in six months. Damaged many properties, land, and infrastructure of Ghulkin village.
July 2015	Lemthang Tsho	Mo Chu	Bhutan	Moraine collapse	0.37 million m^3	No casualties.
July 2016	Gongbatongshaco	Zhangzangbo Valley	Nepal	Moraine collapse	0.11 million m^3	Damage site was affected by the Gortha earthquak, setting debris-covers that was later transported by the GLOF event. 77 houses, 3 bridges, 1 highway and a dam destroyed.

2.3 Methods for studying glaciers with remote sensing

Remote sensing has long been a sought-out way to monitor the glacier changes over the world and is mostly used for the places that are way more complicated to collect ground truth data from. Places like the Himalaya mountains, which contains over 24 000 km^2 of glacier ice (Gardelle, et al. 2011) with a mean altitude of over 5500 m, which is making it difficult to engage field surveys and collect good ground data from. There is a lack of in-situ data when it comes to the studying of Himalayan glaciers, due to it being remote and hard to access (Bolch, et al. 2012), and the data that does exist are mostly bias towards small, debris-free glaciers (Berthier, et al. 2007). Remote sensing has the potential to cover these large areas in a systematic way.

The objectives of this thesis are to investigate the glacier properties of the Lunana glacier system, through remote sensing. To do this there are different methods which one can utilize. Based on the time and the amount of resources, this thesis will focus on these methods: calculation of glacier area changes through glacier classification, change in mass balance through geodetic mass-balance and calculation of glacier velocity by the using feature tracking. The method to distinguish the area of the glacier is divided between different methods, this because of the glaciers complex structure between clean ice and debris-covered ice.

2.3.1 Glacier area

This study is revolving around using multispectral data to efficiently detect, classify, and assess changes on the glaciers within the Lunana region of Bhutan. This can be done through two different methods, either by manual delineation or by automatic classification. A paper by Bishop, et al. (1998) used SPOT Panchromatic satellite data to study and determine if spectral variability can be quantified and used to identify and characterize glacier surfaces. Bishop, et al. (1998) used SPOT data to perceive different features of glacier structure that resulted from glacier movement, ablation, and supraglacial fluvial action, by using semivariogram[3]- and fractal analysis. The study took place on the Batura Glacier, in the Karakoram Himalaya of northern Pakistan and concluded that the semivariogram could be used to describe ice structure and characteristics of the debris load, and that the fractal analysis has the potential to be used to differentiate other characteristics of the glacier surface, but that further research is needed. This research shows and proves that by using spectral variability one can identify and

[3] A semivariogram is a graph showing the changes between observation changes. Bishop, et al. (1998) used this analysis to differentiate different classes of structures directed to the glacier surfaces, and how these classes corresponds to the spatial patterns and their reflectance.

characterize glacier surfaces. Other studies have proved the same point but by using other different methods and different data. Kulkarni and Bahuguna (2002) used high-resolution (5.8 m) stereo data to monitor retreat of the glaciers in the Baspa basin, India. Based on manual digitization and visual interpretation of the glacier snouts for 1997-98 and 1962-63 in the Baspa basin where identified and classified. Both studies used visual interpretations to classify glacier structures, but both in a different way to conclude with the result. Bishop, et al. (1998) used semivariogram analysis and mathematical models to discuss their observations while Kulkarni and Bahuguna (2002) relied on experience and used more remote sensing methods by using photogrammetry and orthorectified images to identify glacier snouts.

To classify glacier system, one needs to account for the structure of the glacier system one is studying. In this case the Lunana glacier system is a combination of clean ice, that are in the north region of the study area, and debris covered glaciers which are more abundant in the south region of the study area. Debris-covered glaciers are usually found in the Himalayas, and even almost all large valley glaciers are covered with debris in the ablation zone of the glaciers (Sakai, et al. 2000). These large valley glaciers are actually known to occupy more than 80% of the glacier areas in the Himalayas (Fujii and Higuchi 1977), and are therefore highly expected to come over when one is classifying glacier outlines in the Himalayan region.

2.3.1.1 Manual digitization

Manual digitization, or manual divinization, is a method where one is using visual tools to manually map certain areas or objects in a GIS system. This method is a well-known method and it is easy to perfect if you know what to classify. When it comes to deriving outlines for glacier areas, there is the conflict on classifying the clean ice vs debris-covered ice. In a paper by Paul, et al. (2013) they tested the accuracy of the glacier outlines derived from remote sensing through manual digitization. This was done by comparing outlines from clean ice and debris-covered glaciers, by using multiple digitization by different or the same analyst on high- (1m) and medium resolution (30m) images. The results proved that manual digitization of clean ice had an overall good accuracy, confirming about 95%. However, the debris-covered outlines did not bear the same result where almost 30% where wrongly classified. It is therefore a clear conclusion. That while manual digitization is a promising method to classify clean ice, it is not a recommended method when one is classifying debris-covered parts because of difference in interpretation (Fig. 2.1).

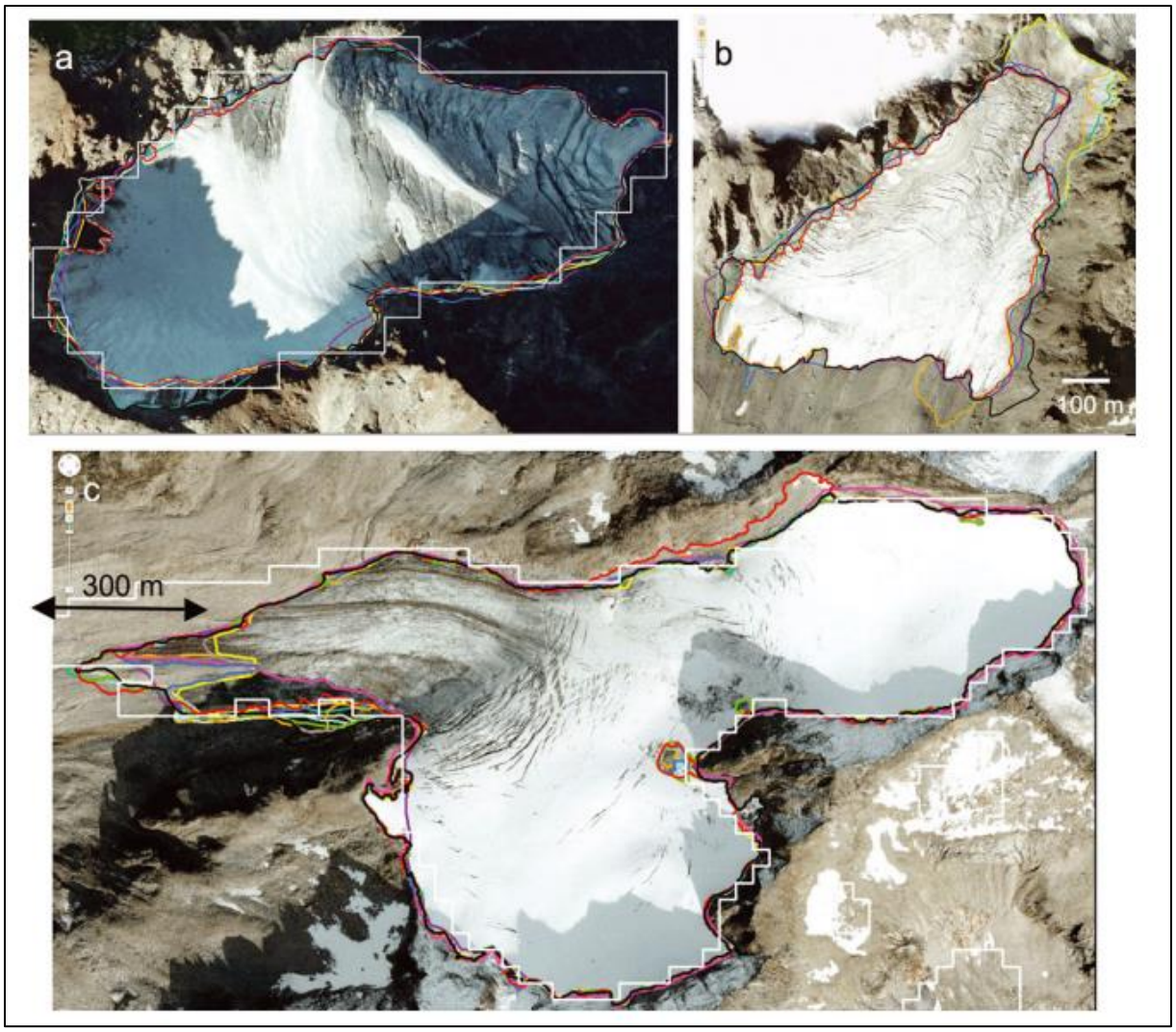

Fig. 2.1: shows an overlay of manually delineated glacier outlines for three test glacier in the Swiss Alps, results from Paul, et al. (2013): (a) Vadret Futschöl, (b) Vadret d'Urezzas and (c) Geren glacier. Notice how the debris-covers on the glacial surfaces (b) and on the glacial tongue (c) is interpreted differently. Background images: screenshots from Google Maps.

2.3.1.2 Automated methods

While there are certain studies revolving around identifying glacier structures and glacier surfaces manually (Kulkarni and Bahuguna 2002; Nuimura, et al. 2015), there are also studies doing this automatically. Automatic classification methods are often using algorithms to identify and classify pixels with certain spatial values. Gupta, et al. (2005) used remote sensing data to identify and classify dry- and wet snow in the Gangotri glacier, located in the Uttarkashi District in India. The project used IRS – LISS – III multispectral data and a digital elevation model. The classification used an algorithm called Normalized-Difference Snow Index (NDSI) as a main parameter for the spectral reflectance classification of snow-covered areas and use the Near-Infrared band (NIR) to differentiate between dry- and wet snow areas. NDSI utilizes the spectral characteristics from snow and ice, which is characterized with a high reflectance value in the visible spectrum (usually green band, 0.5-0.7 μm) and a high absorption in the short-wave infrared (SWIR) spectrum (1.0 – 3.5 μm) (Gupta, et al. 2005; Hall, et al. 1995). They unified a threshold value for the NIR classification between dry- (≥ 0.5) and wet (< 0.5) snow and conclude that based on IRS-LISS-III sensor data it is possible to classify and differentiate between wet- and dry snow areas.While the manual delineation proves a high accuracy when it comes to deriving glacier outlines for clean ice, it is limited by the fact that manual classification is both time consuming and wearisome when it comes to deriving multiple large glacial areas (Paul, et al. 2013). It can therefore be more useful to utilize automated methods such as supervised and unsupervised classification methods.

Supervised classification, the human guided method, is classification method that uses reference data or training sites as references for the classification. The user therefore select and sample pixels within the data files, directing the processing software to these training sites (Belgiu and Dr Guţ 2014). Gratton, et al. (1990) used supervised classification when they were mapping glacial covers of the Columbia Icefield, Canada. They used automated classification based on the maximum-likelihood algorithm, which they concluded with being the most efficient and accurate method to map scattered covers such as snow and vegetation. The problem with using supervised classification in mountains areas like the Himalaya is the issue with identifying good training areas for the classification, due to the shadows.

Unsupervised classification is where the software groups pixels that share the same characteristics without having the user provide sample classes, as they do in a supervised classification. This method is therefore bearing more on the software to classify pixels in GIS. The user is dominate on choosing the specific algorithm the software should be using to perform the classification. The user controls the inputs, how many times this algorithm should be run and the threshold, which tells when the software should end the procedure (Lillesand, et al. 2004: 573). An example of an unsupervised classification is ISODATA clustering. An article by Paul, et al. (2002) used ISODATA clustering as a method to create glacier inventories in the Swiss alps. ISODATA clustering is basically an algorithm that the software uses to split and merge clusters of pixels that were assigned based on their spectral information. These clusters will be split and merged as much as needed to fulfill the users thresholds criteria, which they input before the procedure initiates. Paul, et al. (2002) compared both unsupervised ISODATA clustering with a supervised maximum likelihood method to see what gave the best result when it came the classify glaciers in the Swiss alps. Much like Gratton, et al. (1990) used the same supervised method to classify glacier covers in Canada.

However, to fully classify glacier covers the user also needs to select criteria that will be inserted within the algorithm methods. The most normal criteria for classification methods are band ratios. Band ratios are combination of individual bands within a data image. Examples could be, Normalized Difference Water Index (NDWI), Normalized Difference Vegetation Index (NDVI), Normalized Difference Snow Index (NDSI) and TM4/TM5 also known as NIR/SWIR (see **table 2.2**). In the article by Paul, et al. (2002) he used both supervised and unsupervised classification method with TM4/TM5 as input indices for the algorithm. According to the article TM4/TM5 yields good result when the user is mapping debris-free glacier areas and is therefore normally used to classify clean ice on glacier systems. Other papers such as Robson, et al. (2015) used the same band ratio when they were mapping glacier covers of the Manaslu Region within Nepal.

Table 2.2: Custom indices used in the glacier and glacial lake classification.

Index Acronym	Custom Index Name	Band formula
NDVI	Normalized Difference Vegetation Index	(NIR - Red) / (NIR + Red)
NDSI	Normalized Difference Snow Index	(Green – SWIR) / (Green + SWIR)
NDWI	Normalized Difference Water Index	(Green – NIR) / (Green + NIR)
SWIR/NIR	Commonly referred to as TM4/TM5	SWIR/NIR

2.3.1.3 Difference between pixel-based image analysis and object-based image analysis

The most traditional way of classifying pixels in a GIS software is to use a pixel-based classification. According to Richards (1993); pixel-based classification (PBIA) is defined as an analyzation of individual images pixel containing spectral information. This is the traditional way of classification, given the fundamental value of pixel, as they are spatial units of satellite images, are easy to implement. The method uses the spectral information for every pixel which is stored in the image bands for each dataset. From there the method will classify each individual pixels based on each bands variability of the reflectance values (Lillesand, et al. 2015). Traditionally, in pixel-based classification operates with class characterizations that in theory are well-known and well-defined, but in practice may not be so defined. An example may be glaciers, which can consist of objects like; clean ice and debris-covered ice, all of which can be contained within different pixels. This problem is often related to the spatial resolution and sets up a relationship between spatial resolution and the object that is being classified. Making it so that more than one landform class is include within the same pixel, and therefor misclassify certain landforms with other landforms (**Fig. 2.2).**

This complicates the glacier classification and leads to certain problems involving the pixel-based classification (Rastner, et al. 2014; Robson, et al. 2015).

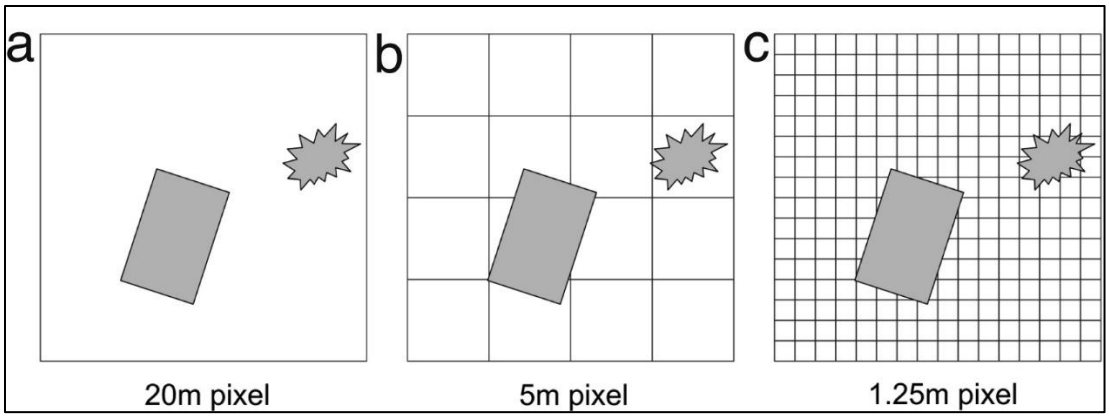

Fig. 2.2: Shows the relationship between spatial resolution and objects that are being classified: (**a**) low resolution, where the pixel is larger than the objects. (**b**) medium resolution, where the pixel and objects are about the same size. (**c**) high resolution, where the pixels are largely smaller than the objects. Figure gathered from Blaschke (2010).

Object-based image analysis is spatial information[4] extraction, used in software's like ArcGIS, PCI Geomatica and eCognition, to process and classify spatial contextual information, e.g shape or texture (Rastner, et al. 2014; Robson, et al. 2015). It starts by segmenting the pixels into objects (Baatz and Schäpe 2000). Which is an algorithm that merges pixels into groups by utilizing three parameters: scale, shape, and compactness. The scale parameter is used for the size of the individual objects, the shape drives the homogeneity of objects. The parameter "compactness" is used to change the compactness of the resulting objects (Baatz, et al. 2005). The segmentation is often applied several times to create different segmentation levels, which amplifies and group finer objects that would not be included in the earlier stages of segmentation (**Fig. 2.3**). After the segmentation, the objects can then be classified using different classification procedures such as: band ratio, slope, elevation, thermal information, SAR coherence.

[4] Spectral information: Spectral imaging is an image that uses multiple bands through the electromagnetic specter. Spectral information is therefore the information from these bands or what color it is (Heywood, et al. 2011).

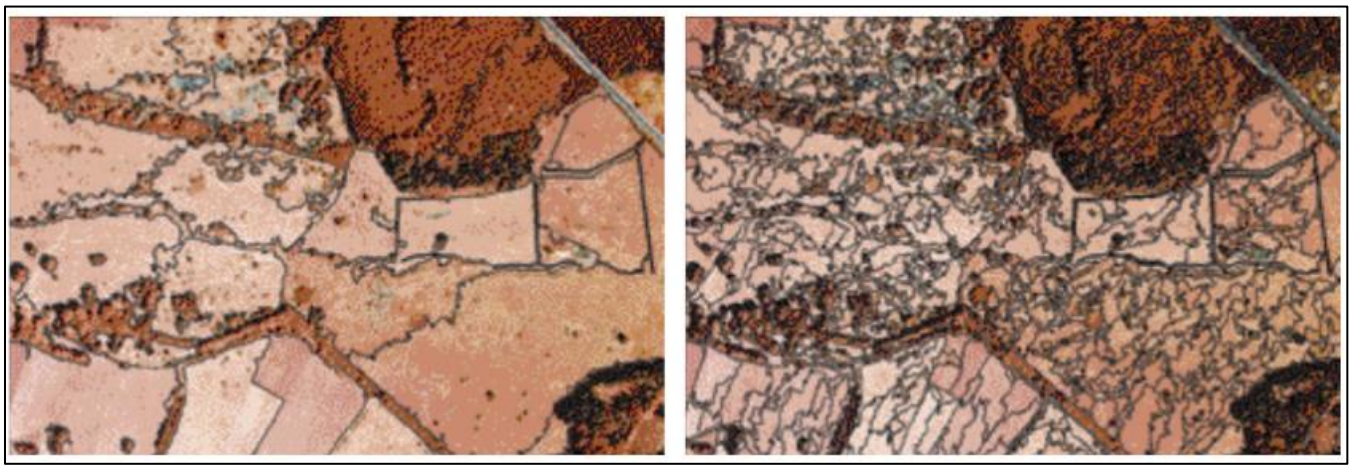

Fig. 2.3: Shows a multiscale segmentation on two different levels of segmentation. On the left is a very coarse segmentation aiming at the pasture fields, and the one on the right is a much finer segmentation aiming at the groups of shrubs. Figure gathered from (Blaschke and Strobl 2001).

Compared to traditional pixel-based methods, OBIA transform pixels into near-homogenous objects. This removed the incident of getting faulty imagery through misclassifications in low spatial resolution images (**Fig. 2.2**) (Paul, et al. 2004; Robson, et al. 2015). For this purpose, OBIA can, e.g., be used to automatically remove water bodies or include/exclude debris-covered glacier tongues. Based on an article by Rastner, et al. (2014), where they compared OBIA and PBIA by mapping glaciers through optical images, they concluded that OBIA had 12% better accuracy of mapping debris-covered glaciers, than PBIA. The disadvantages with PBIA was that misclassification would occur, since PBIA classifies each individual pixel through their spectral information and could therefore classify multiple landforms within the same pixel. On the other hand, Rastner, et al. (2014) noticed that OBIA could miss tiny objects that PBIA would include in the mapping (ice couloirs or nunatakes), but includes the larger objects (e.g., elongated medial morraines). However, they did conclude that OBIA is recommended when one is mapping glaciers in regions where there are multiple spectral information's (e.g. clean ice, debris-covered glaciers) to be mapped.

2.3.1.3 Automatic delineation of Debris-covered ice

Studies have revealed that manual digitization is extremely time-consuming when one is outlining debris-covered glaciers and also known to lead to faulty and inaccurate results (Bhambri, et al. 2011; Bolch, et al. 2008; Paul, et al. 2013). It is therefore not recommended as a method for this part of the classification. Debris-covered glaciers is ice covered with debris from surrounding landslides, and as every other glacier, these parts do also experience glacier movement. This is an important factor when it comes to classifying debris-covered ice. In the article by Paul, et al. (2002) they mentioned that the TM4/TM5 method proved sufficient when one is mapping debris-free glaciers or clean ice, but that the method failed to map debris-covered parts. This is because debris-covered glaciers and stable ground are spectrally similar and can therefore be misclassified as one another. This can be avoided by focusing on the movement of the glacier rather than its reflectance from light. Synthetic Aperture Radar (SAR) is a system that sends out radar waves that backscatter of the ground and back up to the radar. This SAR system measures and records the amplitude and the phase that the backscatter echoes return and produces SAR images. A SAR image pair can be used to measure shift in phase (interferometric fringes), and by using two images with slightly different viewing angels one can monitor change in terrain, also called coherence (Zebker and Goldstein 1986). SAR coherence is a parameter often used to differentiate debris-covered ice with the surrounding stable terrain, and there have been recent studies that have been using this with great result (Frey, et al. 2012; Robson, et al. 2015; Zongli, et al. 2011). Loss in coherence value is correlating to the change over time or movement over the glacier and is therefore often used as a guide to indicate debris-covered glacier parts (Frey, et al. 2012; Robson, et al. 2015). **Fig. 2.4** shows the advantages of using coherence over debris covered ice compared to using the NIR/SWIR band ratio. In the figure one can clearly see that both clean ice and debris-covered parts show very low coherence value, displayed with a dark indication in image **(C).** This is due to the change in geometrical configuration of the scatters (Frey, et al. 2012). Robson, et al. (2015) automatically mapped debris-covered parts in the Manaslu Region, Nepal, by using SAR coherence as a parameter for the classification. It is worth to notice while the coherence data can identify both clean ice and debris-covered ice, it is also able to classify water bodies, which would also display a low coherence value. However, since water bodies already have an easy straightforward method by using optical satellite images and band ratio (see section *2.5 " Methods for studying glacial lakes with remote sensing"*), this means that the coherence method is a more glacier focused classification method (Frey, et al. 2012). As low coherence values measures shift in phase and

therefore identifies changes in terrain, it therefore also identifies change in vegetation and mass movements in non-glaciated terrain. This means that is impossible to compute an automated mapping of a debris-covered glacier based solely on coherence images, one would need other parameters, such as: e.g. NDVI and NDSI. The NDVI is to remove vegetation at the glacier terminus, as the vegetation could be picked up by the coherence, and the NDSI is used to include the dirty ice that would protrude from the debris (Robson, et al. 2015).

It is also possible to use NIR/SWIR bands combined with thermal data over the given study area for mapping debris covered glaciers (Casey, et al. 2012; Karimi, et al. 2012; Shukla, et al. 2010). On the other hand, thermal data over debris-covered ice is limited by the thickness of the debris layer. Reznichenko, et al. (2010) explained in his paper on "Effects of debris on ice-surface melting rates: an experimental study" they noted that the overall melting of ice was considerable smaller under 130 mm of debris. The debris-cover would therefore be less than 130 mm thick for the thermal data to show much sign of activity and since the thickness of the debris-covers from the study areas are unknown, thermal data will therefore not be used for this study.

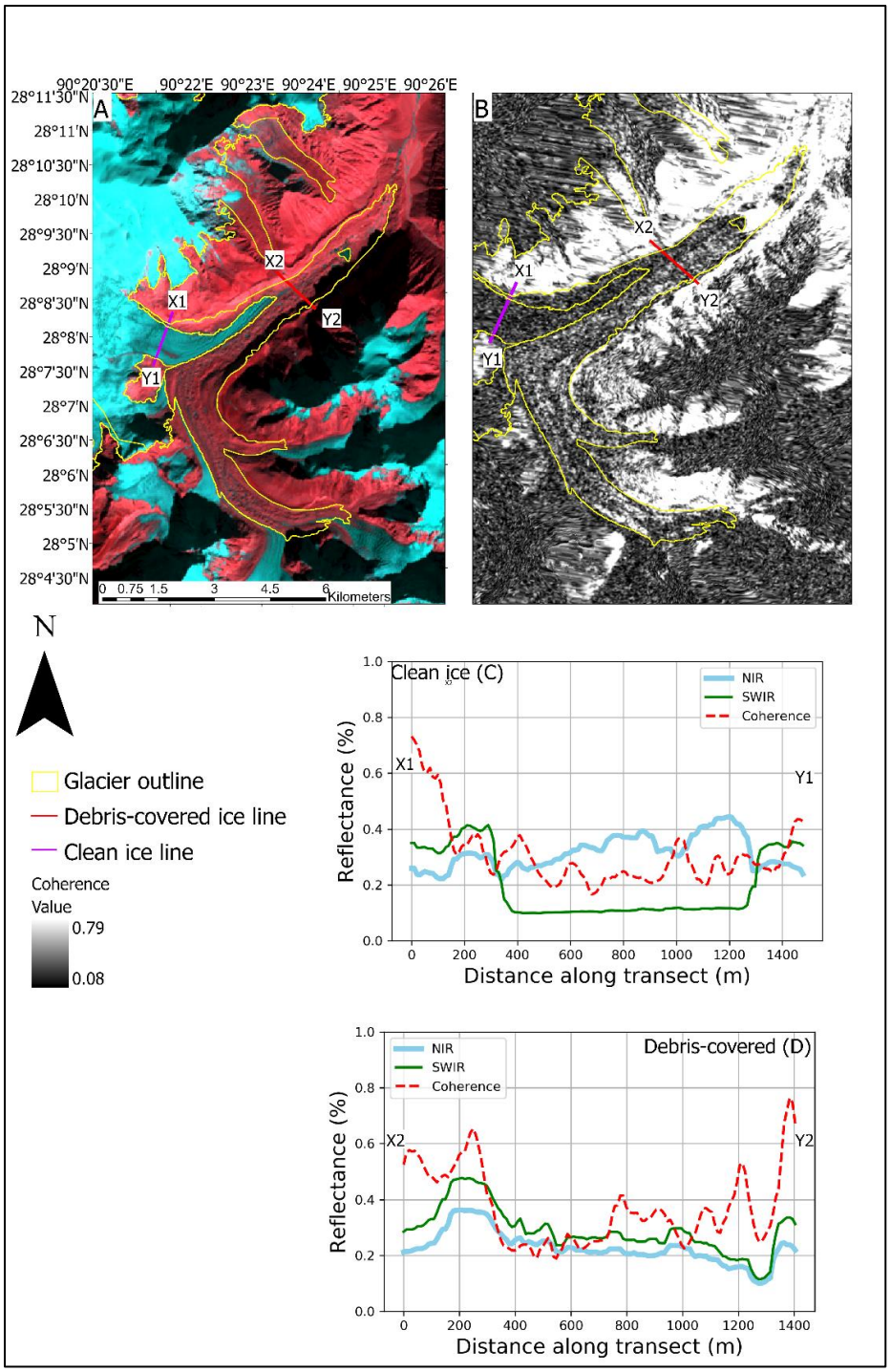

Fig. 2.4: (A) An overview image of the Lianggang glacier located west in the Lunana glacier system. **(B)** Coherence image cropped over the Lianggang glacier; the image shows the glacier movements over the clean ice as well as the debris covered parts. Both of the images are marked with two individual transect lines: the green line represents clean ice and the red line represents debris-covered glacier. **(C)** Graph showing the reflectance values of the NIR/SWIR ratio as well as the coherence values over clean ice, displayed as green transect line**. (D)** Graph showing the reflectance values of the NIR/SWIR ratio as well as the coherence values over the debris-covered glacier, displayed as a red transect line in.

2.3.2 Glacier mass balance

Geodetic mass balance is a way to indirect determine the mass balance of glaciers, this differs from glaciological measures of mass balance which uses field data to directly calculate the changes. Glacier mass balance changes by the result from ablation and accumulation, and is therefore an indicator for volume changes within the glacier (Fischer 2011). Two different DEMs from two different periods are gathered to generate a DEM co-registration (see chapter 4.1.2 for further explanation). The geodetic calculation method uses volume change with the mean density to calculate the mass balance (**Fig. 2.5**). This and most studies estimate the density and is therefore differencing from direct mass balance which uses a calculated density.

Direct mass balance is determined through the direct in situ determination of accumulation and ablation for that mass balance year (Braithwaite 2002). Ablation stakes are drilled down into the glacier and read at the end of the hydrological[5] year (Fischer 2011). While the accumulation is determined by digging snow its and measure the thickness and the density of the snowpack and firn. However, the glaciological method does not account for the mass changes below the surface and therefore only confirms the surface mass balance (Fischer 2011).

$$B_{geo} = \Delta V \times \rho$$

Fig. 2.5: The formula to calculate the geodetic mass balance (B_{geo}) using the volume change (ΔV) times the density (ρ) (Fischer 2011).

Both methods account on good data to present good results, the glaciological method has field survey data and the geodetic method has DEM data. These data processes can lead to certain uncertainties. The ablation stakes can yield small sample size, and as an example, the measuring from the stakes can significantly differ from one stake to another, as a result from surface albedo changes (Fischer 2011). However, as proven by Kuhn, et al. (1999), this is not defined as an error, but that some stakes are valued less important than others. The accuracy of the glaciological mass balance is controlled by the amount of snow pits and stakes. This same statement can be transferred to the geodetic method as the accuracy of the geodetic mass balance is controlled by the resolution of the DEMs.

[5] Hydrological year also known as the water year, is a term used to describe a period of 12 months for which precipitation is measured. Example: in 2010 the water year started on October 1, 2009 and ended on September 30, 2010.

2.3.3 Glacier velocity

Glacier velocity is a last method used to look at the velocity measurements of the Lunana glacier system. This study is focusing at glacier changes with the supplement of GLOF events, and GLOF hazards can have an increase in hazardous effect as active glaciers produces meltwater that can lead to more production of glacial lakes and/or lead to cause of impact to a GLOF event (Emmer 2017).

Dehecq, et al. (2015) used all available Landsat 5/7 pairs that where taken over the Himalaya to produce a large and robust 3-year glacier velocity time series. The displacement was estimated by using repeat-image feature tracking and a complex cross correlation algorithm of the Landsat image pairs. The software used for this study is unknown. Feature-tracking is a method used to estimate a displacement between an image pair, by using generated reference windows that are compared between the image pair using a function of similarity. This is a repeating process and the results yield the maximum similarity which then is translated to be the measure of the displacement (Dehecq, et al. 2015).

Another method was used by Varugu, et al. (2015), where they were using high resolution SAR images to estimate the glacier velocity to Gangotri glacier in India, Himalaya. The explained that the SAR method can be used in two different approaches: the interferometric (InSAR) approach and the offset tracking approach. The interferometric method was executed by using two SAR data sets from ERS-1&2 with a one-day interval and co-registered to record the displacement. The entire process was done through the Gamma Remote Sensing and Consulting (GAMMA) software. The interferometric approach uses coherence to calculate the displacement change, and according to Varugu, et al. (2015) the significant amount of coherence is lost after one day. This limits the interferometric approach to only measure glacier displacement with a maximum one-day interval. This is different for the offset tracking approach which uses intensity values instead of coherence loss, resulting in a fine displacement measurement over glaciers with even longer repeat periods. Varugu, et al. (2015) executed the offset tracking approach by using TerraSAR-X and TanDEM-X image pairs with a low repeat period of 11 days and co-registered through the GAMMA software. Both methods showed valid results and where highly efficient in detriment the displacement in glaciers.

In the end, the feature tracking method versus the SAR offset tracking and interferometric method both uses cross correlation of images. The difference is the speed of the glacier which

can be measured between a short time interval, like the SAR approach, or in a more complex but longer time interval, the optical feature tracking approach.

2.4 Methods for studying glacial lakes with remote sensing

Classifying glacial lakes with multi-spectral data bears a lot of similarities to classifying glaciers. One could for example use manual delineation to identify these lakes. With a trained eye and some geological experience, one could even delineate different types of glacial lakes, e.g. proglacial lakes, and supra glacial lakes.

Key concept in the identifications of various objects through remote sensing is that these objects reflect energy differently and by using the electromagnetic spectrum one can easily identify them (Govindha Raj, et al. 2013), and water bodies absorbs high amount of infrared radi. Band ratios are an easy tool to derive from this concept and has been used in many ways to identify glacial lakes. NDWI is the main band ratio to use to identify water surfaces and has been since index was first used by McFeeters (1996). Water bodies, e.g. glacial lakes, absorbs high amount of infrared radiation as well as green light due to the green pigment in chlorophyll (McFeeters 1996). The NDWI uses the reflected near-infrared (NIR) radiation and the visible green light to intensify the state of features, such as water bodies, but at the same time remove the presence of soil and vegetation features (**Fig. 2.6**). After that there has been several different versions of the NDWI by using different combinations and different equations to improve the classification or to better asses for the different types of lakes, e.g. mudded water, clean water, etc.

$$NDWI = \frac{(X_{Green} - X_{NIR})}{(X_{Green} + X_{NIR})}$$

Fig 2.6: McFeeters (1996) NDWI equation used to classify water bodies in GIS.

An example could be Wessels et al. (2002) which was using spectral analysis, based on ASTER-imagery, to identify terrain features in the region of Mount Everest and locate glacial lakes. They used automatic classification to identify and locate these glacial lakes. By using bands in the NIR (Near Infra-Red) and MIR (Middle Infra-Red) of the ASTER data. The results led to two ratios to distinguish (**Fig 2.6**7:

$$R_1 = \frac{B_{Green}}{B_{NIR}}$$

$$R_2 = \frac{B_{NIR}}{B_{MIR}}$$

Fig. 2.7: Wessels et al. (2002) equation to calculate the location of glacial lakes in Mount Everest region. Where B_i is the ASTER spectral band image. Source: (Gardelle, et al. 2011)

1: With ratio R_1 to distinguish water surfaces from non-water surfaces (Eq. (1)).

2: With ratio R_2 to distinguish solid (ice or snow) from liquid (water) surfaces (Eq. (2)), among already classified water surfaces (from Eq. (1)).

Huggel et al. (2002) studied glacier hazards in the Swiss Alps, using LANDSAT images and applied the NDWI (Normalize Difference Water Index, Eq. (3)) (**Fig. 2.8**). This formula was able to calculate and locate glacial lakes by utilizing the low water reflectance in the NIR (Near Infra-Red) band.

$$NDWI = \frac{B_{NIR} - B_{Blue}}{B_{NIR} + B_{Blue}}$$

Fig. 2.8: Huggel et al. (2002) equation to calculate the location of glacial lakes by using the NDWI formula.

These are just two examples to identify and classify glacial lakes, but there are situations where these types of classifications are not good enough. Situations like; when lakes are frozen and covered by snow, these formulas will not be able distinguish them from water and non-water areas, and solid from liquid (e.g. snowy glaciers). It will be therefore needed to use visual inspections to distinguish them, and still then it could be hard to identify.

2.4.1 Lake monitoring with SAR data

However, using optical data as an input for monitoring glacial lakes have shown to be challenging in the past, reason being that cloud-free image are required as well as the inability to reveal the location during night hours. Therefore, several optical data inputs cannot be used because of their limitations, and the seasonal variations to glacial lakes cannot be observed as well. To prevent this, Wangchuk, et al. (2019) proved in his paper that optical imagery can be substituted with SAR imagery. Which is not limited by cloud cover and nighttime, because of their active remote monitoring. The threshold parameters are the same both for the optical data as the SAR data (figure SAR). Sentinel 1 data will be used as input data for the SAR classification and will be preprocessed through SNAP and then converted to ArcMap for the binary classification.

Chapter 3: Data

This chapter consist of all the different datasets used for this study. The data files are explained accordingly to their different paragraphs: optical data, stereo data, SAR data and DEM data. They are divided up between their different satellites or their data type (e.g. optical and DEM). The datasets used for all the methods are listed in **table 3.1**.

3.1 Optical data

Optical data sets where used for the classification method of both glacial lake- and glacier area. These optical datasets consisted of Landsat 5 & 8 TM and Sentinel 2B. The Landsat data where downloaded for free from earthexplorer.usgs.gov website, with a spatial resolution of 30 m. The Sentinel 2 dataset where downloaded from scihub.copernicus.eu website, with a spatial resolution of 20 m. The Landsat 5 temporal archive ranges from 1984 until 2018 and Landsat 8 ranges from 2013 until present day.

3.1.1 Stereo data

The Stereo data were used to generate DEM for the calculation of geodetic mass balance. These datasets were consisting of 2019 Pléiades data (0.5 m resolution) and 2018 SPOT 6/7 (2.5 m resolution). These high-resolution images cannot be downloaded for free and for this study a quota where applied to the European Space Agency to produce Pléiades scenes and SPOT 6&7 scenes for this project. This application was granted in February 2019 and Pléiades scenes was taken during October. The SPOT 6&7 was accessed through the Geostore for the ESA website with the allocated quota from the application.

3.2 SAR data

The Synthetic Aperture Radar (SAR) data were used for the calculation of glacial velocity as well as for the generating of the coherence parameter used for the glacial area classification. The SAR data was consisting of 2016 TerraSAR – X (TSX) data gathered free of charge from terrasar-x-archive.terrasar.com website and 2018 Sentinel 1A data gathered free from scihub.copernicus.eu website. The TerraSAR – X data had a spatial resolution of 3 m.

3.3 DEMs

Digital elevation models (DEM) where used for the classification method as well as the calculation of the geodetic mass balance, where they were used to calculate surface and volume changes. The DEMs where 2000 Shuttle Radar Topography (SRTM), downloaded for free from srtm.csi.cgiar.org website, 2016 High Mountain-Asia (HMA), downloaded from free from NASA National Snow and Ice Data Center Distributed Active Archive Center (NSIDC DAAC), and a 1976 HEXAGON DEM obtained from King, et al. (2019)

Table 3.1: A table showing all the downloaded satellite scenes that was used for this study.

Scene ID	Date of acquisition	Sensor	Resolution (m)	Bands used	Purpose
LM02_L1TP_148041_19761217_20	17/12/1976	Landsat 2	30	-	Glacial area
LT05_L1TP_138041_19941227_20	12/27/1994	Landsat 5	30	Green/NIR	Lake area
LT05_L1TP_138041_19950128_20	1/28/2995	Landsat 5	30	Green/NIR	Lake area
LT05_L1TP_138041_19961130_20	11/3/1996	Landsat 5	30	Green/NIR	Lake area/glacial area
LT05_L1TP_138041_19970101_20	1/1/1997	Landsat 5	30	Green/NIR	Lake area
LT05_L1TP_138041_19970218_20	2/18/1997	Landsat 5	30	Green/NIR	Lake area
LT05_L1TP_138041_19990208_20	2/8/1999	Landsat 5	30	Green/NIR	Lake area
LT05_L1TP_138041_20001109_20	11/9/2000	Landsat 5	30	Green/NIR	Lake area
LT05_L1TP_138041_20001227_20	12/27/2000	Landsat 5	30	Green/NIR	Lake area
LT05_L1TP_138041_20041104_20	11/4/2004	Landsat 5	30	Green/NIR	Lake area
LT05_L1TP_138041_20050107_20	1/7/2005	Landsat 5	30	Green/NIR	Lake area
LT05_L1TP_138041_20070129_20	1/29/2007	Landsat 5	30	Green/NIR	Lake area
LT05_L1TP_138041_20080116_20	1/16/2008	Landsat 5	30	Green/NIR	Lake area
LT05_L1TP_138041_20081217_20	12/17/2008	Landsat 5	30	Green/NIR	Lake area
LT05_L1TP_138041_20090203_20	2/3/2009	Landsat 5	30	Green/NIR	Lake area
LT05_L1TP_138041_20091001_20	10/1/2009	Landsat 5	30	Green/NIR	Lake area
LT05_L1TP_138041_20091017_20	1/17/2009	Landsat 5	30	Green/NIR	Lake area
LT05_L1TP_138041_20101223_20	12/23/2010	Landsat 5	30	Green/NIR	Lake area
LT05_L1TP_138041_20110108_20	1/8/2011	Landsat 5	30	Green/NIR	Lake area
LT05_L1TP_138041_20111108_20	11/8/2011	Landsat 5	30	Green/NIR	Lake area
LC08_L1TP_138041_20131012_20	10/12/2013	Landsat 8	30	Green/NIR	Lake area
LC08_L1TP_138041_20151119_20	11/19/2015	Landsat 8	30	Green/NIR	Lake area
LC08_L1TP_138041_20161020_20	10/2/2016	Landsat 8	30	Green/NIR	Lake area
LC08_L1TP_138041_20170414_20	4/14/2017	Landsat 8	30	Green/NIR	Lake area
LC08_L1TP_138041_20171108_20	11/8/2017	Landsat 8	30	Green/NIR	Lake area
LC08_L1TP_138041_20171210_20	12/10/2017	Landsat 8	30	Green/NIR	Lake area
LC08_L1TP_138041_20171226_20	12/26/2017	Landsat 8	30	Green/NIR	Lake area

LC08_L1TP_138040_20181213_20	12/27/2018	Landsat 8	30	Green/NIR & SWIR/NIR	Glacial area
S2A_MSIL1C_20181027T043851_N0206_R033_T46RBR_20181027T074001	10/27/2018	Sentinel 2	20	-	Glacial area
S1A_IW_SLC__1SDV_20181006T235450_20181006T235517_024022_029FEB_2D73	10/6/2018	Sentinel 1	Level 1 SLC	-	Coherence
S1A_IW_SLC__1SDV_20181018T235450_20181018T235517_024197_02A59F_5D32	10/18/2018	Sentinel 1	Level 1 SLC	-	Coherence
SRTM_DEM_30m	2/11/2000	SRTM	90	-	DEM/Slope
SEN_SPOT7_20181216_041435900_000_RAW_MS	12/16/2018	SPOT	6	-	DEM/Geodetic mass balance
TPMESA4_SO19043731-5-01_DS_PHR1B_201910160452100_FR1_PX_E090N28_0305_02222	10/16/2019	PLÉIADES	0.5	-	DEM/Geodetic mass balance
TPMESA4_SO19043731-2-01_DS_PHR1B_201910160452208_FR1_PX_E090N28_0505_01880	10/16/2019	PLÉIADES	0.5	-	DEM/Geodetic mass balance
TPMESA4_SO19043731-8-01_DS_PHR1B_201911060441036_FR1_PX_E090N28_0303_00786	11/6/2019	PLÉIADES	0.5	-	DEM/Geodetic mass balance/glacial area
HEXAGON_DEM_BHUTAN_1976	1976	HEXAGON	90	-	DEM/Geodetic mass balance
TDX1_SAR__SSC_____SM_S_SRA_20161126T115334_20161126T115342.xml	26/11/2016	TerraSAR - X	3	-	Glacier velocity
TDX1_SAR__SSC_____SM_S_SRA_20161218T115334_20161218T115342.xml	18/12/2016	TerraSAR - X	3	-	Glacier velocity

Chapter 4: Methods

In this chapter the different types of remote sensing methods used in this study will be explain. The glacier classification consisted of two OBIA classification of the Lunana glacier system: one where based solely on the optical satellite data and focused on classifying clean ice and glacial lake, while the second included SAR coherence images to classify the debris-covered parts of the glacier system. The glacial lake classification included identification of the shape and area of Raphstreng Tsho- and Luggye Tsho proglacial lake from 1993 until 2018. The geodetic mass balance includes calculation of both the surface elevation- and the volume change for the Lunana glacier system, between 1976 and 2019. The glacier velocity where calculated from TerraSAR-X data and shows a 22 days displacement change over Lunana from 2016.

4.1 Preprocessing

The preprocessing step is a crucial step before exerting the methods used to identify glaciers and or calculate the geodetic mass balance. The step is needed transform input data into output data that can be used as input into another method. It consists of methods like e.g. cleaning, normalization, transformation, and more (Frey, et al. 2012; Gardelle, et al. 2013; Robson, et al. 2015). In this study, the preprocessing steps consist of DEM creation and DEM co-registration, as well as SRTM radar penetration correction.

4.1.1 DEM creation

To calculate the geodetic mass balance for the Lunana glacier system, several DEMs where required. Some of the DEMs like the SRTM and HMA where freely accessed and generated. Stereo imagery was used to generate DEMs from 2018/9. This study is using Pléiades data from 2019 and SPOT data from 2018 as raw images to generate DEM data. The data was processed through the software PCI Geomatica and created the DEMs by using Normalized Cross-Correlation (NCC) as method and parameters such as rational polynomial coefficients and tie points. The method used 3000 tie points to generate a 30 m resolution DEM

4.1.2 DEM Co-registration

To calculate the linear co-registration the method by Nuth and Kääb (2011) was utilized. This co-registration is done by looking at the elevation bias (dh) over the stable terrain by using the minimization of the root mean square residuals of said stable terrain. To calculate the elevation bias the formula by Nuth and Kääb (2011) (**Fig. 4.1**) was used, and the elevation bias has proven to be more visible on steeper slopes. Therefore, the elevation bias over the slope (tan α) is calculated by the magnitude and direction (a & b) of the co-registration shift and plotted against the aspect (ψ). The process is then iterated until the shift and the standard deviation of the residual over stable terrain is less than 2 % (Robson, et al. 2018). The co-registration shifts are shown in **Fig. 4.2**, where it shows a graph of the normalized elevation bias before and after co-registration process.

$$\frac{dh}{\tan \alpha} = a \cos(b - \psi) + c$$

Fig. 4.1: Formula to linearly co-register DEM's. The elevation bias (dh) is calculated given that the elevation differences are larger on steeper slope, considering the magnitude (a), the direction of the co-registration shift (b) and the tangent of the slope terrain (α). This concept is then plotted against the aspect (ψ) and the mean elevation bias (c). Gathered from Robson, et al. (2018).

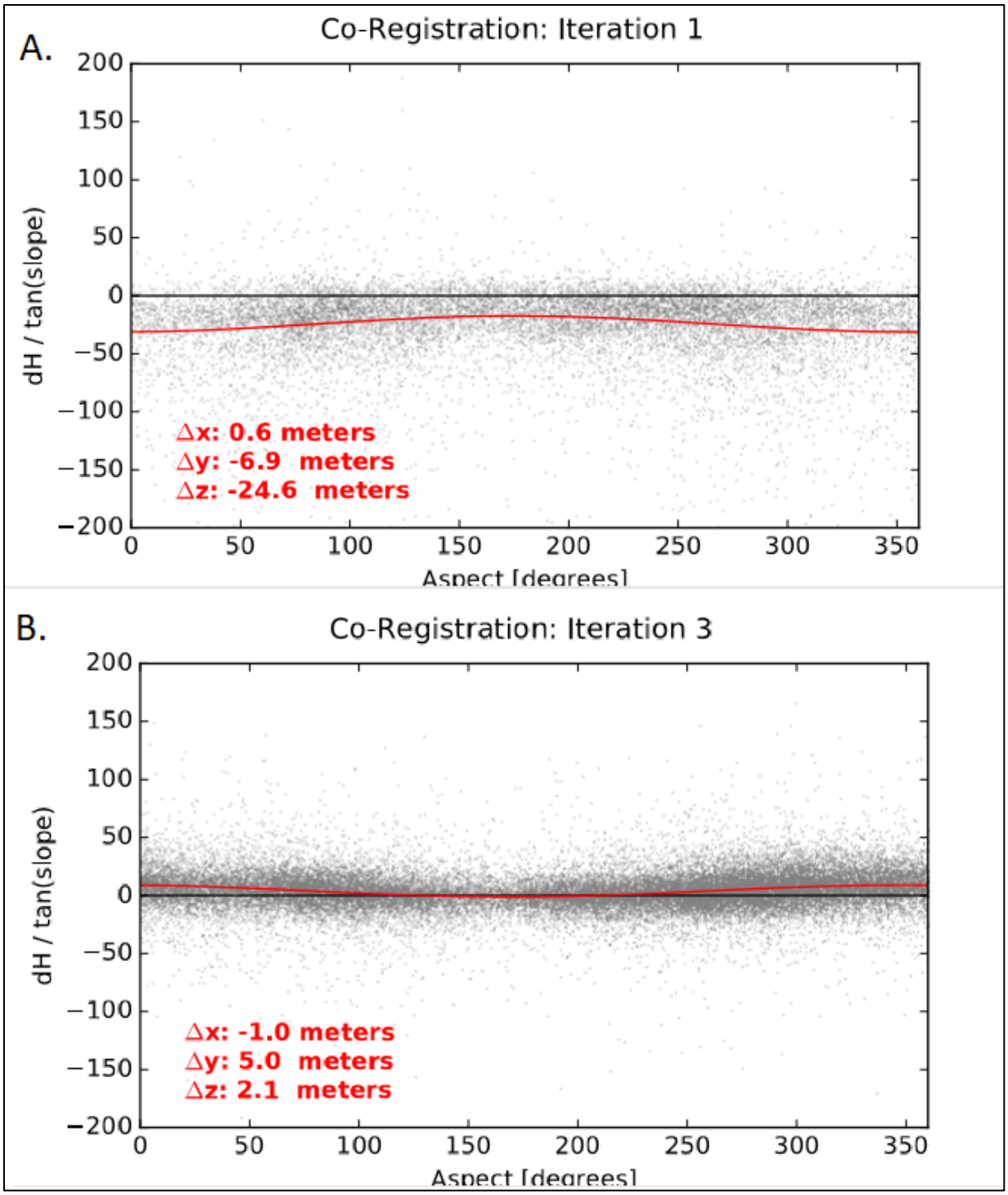

Fig. 4.2: Shows the co-registration shifts between the 2019 Pléiades DEM and the 2000 SRTM DEM. The graphs show the co-registration before (**A)** and after three iterations of co-registration (**B**). The co-registration shifts that where applied are displayed in red text, which includes the z-residual.

4.1.3 SRTM radar penetration correction

According to Rignot (2001) the X-band in the SRTM DEM can penetrate the snow and firn by several meters, and will therefore cause a problem when calculating the co-registration with a DEM pair that includes the SRTM dataset. To prevent this a penetration correction was made, and there have been several estimates on the level of penetration in the Himalayas. Estimates like 1.4-3.4 m (Gardelle, et al. 2013) and even 8-10 m (Kääb, et al. 2012). The final decision was to use the same estimates as Robson, et al. (2018), which was the correction stated in Kääb, et al. (2012) for clean ice as 1.5 m. These value changes will be added to the results for the co-registration files through modelbuilder and by using the raster calculator tool in ArcMap.

4.2 Glacial lake time series

This thesis is focusing on deriving and classifying two important glacial lakes that have been categorize as potential dangerous glacial lakes (PDGLs) by Mool, et al. (2001), that is Raphstreng Tsho and Luggye Tsho. These glacial lakes will be classified in temporal listing from 1993 until 2018. By doing so this inventory should be able to reveal the state of Luggye Tsho lake before and after the 1994 GLOF event which outburst from Luggye Tsho (Watanbe and Rothacher 1996). To fully compile a time series showing the change in physical states of the two PDGLs lake, Raphstreng Tsho and Luggye Tsho, a digital data base of these two glacial lakes was necessary to calculate the temporal change in area. To identify these two glacial lakes over several optical datasets an automatic classification method was needed. As a manual delineation over several optical datasets would be time consuming and therefore not be suited for this sort of classification. For this study I developed a model in ArcGIS that can automatically chose a threshold in the NDWI to separate water surfaces from non-water surfaces, as a binary classification. and applied on a stack of optical imagery **(Fig. 4.3**).

The PBIA classification process:

1. Pre-processing: The SRTM DEM were resampled to 30 m resolution, as well as projected to 45 UTM. This was done to match up geographically with the Landsat 5 & 8 data files and to bear the same spatial resolution. A slope file was generated from the SRTM file as it would be used as a parameter for the classification. A raster calculator tool was used to set up the NDWI calculation of the NIR- and green band for all of the Landsat images.
2. Classification: **Fig. 4.3** shows the flowchart of the PBIA classification done for Raphstreng Tsho and Luggye Tsho glacial lake. The classification uses NDWI as main parameter and derived a binary classification to create a raster consisting of two classes: 1 – potential water pixels and 0 – non-water pixels. The elevation and slope data from the SRTM DEM were added trough “add surface information” tool. These parameters where adjusted with different values to further assess the potential water pixels.
3. Clean up: The potential water pixels derived from the binary classification where adjusted through some clean-up methods. Firstly, the pixels where added area values in km^2 through the geometry calculator. Secondly, any potential water pixels smaller than 0.09 km^2 where removed. Lastly, every potential water pixel where enclosed and adjusted through manual editing.

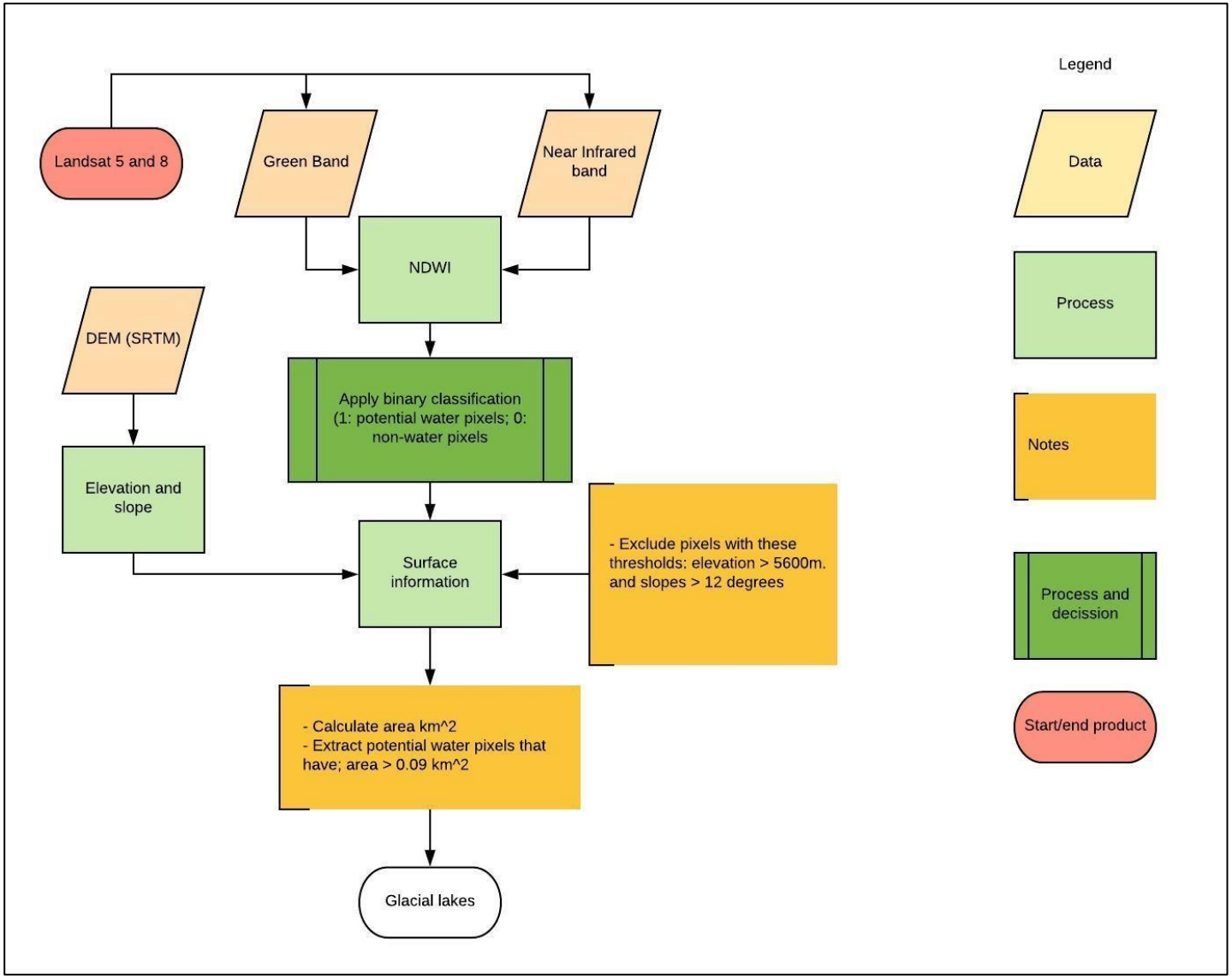

Fig. 4.3: Flowchart showing the essential parameters and methods used to classify the glaclial lakea areas through the optical classification method.

4.3 Glacier area change

To classify the glacier surfaces of the Lunana glacier system, the classification will be separated between classification of clean ice and debris covered ice, as they need different algorithms and parameters to be identified. The debris-covered glacial areas are mostly abundant in the southern part of the Lunana glacier system, the northern parts are dominated by clean ice. By applying a threshold to the ratios of Landsat TM bands, mainly TM4/TM5 (NIR/SWIR band) or TM3/TM5 as a main parameter, one could classify clean ice areas (Paul, et al. 2004). The debris-covered parts will be classified by using low coherence values (**Fig. 4.4**). This will be all achieved through automatic classification (OBIA) in the eCogntion software.

To be able to estimate the glacier change over Lunana glacier system, there will be three different glacier outlines derived for this study. A glacier inventory for 2018 will be made through the OBIA classification method, and two individual glacier inventories for 1996 and 1976 will be made through the manual delineation method.

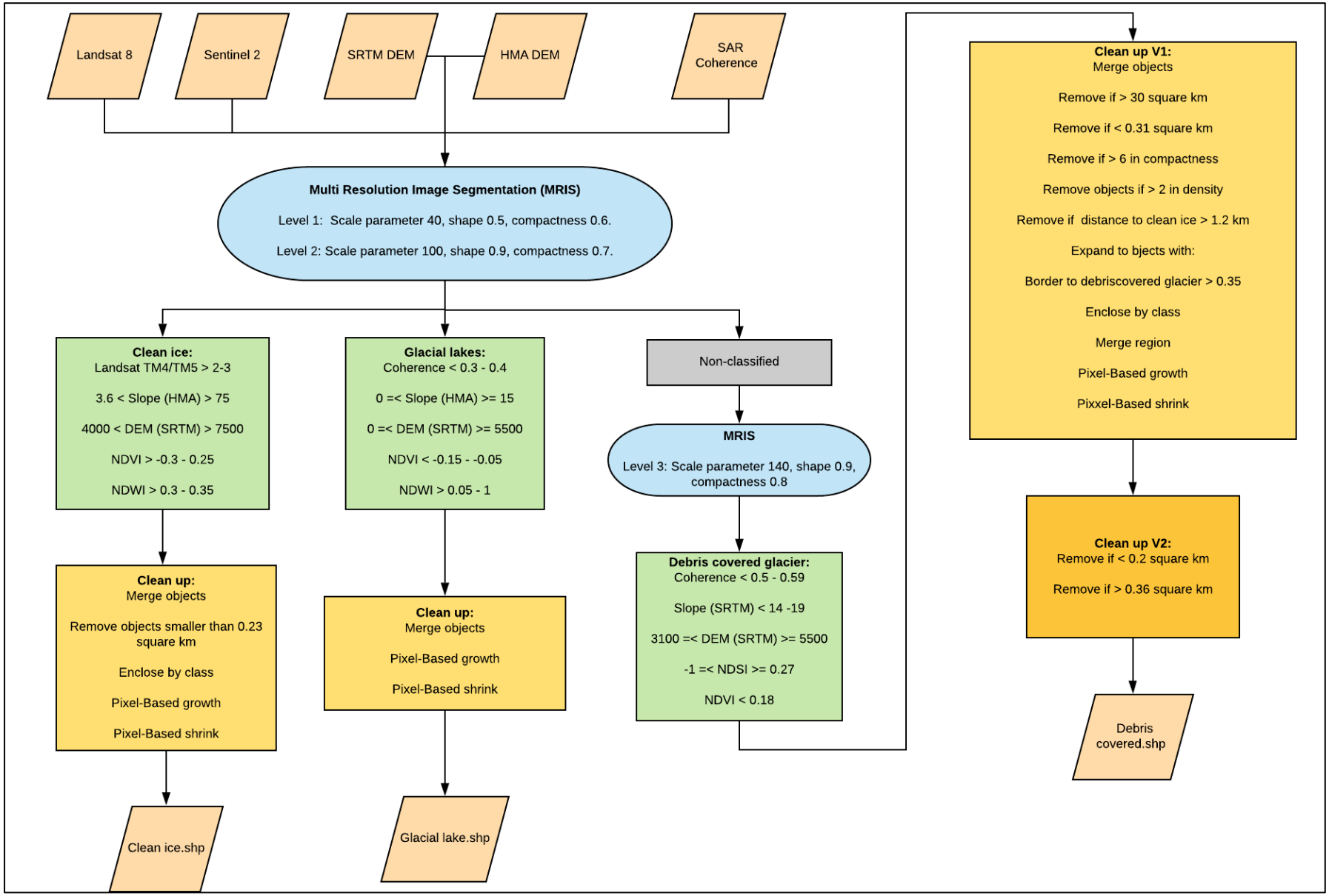

Fig. 4.4: A flowchart showing the processes to classify clean ice, glacial lakes and debris-covered ice. The clean ice was classified solely on the use of optical and elevation

4.3.1 Creation of 2018 glacier inventory

The 2018 glacier inventory was made through OBIA classification. The method is consisting of pre-processing, image segmentation, classification, mapping of glacial lakes and clean ice, and mapping of debris-covered ice. The individual mappings are then merge together to make one complete glacier inventory of the Lunana glacier system of 2018.

The OBIA classification process:

1. Pre-processing: The first step will be consisting of pre-processing steps, to make sure that one can use the individual raw data files. The SRTM and HMA DEMs were resampled to 30 m resolution, as well as projected to 45 UTM to match the Landsat 8 image, at the same time a slope raster was generated both from the SRTM and the HMA. Different indices and band ratios where generated in eCognition. The SAR coherence where created in SNAP, using Sentinel 1 data. Two Sentinel 1 data files where co-registered, terrain corrected and geocoded within the same remote sensing software, before they were made into a single coherence data file.
2. Image segmentation: The image segmentation is a crucial step within OBIA, and is a near-homogenous process, done to group pixels into objects. These objects can than again be merged into individual objects, called hierarchical levels (Robson, et al. 2015). By using the multi-resolution segmentation in eCognition, image objects where created for three classifications; both glacial lakes and clean ice used the same two hierarchical leveled segmentation. In Robson, et al. (2015) paper, he mentioned that by using multiple image objects helps grouping the non-glacier features together, this makes it easier to exclude these features from the classification, and this paper is therefore using multiple hierarchical[6] levels. For the debris-covered glacier classification the image segmentation was processed one finale time, making it the third hierarchical leveled segmentation.
3. Classification: **Fig. 4.4** shows the workflow used for the OBIA classification, this includes all the pre-process steps, parameters and thresholds used for the classification, and the post-classification filtering used to clean up the classification. The different indices and their thresholds used for the classification where gathered from the literature: NDVI, NDSI, SWIR/NIR ratio (see **Table 2.1**), slope and the SAR coherence where gathered from Robson, et al. (2015) & Bajracharya, et al. (2014),

[6] Hiercarchial: meaning a way to organize. In this case, the hierarchical level is used to organize the different levels of the segmentations used in the OBIA classification.

while the NDWI where partly gathered from Wessels, et al. (2002), and was also used in the pixel based classification of glacial lakes in chapter *"4.2 Glacial lake time series"*.

4. Mapping of lakes and clean ice: Firstly, the glacial lakes and the clean ice was first classified as they were the easiest to classify and can therefore be masked out for the rest of the classification. By using the NIR/SWIR or TM4/TM5 ratio, the slope, elevation and the NDVI and NDWI as thresholds, clean ice was classified. It is important to notice that instead of using the SRTM for slope, the HMA DEM was used instead. This is because the classification was based of Sentinel 2 data and Landsat 8 data from 2018, and the SRTM DEM was generated in 2000. Therefore, the slope generated from the SRTM DEM would read glacier slope from the 2000, and because of glacier movement this would not suffice for a classification of 2018 data. Since HMA data set was generated in 2016 it is therefore more sufficient for this classification, then the SRTM DEM from 2000. To classify the glacial lakes, the same inputs as for the clean ice classifications where used, but instead of the NIR/SWIR ratio the SAR coherence where used instead. The SAR coherence is mainly used to track changes over time and should therefore be able to measure movement inn individual glacial lakes, as certain lakes have water outputs through runoff. These runoff causes movements in the lakes and can therefore be picked up by the coherence as low values, see **Fig. 4.4** for these values. Certain supraglacial lakes are considered to be rather troublesome when one is classifying debris-covered glaciers and comparing it to other images and classifications. If a supraglacial lake is small enough and frozen, it can easily be classified as clean ice and therefore be mistaken as part of the debris-covered glacier. To avoid this, a certain threshold was introduced and removing any glacial lake classification less than 0.1 km^2.
5. Mapping of debris-covered glacier: As mentioned, certain glacier areas in the Himalayas are covered in a layer of supraglacial debris from surrounding environments and are observed through their typical shape and the supraglacial lakes located on the top of the glaciers. The debris covered parts are classified using SAR coherence, as the coherence will be able to pick up the glacier movement over time. The usual classification parameters as: slope, elevation, NDSI and NDVI will also be used to classify the debris covered parts.

4.3.2 Creation of 1976 & 1996 glacier inventory

The glacier area change was divided in to three different time periods: 1976, 1996 and 2018. In order to determine the glacier area, change between 2018 and 1996, a glacier polygon for 1996 was needed. Therefore, a manual delimitation of 1996 where created, by using the polygon for 2018 and manually adapt it with reference of a Landsat 5 image from 1996. The polygon will have no other variables than the optical image and is therefore only to be consider a sudo classification of the glacier in Lunana in 1996. The same was done for the glacier outline of 1976. The glacier polygon from 1996 was manually adapted with reference of a Landsat 2 image from 1976. These two manually delineated polygons where only created to compare with the OBIA glacier outline from 2018.

4.3.3 Glacier area change calculation

The areas (km^2) for both of the glacier inventories was calculated through the geometry calculator tool in ArcMap. The differentiate between the two inventories are displayed as north area change, south area change, and area change for the whole glacier system. The percentage of area change was also calculated for the Lunana glacier system with the same layout. The glacier outlines where individually divided based on the glacier borders from the GLIMS outline polygon.

4.4 Glacier geodetic mass balance

The geodetic mass balance was calculated based on the surface elevation changes and the glacier outlines from given time periods (1974-2019). After the DEM co-registration; pixels that yield a surface change over 300 m, which is to remove impossible values like cloud and shadows, and/or has a value greater than three standard deviations based on (Gardelle, et al. 2013), was masked out. To convert the volume to mass a conversion factor was used by assuming a density of 850 kg m^{-3} following Huss (2013). It is worth to note that the PLÉIADES and SPOT DEM does not cover the same type of area as the SRTM and Hexagon does (see **Fig. 1.1**). The stereo data does only cover about 225 km of the Lunana glacier system, and therefore about only half of the study area, which covers 500 km of the Lunana glacier system.

4.5 Glacier velocity

TerraSAR-X images was used to determine glacier velocity. The TerraSAR-X images was processed through the offset tracking tool within SNAP, which uses patch intensity cross-correlation optimization to measure feature motion between to images (Lu J. 2016; Schellenberger, et al. 2015). This will ultimately calculate the displacement of the debris-covered glaciers located in the southern end of the glacier system. The absolute accuracy is dependent on the overall surface displacement and the orbital errors from the satellites (Floricioiu, et al. 2009). The two TerraSAR-X images where taken on 22.10.2016 and 18.10.2016, the displacement was therefore calculated to be between 22 days. Because of the lack of time management this thesis will not include any normalized cross-correlation calculations of the glacier velocity for the Lunana glacier system, which would have given a broader depth to the glacier velocity change.

4.6 Uncertainty assessment

The uncertainty assessment is divided up between the different methods and their field of target. The accuracy was measured through error assessment and target field to ground truth method within the ArcMap software.

4.6.1 Glacier outline accuracy

The accuracy of the glacier outline OBIA classification was achieved by computing a confusion matrix. The confusion matrix is a summary of the classification performance and is achieved by using the incorrect and the correct predications of the classification. The accuracy is achieved by doing an error matrix, a class-by-class comparison between the ground truth data, also known as reference data, and the corresponding results of the classification (Sammut and Webb 2010: p. 209). For this accuracy assessment, the ground truth data where glacier outlines downloaded from Global Land Ice Measurements glacier database (GLIMS), which where contributed by Nuimura, et al. (2015) and their manual derived "Glacier Area Mapping for Discharge from the Asian Mounatins" (GAMDAM). Based on the accuracy there are two error assessments one needs to take account to: producer's accuracy (omission error) and user's accuracy (commission error). The producer accuracy represents how accurate the reference pixels of the land cover are classified, and the user accuracy represents how accurate the pixel classified represent that category on the ground (Lillesand, et al. 2015; Sammut and Webb 2010: p. 209). For this accuracy, the producer accuracy for the glacier classification was 98% accurate, while the user accuracy was 99% accurate. The total results where therefore 98% accurate for the glacier outline OBIA classification.

4.6.2 Glacial lake outline accuracy

The accuracy of the glacial lake outlines PBIA classification was calculated with the same tool output as that of the glacier outline accuracy assessment. The ground truth data used for the assessment where a glacial lake inventory downloaded from the Japan Aerospace Exploration Agency database (JAXA). For this classifcaiton the producer accuracy was 97% accurate, while the user accuracy was 92% accurate. The total results where therefore 94% accurate for the glacial lake outline PBIA classification.

4.6.3 Glacier mass balance accuracy

The accuracy for the glacier mass balance was estimated through the error assessment based on analysis of the stable terrain (Robson, et al. 2018). The analysis was consisting of calculating the standard error (SE), which was needed to calculate the DEM differencing uncertainty (e). The standard error was calculated based on the standard deviation over stable terrain (SD_{STABLE}) divided by the number of pixels included in the DEM differencing (n) (**Fig. 4.5**).

$$SE = \frac{SD_{STABLE}}{\sqrt{n}}$$

Fig. 4.5: The standard error (SE) equation based on standard deviation over stable terrain ($SD_{STABLLE}$) and the number of pixels from the DEM differencing (n) (Robson, et al. 2018).

The pixels included in the DEM differencing is calculated from the original number of pixels (N_{tot}), the pixel size (PS) and the spatial autocorrelation (d) (**Fig. 4.6**).

$$n = \frac{N_{tot} \times PS}{2d}$$

Fig. 4.6: The number of pixels from the DEM differencing (n) equation. Calculated from the original number of pixels (N_{tot}), the pixel size (PS) and the spatial autocorrelation (d) (Robson, et al. 2018).

The spatial correlation distance for the SRTM, SPOT, HEXAGON, and PLÉIADES DEM was concluded to be at 400 m based on the work of others (Robson, et al. 2018). The DEM differencing uncertainty (e) was then calculated (**Fig. 4.7**), which is the sum of root mean square of the standard error (SE) and the z-residual (Z) from the triangulation of the DEM co-registration (**Fig. 4.2**).

$$e = \sqrt{SE^2 + Z^2}$$

Fig. 4.7: The DEM differencing uncertainty (e) equation. Calculated from the root mean square of the standard error (SE) and the z-residual (Z) from the triangulation of the DEM co-registration (Robson, et al. 2018).

4.6.4 Glacier velocity accuracy

The accuracy for the glacier velocity measurement was determined by measuring the displacements over the stable ground around the Lunana glacier system. The stable ground where defined as the terrain with little to no displacement. The final velocity data where modified to only show the stable ground, by removing the glacier (consisting of clean ice and debris-covered glacier), slope that exceed 30°, and glacial lakes. The stable ground where then calculated to the mean displacement which revealed to be about 0.04 m. The displacement was calculated from November 22 to December 18 2016, which is a displacement of 22 days.

Chapter 5: Results

The study area covers large parts of the Lunana glacier system that is divided between the southern glacier system and the northern glacier system and will be referred to as such in this chapter. The results from the glacial lake classification is restricted to the Raphstreng Tsho and Luggye Tsho glacial lake, both located on the southern parts of the Lunana glacier system.

5.1 Glacier area change

The classification of the glacier in the study area where, as explained in chapter 4.3 "Glacier area change", divided into two classification parts; debris covered glacier and the clean ice glacier. The total area of study in 2018 was 513 km^2 of which 64.1 km^2 (12.5%) was debris-covered ice. The glacier area change covers the physical change of state of the Lunana glacier system from three different time periods: 1976, 1996 and 2018. The debris covered glacier was dominant in the southern part of the glacier and the clean ice was dominant in the northern part. Because of this, the two classifications will therefore be explained accordingly:

5.1.1 Glacier area change - Southern glaciers

The classification revealed several glacier tongues consisting of only debris-covered ice, everything else was classified as clean ice. Between 1996 and 2018 the glaciers lost 30.2 km^2 an approximant of 12.1 % reduction in area **(Table 5.2)**. The results are about the same for the ice loss between 1976 and 2018, where the reduction in area is at ca. 12.7%. Glacier G090157E28136N had the biggest retreat of over 3.2 km between 1996 and 2018 and was classified as debris-covered ice (**Fig. 5.1**), it had a 17.1% reduction in area, and was classified to have the same frontal retreat between 1976 and 2018 at about 17% reduction in area. The glacier does not terminate into any lake but terminates into the Pho Chu river. The Luggye glacier 1, which terminates in the Luggye Tsho lake had a frontal retreat of 1.2 km between 1976 and 2018 and had a 41.7% reduction in area. These numbers increased between 1976 and 2018, where the frontal retreat of the glacier was about 1.9 km and had a 47% reduction in area, resulting in that the Luggye glacier 1 almost halved in size from 1976 to 2018. The Raphstreng glacier had a 0.9 km^2 reduction in area between 1976 and 2018, calculating to be a 21 % reduction in area. The glacier terminates directly in Raphstreng Tsho glacial lake and between 1976 and 2018 the glacier had a frontal retreat of about 0.9 km. The Thorthormi glacier has several supraglacial lakes on the terminating tongue, these supra glacial lakes where difficult to classify and calculate between this timeline, as some of the would merge or freeze and melt over time. It where therefore decided that the supraglacial lakes would only

be classified when they were at minimum of 0.1 km^2. This was done so that the classification of the clean ice at the Thorthormi glacier would not be compromised with very small inconvenient supraglacial lakes, and only be taking acquaintance to when they are of suitable size and therefore not be classified as part of the glacier . The Thorthormi glacier had a small frontal retreat between 1976 and 2018 of about 0.2 km, but had an 1.3 % increase in size between 1976 and 1996 as the supraglacial lakes that where observed in 1976 (<0.1 km^2) where frozen solid in 1996, and between 1996 and 2018 the glacier had a 8.3% reduction in area with no new supraglacial lakes being observed in 2018. The debris covered glacier with the glacier id G090157E28136N (no name) had a large frontal retreat of 2.3 km between 1976 and 2019 and is consisting of both clean ice and debris covered ice, but the whole glacier tongue is completely covered by debris. Glacier G090157E28136N went from 61.2 km^2 in 1976 to 53.9 km^2 in 2018, a total of 7.3 km^2 loss in area and a 12 % reduction in size.

5.1.2 Glacier area change - Northern glaciers

Based on the classification the Northern glaciers of the Lunana glacier system, consists of dominantly clean ice, if one is overlooking the Lianggang glacier which consists of both clean ice and debris-covered ice. Between 1996 and 2018 the northern glaciers lost ca. 45 km^2 of ice, equating to approximately a reduction of 14.7 % **(Table 5.2**). The same result is presented between 1976 and 2018, where the loss of ice is about 45 km^2. The Shimo glacier (G090045E28198N), which terminates in a pro glacial lake, had a retreat of 1.27 km with an 8.1% area reduction between 1996 and 2018, and had a retreat of 1.65 km with an 9.52% area reduction between 1976 and 2018 (this retreat is visible in **Fig. 5.1**). Which lead to an increase in area of the pro glacial lake it was terminating in. The Zeng glacier had one of the least frontal retreat of the northern glaciers, it had a retreat of under 0.1 km between 1996 to 2018 but had a 11.3% area reduction. The same glacier showed no frontal retreat between 1976 and 2018 but did however had a 9.9% area reduction. The Lianggang glacier was consistent of both debris-covered ice and clean ice and showed no significant retreat from 1996 to 2018 and a it had a 1.3% area reduction. The results are the same between 1976 and 2018.

Table 5.1: Glacier area change for some of the individual glaciers in the Lunana glacier system. The general timespan has been divided into three zones: 1976, 1996 & 2018.

Glacier name	Glacier id	Area 1976 (km^2)	Area 1996 (km^2)	Area 2018 (km^2)
Lianggang Glacier (North)	G090383E28118N	46.92	46.92	46.33
Luggye Glacier 1 (South)	G090326E28109N	7.56	7.07	4.41
Luggye Glacier 2 (South)	G090305E28114N	2.46	2.46	1.35
Raphstreng Glacier (South)	G090246E28129N	4.27	3.62	3.37
Bechung Glacier (South)	G090217E28130N	12.05	12.05	10.76
None (South)	G090157E28136N	61.2	61.17	53.89
Shimo glacier (North)	G090045E28198N	31.09	30.61	28.13
Zeng glacier (North)	G090273E28197N	92.068	93.58	82.96
Thorthormi glacier (South)	G090278E28132N	18.79	18.50	17.2

Table 5.2: Glacier area change for the Lunana glacier system. Calculated from three different time periods: 1976, 1996 & 2018. The area change (%) is calculated with the values from 1976 vs 2018.

Glacier region	Number of glaciers	Median elevation (m a.s.l.)	Area 2018 (km^2)	Area 1996 (km^2)	Area 1976 (km^2)	Area change (%)
Northern	74	5873	306.12	351.5	350.9	12.8
Southern	51	5953	219.42	249.63	251.19	12.65
All Glaciers	125	5913	525.54	601.13	602.09	12.73

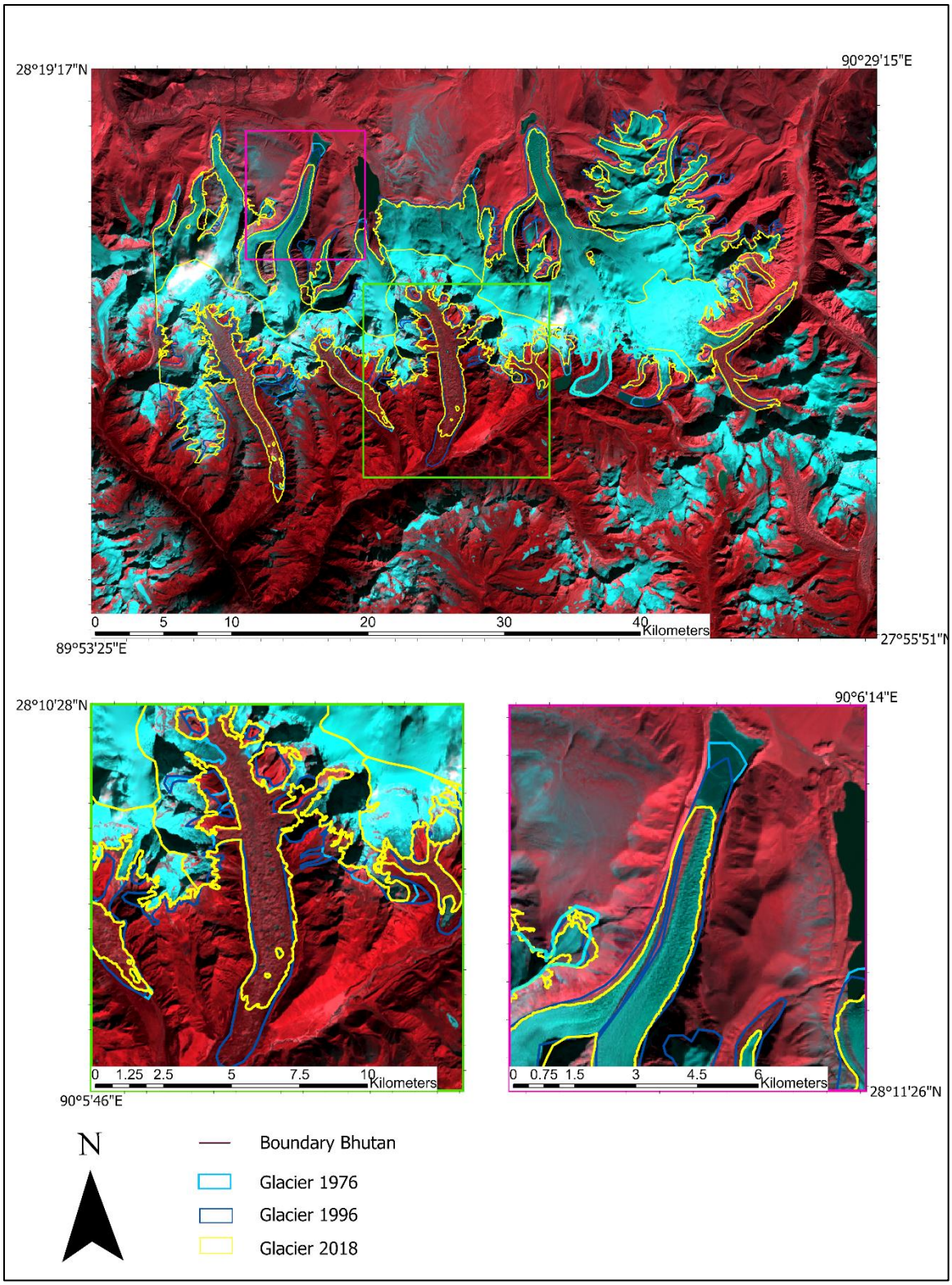

Fig. 5.1: **(A)** Shows the glacial area change of the Lunana glacier system from 1996 to 2018. The OBIA classification is marked with a yellow polyline indicator and the visual classification based on a Landsat 5 dataset from 30.11.1996. **(B)** A close-up image of glacier G090157E28136N, a glacier compiled of both debris-covered glacier and clean ice from the southern parts of the Lunana glacier system. **(C)** Close-up image of the Shimo glacier located in the northern parts of the Lunana glacier system. Background image: False color composite Landsat 8 (13.12.2018).

5.2 Glacial lake area change

Luggye Tsho- and Raphstreng Tsho lake was both rated as potential dangerous glacial lakes given their physical state today and the past outburst event. The result for Luggye Tsho glacial lake shows a gradient growth in area, where the lake increased from 0.9 km^2 in 1994 to 1.47 km^2 in 2018. **Fig. 5.2** displays this gradient growth in area and shows the overall change of the Luggye Tsho lake from 1994 post GLOF event and in 2017, which is closer to today. The graph in the figure plots all of the recorded data of the pixel-based image classification (PBIA) of the two pro glacial lakes. The graph shows an immediate reduction in area of the Luggye Tsho lake, from 1993 to 1994, where the area changes from 1.12 km^2 to 0.92 km^2. From there, Luggye Tsho has been classified to have a general increase in area up to 1.27 km^2 in 2005, before it drops to 1.07 km^2 in 2007 and after the area grows to 1.47 km^2 in 2017 and drops to 1.40 km^2 in 2018.

The outburst of Luggye Tsho in 1994 left a trace from the water streaming down towards Pho Chhu river and following the flowline further south, these traces are possible to see in **Fig. 5.3**, where a polygon has been manually generated to highlight these traces. In the figure there are also indications of an outlet zone as a result of the event. After the event in 1994 the Lugge Tsho lake increased in area, and today it is about 0.5 km^2 bigger than what it was before the GLOF event.

The Rampstreng Tsho lake has, according to **Fig. 5.2**, had almost no increase in lake area from this time period. While Luggye Tsho glacial lake decreased in size from 1993 to 1994, Raphstreng Tsho lake increased in area from 1.27 km^2 to 1.31 km^2. Raphstreng Tsho did however have a drop in area from 2005 to 2007 where it decreased from 1.12 km^2 to 1.07 km^2, this decrease corresponds with the same decrease in lake area that was classified for the Luggye Tsho glacial lake. After 2007 Raphstreng Tsho had a small increase before it stagnated around 1.3 km^2 in 2017/2018.

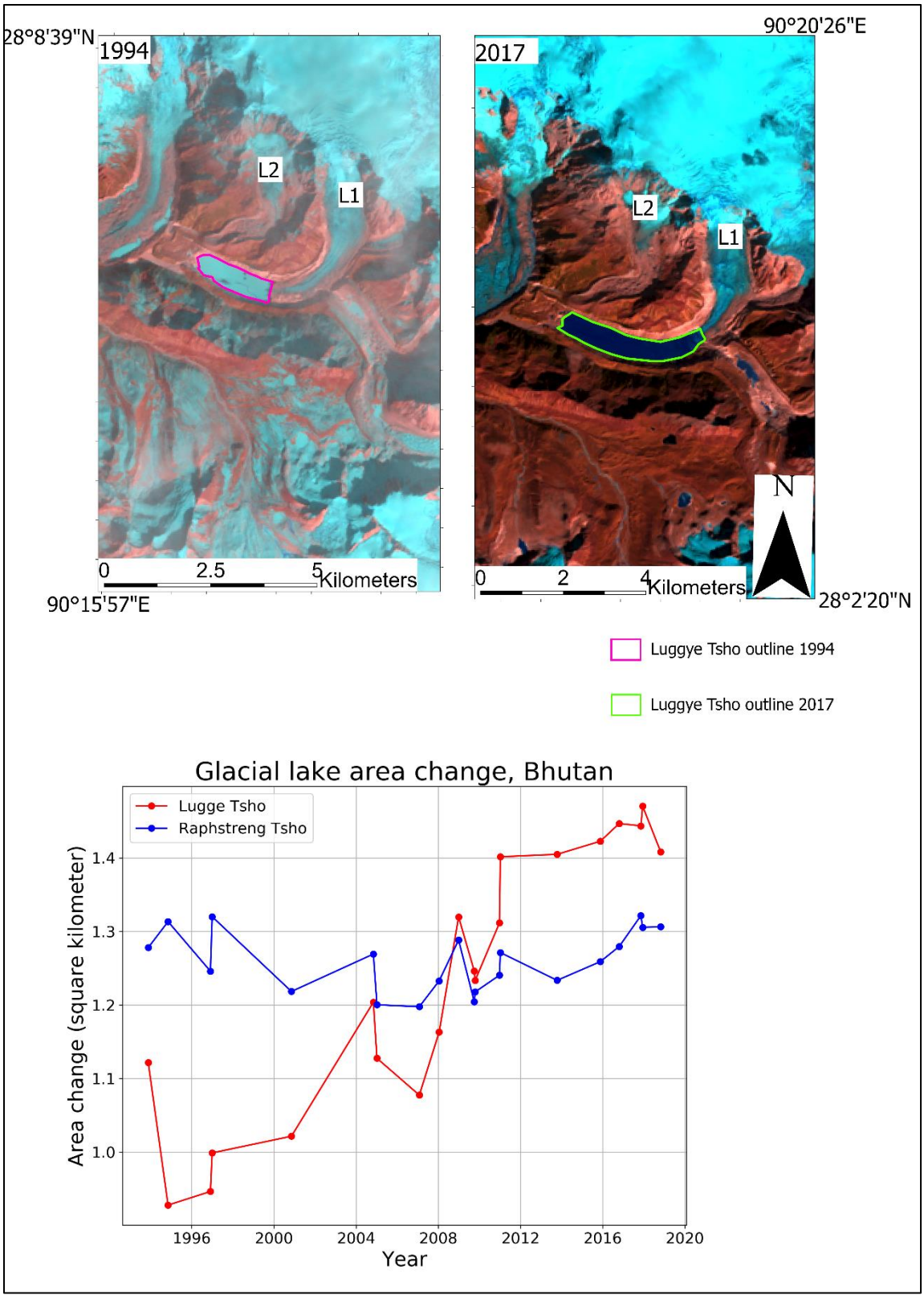

Fig. 5.2: Shows the change in area for the Luggye Tsho proglacial lake between 1994 and 2017, while including the location of Luggye glacier- 1 (L1) and 2 (L2) . Both images are displayed with a respective glacial lake outline that was generated through the PBIA classification of Raphstreng Tsho and Lugge Tsho lake. It displays a graph showing the area change (km^2) of both Raphstreng Tsho- and Luggye tsho lake, from 1993 until 2018. Background image: false colour composite Landsat 5 (27.12.1994 & 26.12.2017).

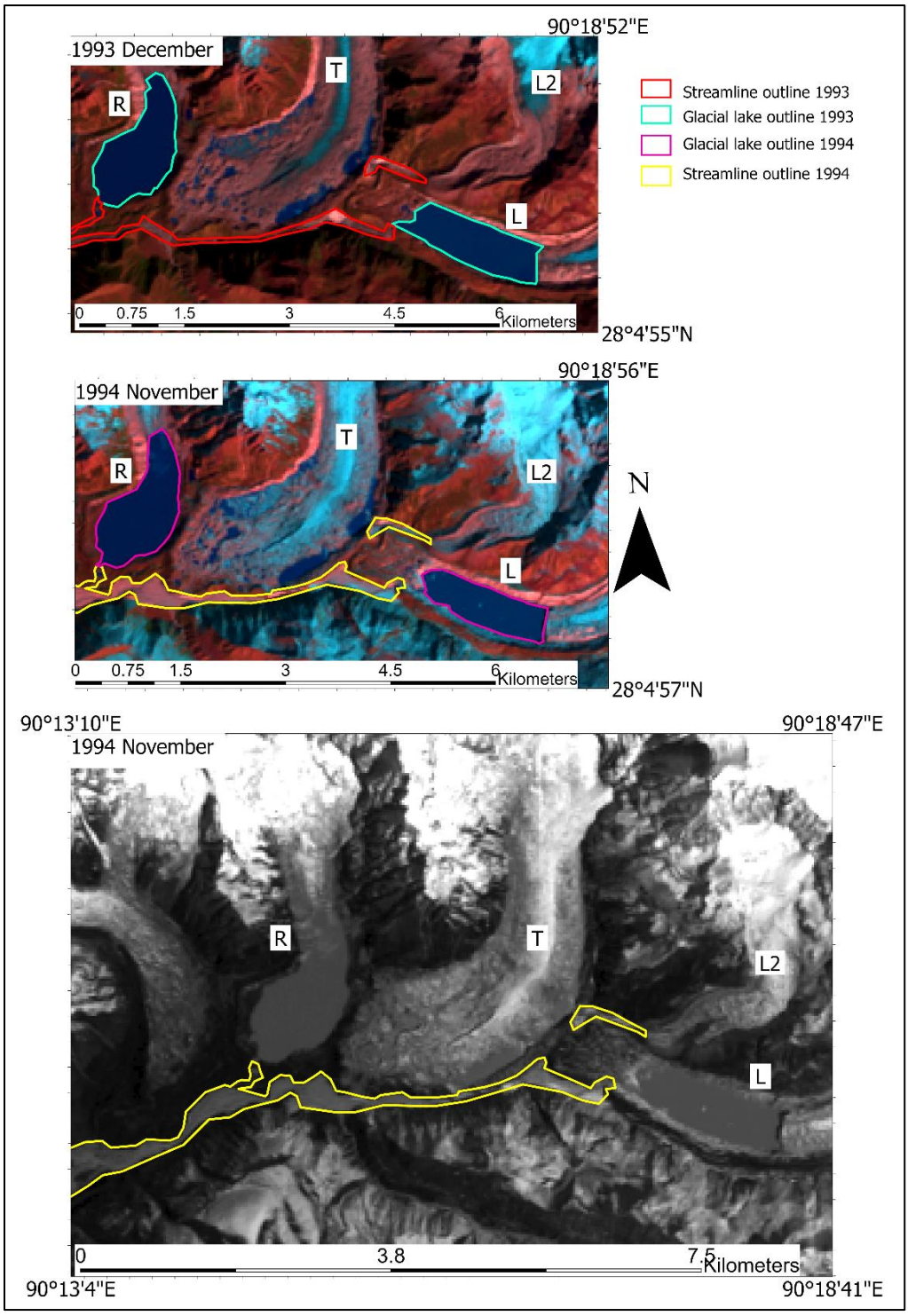

Fig. 5.3: Displaying the state of Luggye Tsho (L)- and Raphstreng Tsho (R) glacial lake, pre- and post Luggye Tsho GLOF event in October 1994. It also displayes to location of Thorthormi glacier (T) where one can clearly see a abundance of supraglacial lakes. The figure highlights a manual delineation of the flowline to Pho Chhu river both before and after the event as well as the outlet channel for the two glacial lakes and Luggye glacier 2 (L2). The last image is he green band of the Landsat 5 1994 November image displayed right above; it easily shows the missing debris from the flowline as the soil is fresher contra the stable ground around it. Background image: false color composite Landsat 5 (December 1993 & November 1994) and green band Landsat 5 (November 1994).

5.3 Glacier mass balance- and surface elevation change

The mean geodetic mass balance change and the mean surface elevation change was divided and the result are presented for some individual glaciers (**Table 5.4** & **5.5**) and the glacier changes for all of the glaciers are calculated as a mean change value in **Table 5.3**. The individual glaciers are divided in cardinal directions, north and south, separated by the Bhutan border in the Lunana glacier system. The northern parts are mostly dominant of clean ice sections and the southern parts are dominated by glacier tongues covered with debris. Seven of (225 km^2) the glaciers were covered by Pléiades- and SPOT imagery from 2018/9, while the SRTM and HEXAGON DEM covered the whole Lunana glacier system. This means that the calculation of geodetic mass balance and surface elevation changes between 2000-2018/9 and the total calculation between 1976-2018/9 are limited to the stereo data outlines and will affect the results and the discussion of this study. All an all, the Lunana glacier system has had a decrease in both mass balance (m w.e. a^{-1}) and in surface elevation (m a^{-1}). Between 1976 and 2018/9 the Lunana glacier system had a mean reduction in surface elevation of 0.48 ± 0.08 m a^{-1}. This was divided up between two time periods: from 1976 until 2000 the glacier system had a mean reduction in surface elevation of 0.79 ± 0.0075 m a^{-1}, which calculates to a total mean value of 19 ± 0.18 m, and from 2000 until 2019 where the mean reduction in surface elevation was 0.24 ± 0.15 m, which calculates to a total mean value of 4.6 ± 2.9 m. The mean mass balance shows the same type of gradient as the surface elevation change. Between 1976 and 2000 the glacier system had a mean reduction in mass balance of about 0.67 ± 0.0081 m w.e. a^{-1}, which calculates to a total mean value of about 16.1 ± 0.2 m w.e. This mass balance reduction where smaller between 2000 and 2019, where the mean mass balance where measured to be 0.2 ± 0.13 m w.e. a^{-1}, which calculates to a total mean reduction of about 3.8 ± 2.5 m w.e. In total the mean mass balance where processed between 1976 and 2018/9 and calculated to be a reduction of 0.41 ± 0.068 m w.e. a^{-1}. The nine individual glaciers from **Fig. 1.1**, and their mass balance change values can be seen in **Table 5.5**, as well as their surface elevation change values in **Table 5.4**. Both Bechung glacier and glacier G090157E28136N where located outside the range of the Pléiades and SPOT data and has therefore no mass balance- nor surface elevation change value after 2000.

5.3.1 Glacier mass balance- and surface elevation change - Northern glaciers

In the north the two glaciers, Lianggang- and Zeng glacier, both experienced a great loss in mass balance and surface elevation (**Fig. 5.4**). The Lianggang glacier had a 0.97 ± 0.06 m w.e. a^{-1} mass balance reduction and a 1.14 ± 0.08 m a^{-1} surface elevation loss of between 1976 and 2019, calculated to a total of 49 ± 3.4 m surface elevation reduction. Based on **Fig. 5.5**, the surface elevation change is considerably larger between 2000-2019 then 1976-2000. The glacier was partly made of debris covered glacier at the tongue and clean ice near the mid region of the glacier. The Zeng glacier had a 1.17 ± 0.06 m w.e. a^{-1} mass balance reduction and a 1.37 ± 0.08 m a^{-1} surface elevation loss between 1976 and 2019, calculated to a total loss of 58.9 ± 3.4 m in surface elevation, and the glacier was solely consisting of clean ice.

5.3.2 Glacier mass balance- and surface elevation change - Southern glaciers

In the south the glaciers, Luggye glacier 1 and 2, both experienced great loss in surface elevation as well as great reduction in mass balance (see **Table 5.4** & **5.5**). Both of these glaciers are connected to the Luggye Tsho glacial lake, however Luggye glacier 1 is the glacier that is terminating directly into Luggye Tsho lake. From 1976 to 2019 Luggye glacier 1 had a 1.01 ± 0.069 m w.e. a^{-1} reduction in mass balance and a 1.19 ± 0.07 m a^{-1}, calculating to a total loss value of 51.2 ± 3.0 m in surface elevation. During the same period, Luggye glacier 2 experienced a 0.89 ± 0.06 m w.e. a^{-1} reduction in mass balance and a 1.04 ± 0.07 m a^{-1} in surface elevation, calculating to a total loss value of 44.7 ± 3.0 m in surface elevation. Other southern glaciers such as the Raphstreng glacier, terminating directly in Raphstreng glacial lake, did also experience loss in mass balance and surface elevation between 1976 and 2019, but was the only glacier that had an increase in both surface elevation and mass balance between 1976 and 1996. Raphstreng glacier had a 0.33 ± 0.0081 m w.e. a^{-1} increase in mass balance and a 0.39 ± 0.0088 m a^{-1} increase in surface elevation, calculating to a total increase value of 7.8 ± 0.18 m in surface elevation. Between 1996 and 2019 the same glacier had a 0.52 ± 0.1 m w.e. a^{-1} reduction in mass balance and a 0.62 ± 0.11 m a^{-1} loss in surface elevation, calculating to a total loss value of 14.3 ± 2.5 m in surface elevation. As a result, between 1976 and 2019 Raphstreng glacier had a 0.21 ± 0.06 m w.e. a^{-1} reduction in mass balance and a 0.28 ± 0.07 m a^{-1} loss in surface elevation.

Table 5.3: Mean glacier mass balance- and surface elevation changes on the Lunana glacier system between 1976 and 2019.

Timeline	Mean mass balance (m w.e. a^{-1})	Mean surface elevation change (m a^{-1})
1976-2000	-0.67 ± 0.0081	-0.79 ± 0.0075
2000-2019	-0.2 ± 0.13	-0.24 ± 0.15
1976-2019	-0.41 ± 0.068	-0.48 ± 0.08

Table 5.4: Surface elevation (m a^{-1}) changes divided into individual glaciers located in the Lunana glacier system, between 1976 and 2018/9.

Glacier name	Glacier id	1976-2000 (m a^{-1})	2000-2018/9 (m a^{-1})	1976-2018/9 (m a^{-1})
Lianggang Glacier (North)	G090383E28118N	-0.8 ± 0.0093	-0.14 ± 0.15	-1.14 ± 0.08
Luggye Glacier 1 (South)	G090326E28109N	-0.52 ± 0.0088	-0.695 ± 0.2	-1.19 ± 0.07
Luggye Glacier 2 (South)	G090305E28114N	-0.23 ± 0.0083	-0.82 ± 0.15	-1.04 ± 0.07
Raphstreng Glacier (South)	G090246E28129N	0.39 ± 0.0088	-0.62 ± 0.11	-0.28 ± 0.07
Bechung Glacier (South)	G090217E28130N	-1.38 ± 0.0088	-	-
Shimo glacier (North)	G090045E28198N	-1.42 ± 0.0090	-	-
Zeng glacier (North)	G090273E28197N	-1.06 ± 0.0094	-0.33 ± 0.12	-1.37 ± 0.08
None (South)	G090157E28136N	-0.73 ± 0.0091	-0.004 ± 0.1	-0.69 ± 0.12
Thorthormi glacier (South)	G090278E28132N	0.23 ± 0.0087	-0.43 ± 0.18	-0.59 ± 0.07

Table 5.5: Glacier mass balance (m w.e. a^{-1}) changes divided into individual glaciers located in the Lunana glacier system, between 1976 and 2018/9.

Glacier name	Glacier id	1976-2000 (m w.e. a^{-1})	2000-2018/9 (m w.e. a^{-1})	1976-2018/9 (m w.e. a^{-1})
Lianggang Glacier (North)	G090383E28118N	-0.67 ± 0.0081	-0.12 ± 0.17	-0.97 ± 0.06
Luggye Glacier 1 (South)	G090326E28109N	-0.45 ± 0.0081	-0.65 ± 0.2	-1.01 ± 0.069
Luggye Glacier 2 (South)	G090305E28114N	-0.12 ± 0.0081	-0.74 ± 0.17	-0.89 ± 0.06
Raphstreng Glacier (South)	G090246E28129N	0.33 ± 0.0081	-0.52 ± 0.1	-0.21 ± 0.06
Bechung Glacier (South)	G090217E28130N	-1.17 ± 0.0081	-	-
Shimo glacier (North)	G090045E28198N	-1.22 ± 0.0081	-	-
Zeng glacier (North)	G090273E28197N	-0.9 ± 0.0081	-0.28 ± 0.1	-1.17 ± 0.06
None (South)	G090157E28136N	-0.62 ± 0.0081	-0.003 ± 0.09	-0.65 ± 0.04
Thorthormi glacier (South)	G090278E28132N	0.19 ± 0.0081	-0.37 ± 0.15	-0.5 ± 0.06

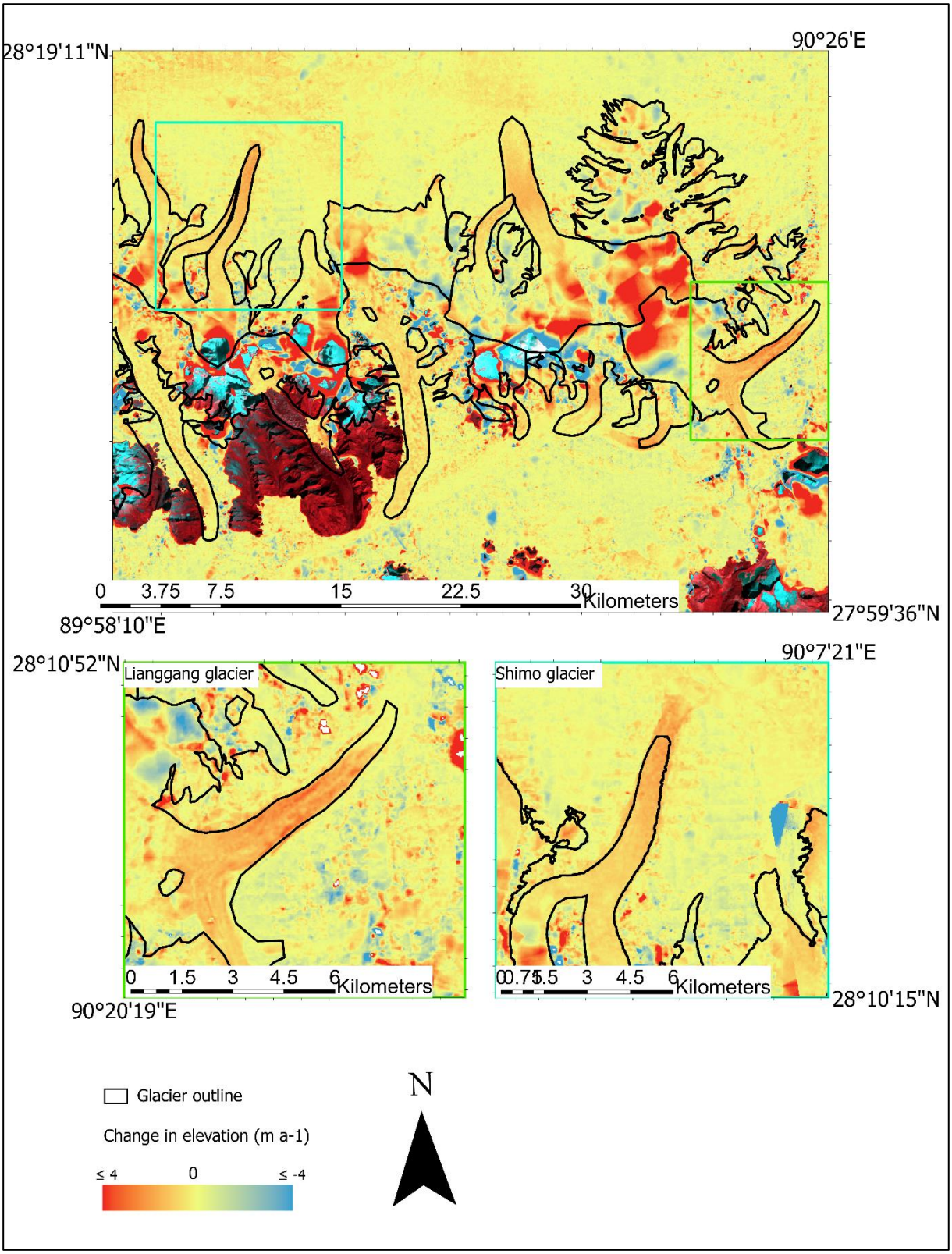

Fig. 5.4: Change in surface elevation change in the Lunana region between 1976 and 2000. Two individual images show the difference between the surface elevation change on clean ice (right), Shimo glacier, and the surface elevation change on debris-covered glacier (left), Lianggang glacier. The noise visible in the figure comes most likely from bad elevation points from the Hexagon DEM.

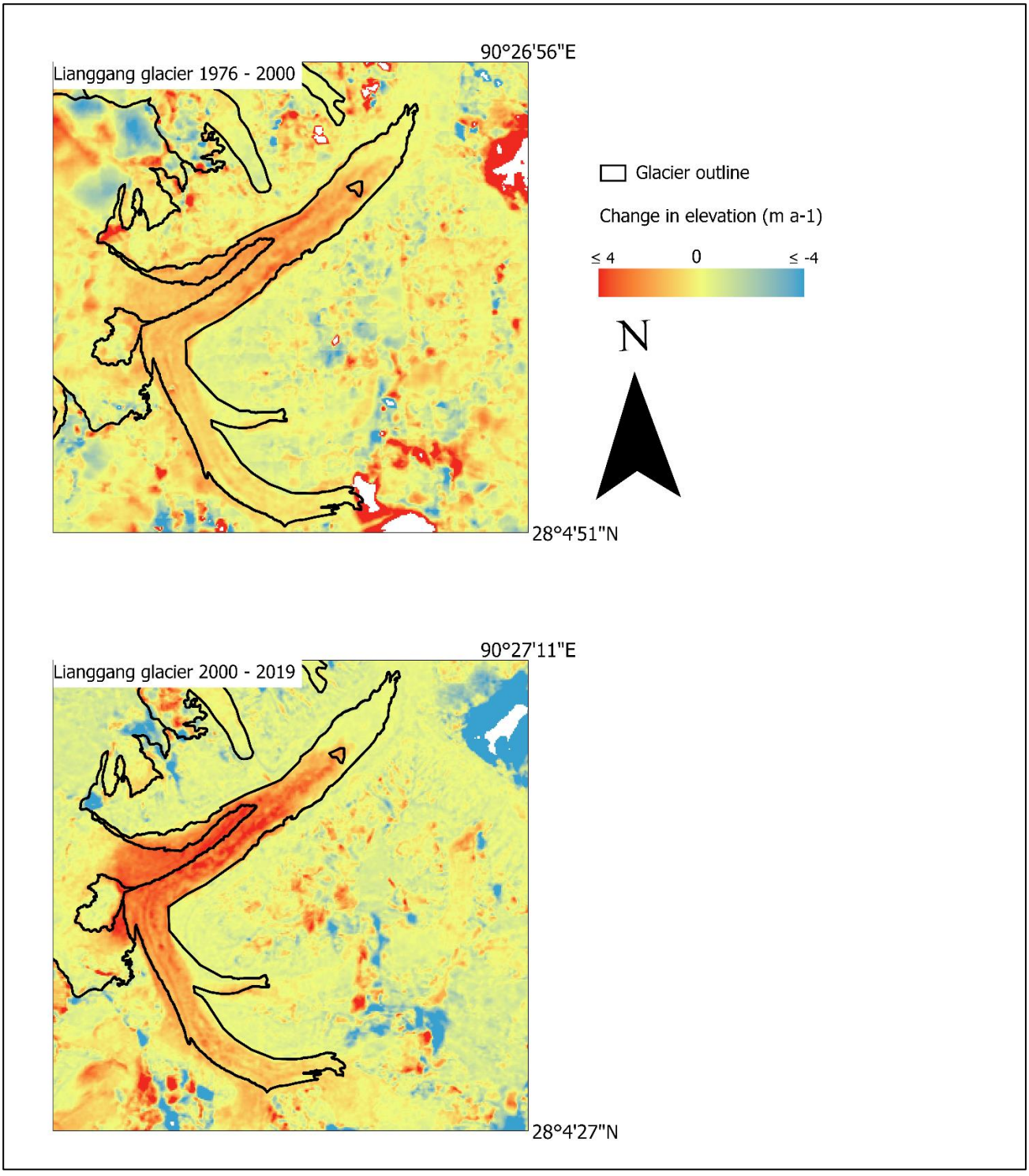

Fig. 5.5: Change in surface elevation for the Lianggang glacier. The two images display how the surface elevation change has evolved from 1976-2000 to 2000-2019. There is a clear indication that the surface elevation change is higher between 2000-2019 then 1976-2000.

5.4 Glacier velocity

The glacier velocity over the Lunana glacier system was divided up between the nine glaciers (**Fig. 1.1**). These glaciers have been calculated individual mean glacier velocity, displayed in both velocity per day (m d^{-1}) and velocity per year (m d^{-1}). The velocity per year was calculated from the velocity per day value that was generated from the offset tracking tool. The glacier velocity is divided up between the respective region, north and south, of the Lunana glacier system.

5.4.1 Glacier velocity – Northern glaciers

The highest achieved glacier velocity in 2016 is both located in the north and south region of Lunana, Lianggang glacier and Luggye glacier 1. The Lianggang glacier had a mean glacier velocity of 0.013 ± 0.002 m d^{-1} calculated to be about 4.75 ± 0.73 m a^{-1}. However, the Lianggang glacier was not completely covered by the TerraSAR – X data, and the velocity data was therefore partly generated (**Fig. 5.6**). The velocity over Lianggang glacier is measured mostly over the clean ice parts and covers almost no part of debris covered tongue. This result is therefore to be partly weighted later in the discussion. The Zeng glacier had a mean glacier velocity of 0.012 ± 0.002 m d^{-1} calculated to be about 4.4 ± 0.73 m a^{-1}. Based on **Fig. 5.6** the majority of the Zeng glacier velocity is allocated in the mid region of the glacier and weakens further down the tongue.

5.4.2 Glacier velocity – Southern glaciers

As said in the last paragraph, Luggye glacier 1 was one of the glaciers calculated to have had the largest glacier velocity in 2016. Luggye glacier 1 had a mean glacier velocity of 0.013 ± 0.002 m d^{-1}calculated to be 4.75 ± 0.73 m a^{-1}. Luggye glacier 1 is connected to Luggye glacier 2 which had a mean glacier velocity of 0.006 ± 0.002 m d^{-1}, which calculates to a velocity of 2.2 ± 0.73 m a^{-1}. In comparison this is less than half the speed of Luggye glacier 1. The Raphstreng glacier had a mean glacier velocity of 0.010 ± 0.002 m d^{-1}, which calculates to a velocity of 3.65 ± 0.73 m a^{-1}. According to **Fig. 5.6** the Raphstreng glacier as well as Luggye glacier 1 showed similar placement of the glacier's velocity as the Zeng glacier, where most of the velocity was located in mid part region of the glaciers. The Thorthormi glacier had a mean glacier velocity of 0.009 ± 0.002 m d^{-1}, which calculates to a velocity of 3.29 ± 0.73 m a^{-1}. This glacier had most of its velocity allocated in the top region of the glacier, while the results show some parts of it moving down in the mid and bottom region (**Fig. 5.6**). Glacier G090045E28198N had a mean glacier velocity of 0.007 ± 0.002 m d^{-1}, which calculates to a velocity of 2.56 ± 0.73 m a^{-1}. G090045E28198N was corresponding of part debris covered ice and clean ice, where the majority of the velocity was located in clean ice region of the glacier (**Fig. 5.6**). The result shows some movement in the debris covered region, but most of the glacier is stagnant in this region.

Table 5.6: Mean glacier velocity of the nine glaciers located in the Lunana glacier system, measured based on data from 2016. The glaciers velocities are displayed in both meter per day (m d^{-1}) and meter per year (m a^{-1}).

Glacier name	**Glacier id**	**Mean glacier velocity (m d^{-1})**	**Mean glacier velocity (m a^{-1})**
Lianggang Glacier (North)	G090383E28118N	0.013 ± 0.002	4.75 ± 0.73
Luggye Glacier 1 (South)	G090326E28109N	0.013 ± 0.002	4.75 ± 0.73
Luggye Glacier 2 (South)	G090305E28114N	0.006 ± 0.002	2.2 ± 0.73
Raphstreng Glacier (South)	G090246E28129N	0.010 ± 0.002	3.65 ± 0.73
Bechung Glacier (South)	G090217E28130N	0.005 ± 0.002	1.83 ± 0.73
Shimo glacier (North)	G090045E28198N	0.006 ± 0.002	2.2 ± 0.73
Zeng glacier (North)	G090273E28197N	0.012 ± 0.002	4.4 ± 0.73
None (South)	G090157E28136N	0.007 ± 0.002	2.56 ± 0.73
Thorthormi glacier (South)	G090278E28132N	0.009 ± 0.002	3.29 ± 0.73

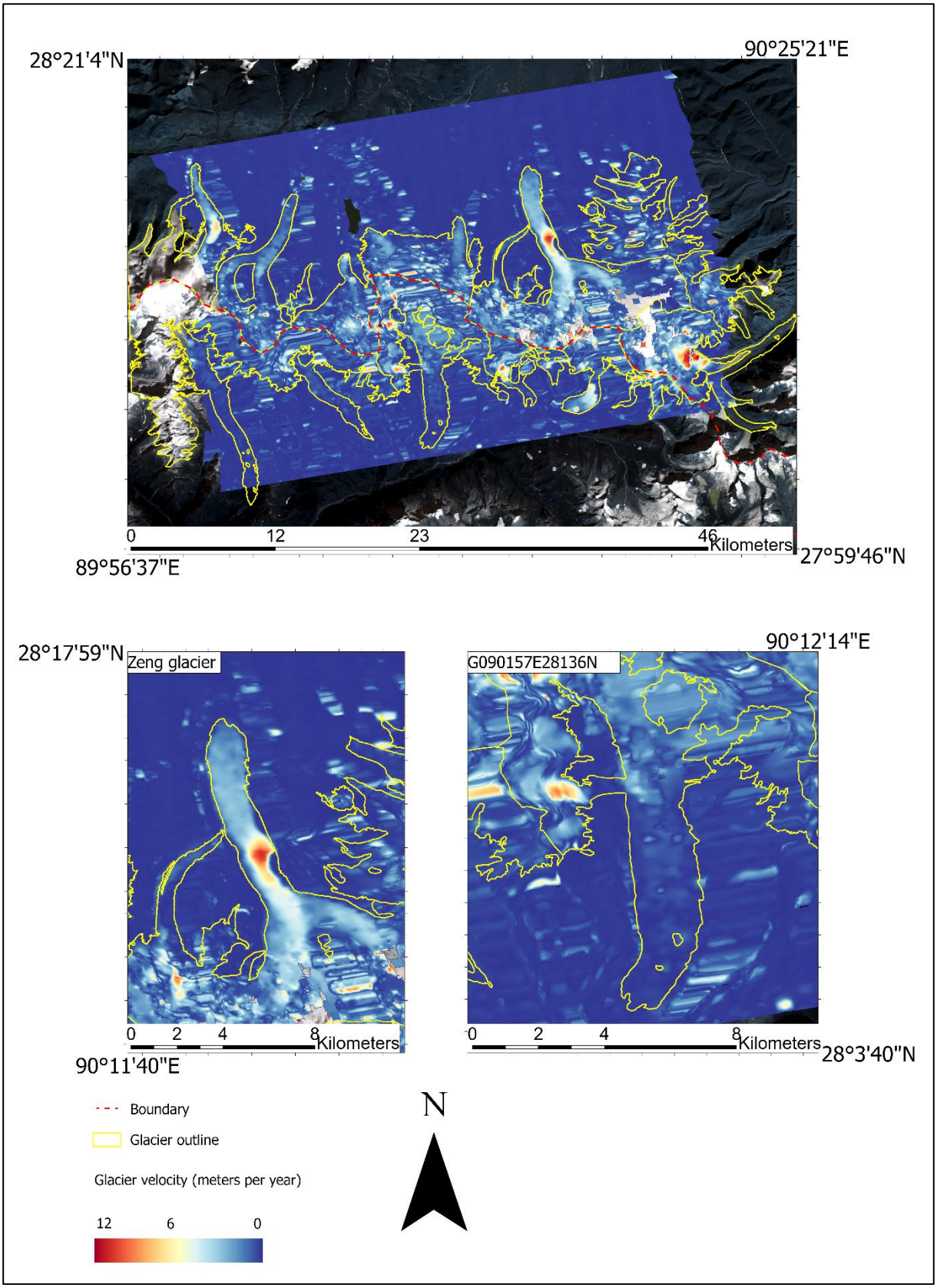

Fig. 5.6: Displaying the velocity changes over the Lunana glacier system by the outline of the TerraSAR-X data. The values are displayed as meters per day and the glacier outline was limited due to the TerraSAR-X outline. Background image Landsat 8 true color composite (13. Dec.2018).

Chapter 6: Discussion

In this chapter the presented result of the glacier changes of the Lunana glacier system and the evolution of the Luggye Tsho and Raphstreng Tsho glacial lakes will be discussed. The main objectives for the glacial lakes are to summarize their evolution and investigate their physical state as of today and discuss what sort of risk they possess as being labeled potential dangerous glacial lakes. The chapter will also include a discussion on how the surface melt are displayed on debris-covered glacier parts as oppose to on clean ice, and how the debris covers effect the glacier flow of the glacier. Discuss the compatibility between the glacier flow and the glacier mass loss, and as a last subject, discuss the importance of using coherence data when one is classifying debris-covered glaciers.

6.1 Evolution of Luggye Tsho glacial lake and the Luggye glaciers

Given the past event of the outburst of Luggye Tsho glacial lake in October 1994, the glacial lake has been labeled as a potential dangerous glacial lake and should be monitored with the caution. In November 1993, 11 months before the time of the GLOF event, Luggye Tsho was classified with a 1.12 km^2 area. After the event, the area reduced to 0.92 km^2 which was classified about a month after the event. The theory is therefore that minimum 0.2 km^2 area of the Luggye Tsho glacial lake where the main discharge that caused the outbreak of Tshopdak Tsho, leading to initiation of the 1994 GLOF event. Fountain, et al. (2000: p. 169) mentioned in the workshop that the western end of the Luggye Tsho glacial lake recede by about 500 m because of the GLOF event, and this statement corresponds with **Fig. 5.2** in this study which showcases the area change of Luggye Tsho between 1993 and 1994.

In 2018 Luggye Tsho stands at a size of 1.41 km^2, which is 29 km^2 greater than before it outburst in 1994, and it can therefore cause more harm and damage if it were to outburst at its current state. Fountain, et al. (2000: p. 169) raised the awareness that if the outlet zone to Luggye Tsho where to be blocked in the future a rise of water level would increase the risk of another GLOF event happening. The blockage could be caused by such events as: a landslide originating just above the inner lateral moraine of Luggye Tsho, or a large-scale failure of the damn caused by melting of the ice core within the lateral moraine (Fountain, et al. 2000: pp. 169). Where the last event is similar to what happened originally during the 1994 GLOF event. The outlet zone was expanded as a result of the 1994 GLOF event and is easily recognized on the Landsat image taken just before and after the event in **Fig. 5.3**. Based on observations from these Landsat 8 images, the SPOT image taken in December 2018 and the

Pléiades images taken in November 2019, the outlet zone seems presumably just as expanded as it was after the GLOF event. There is no newer study of the state of Luggye Tsho's outlet zone after Fountain, et al. (2000), and therefore no newer field study can confirm the state of Luggye Tsho outlet zone after 1994.

The Luggye glacier 1 & 2 are both connected to Luggye Tsho glacial lake and has been since the appearance of Luggye Tsho in the 1980s (Fountain, et al. 2000: p. 169). These two glaciers have since 1976 reduced in size by a total of 4.66 km^2, both experiencing greater loss after 2000. Luggye glacier 1 went from an area of 7.56 km^2 in 1976 to an area of 4.41 km^2 in 2018, almost halving in size, and had a mass balance change of 1.01 ± 0.069 m w.e. a^{-1} between the same time frame. The glacier changes correspond to the change in physical state of Luggye Tsho. As the proglacial lake increased in size from the GLOF event in 1994 until 2018, Luggye glacier 1 had a frontal retreat of 1.2 km and a 41.7% area reduction during the same time-period. At the same time, Luggye glacier 1 experienced increase reduction in size and mass balance after the 2000. This corresponds with increase in area of Luggye Tsho after 1994. The frontal retreat of Luggye glacier 1 after 2000 and the area reduction of 41.7% could indicate an increase in production of meltwater. The glacier was calculated to have an average velocity of 4.75 ± 0.73 m a^{-1}, making it a highly active glacier. The Luggye glacier 1 is classified of consisting of both debris-covered ice parts and debris-free ice parts, and according to **Fig. 6.1** there is a clear difference between the two parts regarding surface melt and glacier flow. The surface melt over the bottom part tongue region of Luggye glacier 1 is considerably larger (0.5 m a^{-1}) over the clean ice parts, than the debris-covered parts, and at the mid part the parts seems to uniformly reduce in surface melt. However, close to the bottom of the tongue where the glacier is terminating in Luggye Tsho, the surface melt is actually larger over the debris-covered part. This could indicate that debris-covered is mostly absent at the bottom of the glacier tongue creating a relative thin cover of debris over the glacier. The surface melt difference between debris-covered and clean ice will be discussed and elaborated more, later in this chapter. The glacier velocity over Luggye glacier 1 seems to be acting opposite to how the surface melt is, meaning that if there is an increase in surface melt than there is a reduction in glacier velocity. The velocity is increasing at a higher elevation as oppose to the surface melt which decreases at the same elevation, and this is due to state of equilibrium that the glacier is maintaining. The glacier flow concept balances the inputs and outputs by transferring ice from the accumulation zone (higher elevation) to the ablation zone (lower elevation), called balance velocity (Benn and Evans 2013). The glacier

flow is controlled by the surface melt rate, and therefore the higher the surface melts the faster the mass turnover rate (glacier movement) (Benn and Evans 2013; Chandler and Evans 2019). Also, the glacier velocity acts differently regarding if it is over debris-covered or clean ice. The glacier velocity is considerably high over the mid part region of the clean ice, and considerably low over the debris-covered parts with the same elevation (see chapter 6.4.2.

Between 2000-2018, Luggye Tsho had a lake area increase of 28% (according to the graph at **Fig. 5.2**) and the runoff from Luggye glacier 1 seems to be flowing directly into Luggye Tsho, as the glacier is terminating directly into the glacial lake (**Fig. 5.2**). The meltwater should therefore be an input source to Luggye Tsho, and therefore, an increase in meltwater production could lead to an increase in glacial lake area. This seems a little different for Luggye glacier 2. Based on observing Landsat 5 & 8 (**Fig. 5.2**), SPOT and Pléiades images of Luggye glacier 2, its outlet channel does not seem to connect to Luggye Tsho but seems to outlet down towards Thorthormi glacier. It then may work as an input source for the supraglacial lakes located on the southern parts of the tongue of Thorthormi glacier. According to the results, Luggye glacier 2 reduced in area from 2.46 km^2 in 1976 to 1.35 km^2 in 2018, with a 0.89 ± 0.06 m w.e. a^{-1} reduction in mass balance. While Luggye glacier 2 did have a considerable amount of glacier loss during the total time period, it was calculated to have an average velocity of 2.2 ± 0.73 m a^{-1} which is only half as fast as Luggye glacier 1. Glacier tongue of Luggye glacier 2 is classified to contain large amount of debris-covered parts, and the glacier tongue of Luggye glacier 1 is only partly covered with debris, which could be an indication to why the velocity over Luggye glacier 2 is considerably slower than Luggye glacier 1.

According to **Fig. 5.3** there is a clear visual that there are several supraglacial lakes located on the top of the tongue of Thorthormi glacier. However, this study does not take account for the formation nor the classification of these supraglacial lakes located on Thorthormi glacier and this paper can therefore not discuss if there are or seems to be any correlation between the reduction of Luggye glacier 2 and the formation of supraglacial lakes on Thorthormi glacier. If Luggye Tsho glacial lake where to outburst again by a blockage of the outlet channel today, the glacial lake area would be around 1.42 km^2 of water with a depth ranging from 60-100 meters (Ahmed, et al. 2020).

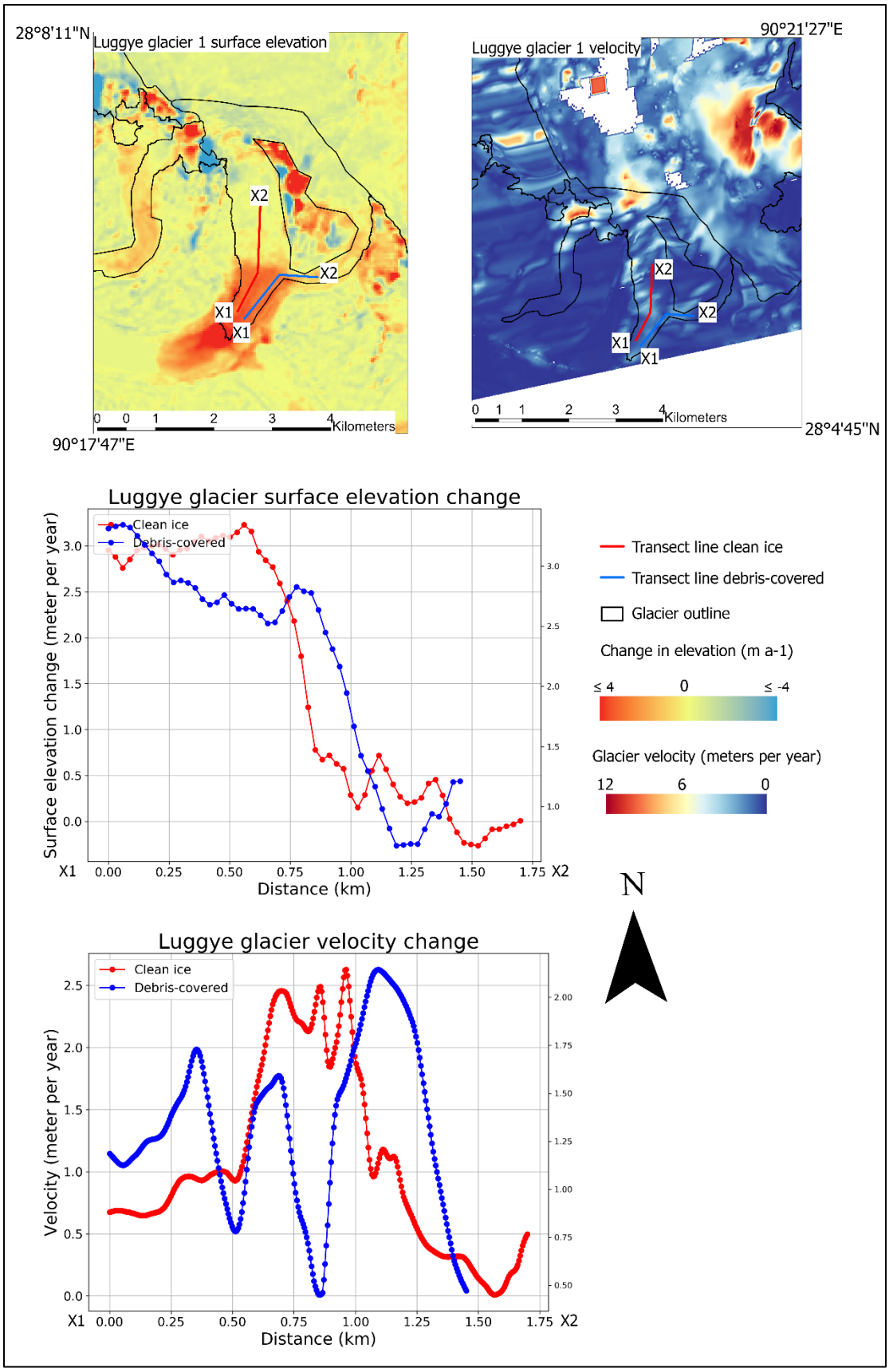

Fig. 6.1: Surface elevation change and glacier velocity measured over Luggye glacier 1. The two transect lines is divided between clean ice (red) and debris-covered ice (blue).

6.2 Evolution of Raphstreng Tsho and Raphstreng glacier

Based on previous research there has been no trace that Raphstreng Tsho glacial lake has ever been part of a GLOF event before its appearance in the 1980s (Fountain, et al. 2000: pp. 171). The lakes condition is based on the result of this study, very stagnant. The timeseries in **Fig. 5.2** shows that Raphstreng Tsho has been maintaining its same state from 1993 until 2018, increasing by only 0.03 km^2 in area. The fluctuation in water area that is visible in the timeseries is most likely caused by drop in water level as water seeps out of a small outlet channel, that is located on southern part of the glacial lake. The outlet channel is not so easily visible on the low-resolution Landsat 5 & 8 images but can be seen in the higher resolution Pléiades image from 2019. The Raphstreng Tsho moraine dam where fixed due to the structural mitigation done by *The Raphstreng Tsho Outburst Flood Mitigation Project*, which lowered the risk of Raphstreng Tsho outbursting quite gradually. It has been reported by several studies that the Raphstreng Tsho glacial lake does not pose any GLOF threat on its own. However, given its large volume consisting with an area of 1.3 km^2 and an average depth of 100 meters (Fountain, et al. 2000: p. 169) and its location being just 80 meter below Thorthormi glacier which is separated by an unstable 32 meter, at its thinnest, high ice-core moraine, one cannot overlook that Raphstreng Tsho could outburst in the future if the supraglacial lakes on Thorthormi glacier where to outburst first (Singh 2009).

Based on the result the Raphstreng glacier had a glacier reduction of 0.9 km^2 in area as well as 0.21 ± 0.06 m w.e. a^{-1} reduction in mass balance between 1976 and 2018. The glacier is terminating directly in Raphstreng Tsho and therefore works as an input source for the proglacial lake. Observing the different Landsat 5 & 8 images (**Fig. 5.3**) as well as the Pléiades data from 2019 and the SPOT data from 2018 there seems to be no other glacier input sources for the expansion of Raphstreng Tsho. Between 1976 and 1996 the glacier area reduced by 0.65 km^2, which was about three times as much as it did between 1996 and 2018 where the glacier reduced by mere 0.25 km^2. Which is a quite opposite behavior than for e.g. Luggye glacier 1, which according to the result reduced gradually more between 1996 and 2018 than it did between 1976 and 1996. The surface melt over Raphstreng glacier is mostly oriented around the bottom part of the glacier tongue, much like Luggye glacier 1 (**Fig. 6.2**). This is opposite for the velocity as the glacier flow is highest around the mid/top part of the glacier tongue (Fig. 6.2). This again proof of balance velocity, where the glacier is trying to maintain a state of equilibrium.

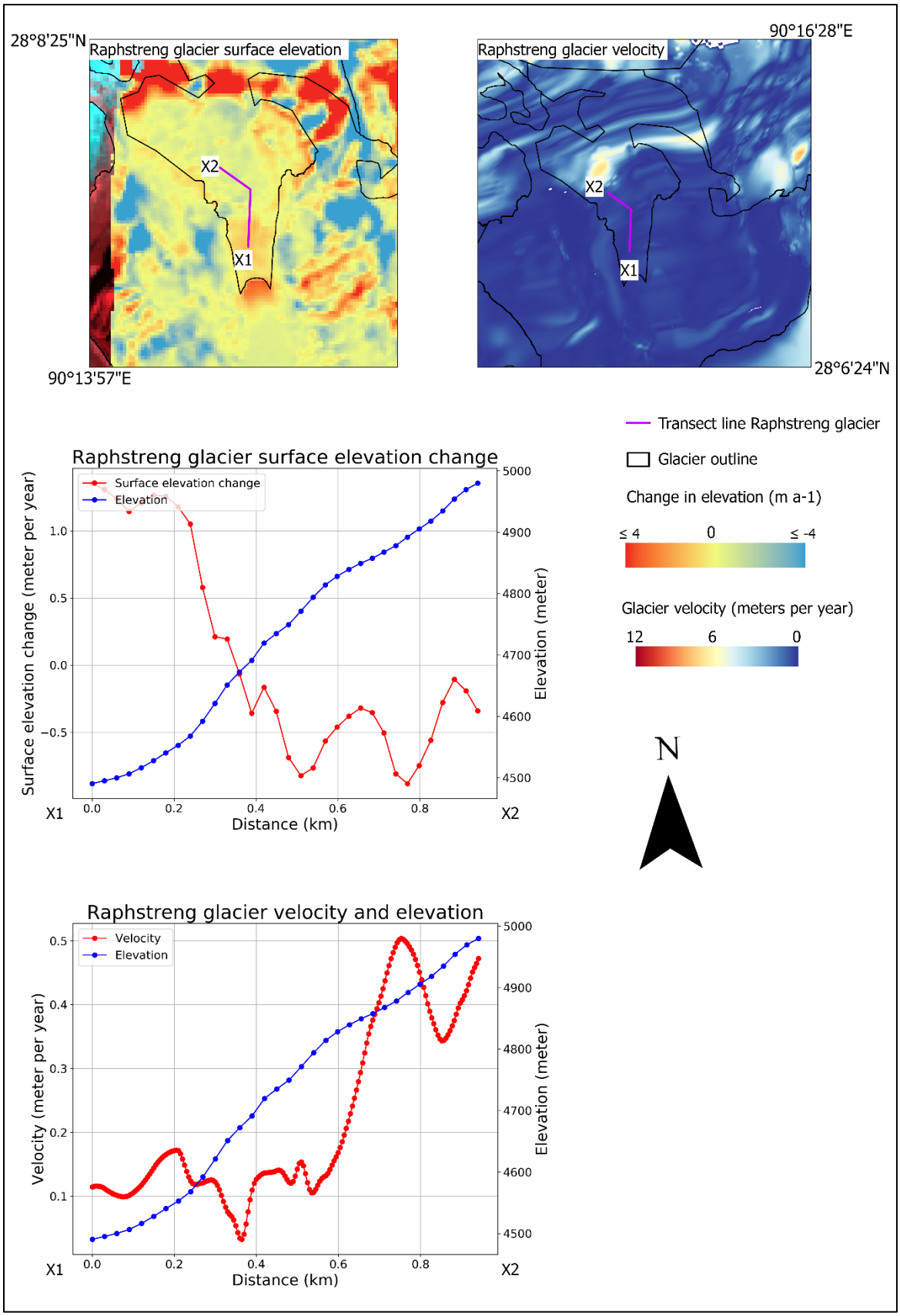

Fig. 6.2: Surface elevation and velocity change over Raphstreng glacier, with regards to rise in elevation.

6.3 Further investigation of the potential GLOF threat

The results from this study does not invoke any direct answer to if Luggye Tsho or Raphstreng Tsho will be a potential GLOF outbreak in the future. The results show only the potential outcome if the lakes where to outbreak. As a further investigation for this study I would recommend monitoring and study the stability of the ice-moraines that dam these two glacial lakes. This can be done by using SAR interferometry (InSAR) and coherence mapping. InSAR mapping is an important tool to monitor and measure surface displacements, and can also measure moraine degradation (Chen, et al. 1999; Joughin, et al. 2010). By doing so, the investigations will provide further assessment to the GLOF risk that these two PDGLs contains. It will also provide with further learning on how to prevent certain outbreaks or at least minimize their potential outbreaks by enforcing the structural integrity of the ice-moraine dam, which has proven to be successful in the past (Fountain, et al. 2000: p. 169).

6.4 Surface change over debris-covered and clean ice surfaces

Debris-covered glacier relative to clean ice glaciers have some certain differences when it comes to the thinning rate. According to the result it seems that the average surface melt is slower over a debris-covered glacier than clean ice glaciers at low elevations. Looking at **Fig. 5.4** the surface melt is displayed by the change in surface elevation between 1976 and 2000. The figure reveals an overall similar surface melt for debris-covered glaciers, e.g. Lianggang glacier, G090157E28136N, Luggye glacier 2, Bechung glacier. Which is a low surface melt at the lowest part of the glacier, but as the elevation rises towards the mid part of the glacier, there is an increase in thinning rate. However, as the elevation rises the surface melt seems to slow more and more down, and at the high parts where it transitioned into clean ice the surface melt would be equal to zero. **Fig. 6.3** displays how the surface melt are changing, between 1976-2000, with the rise in elevation, and shows a measurement for the debris-covered glacier G090157E28136N. The mid-range elevation of a debris-covered glaciers are where the debris covers are not settled in or sparse, but also where the majority of the glacier area are resided (Maurer, et al. 2019). The surface melt seems to increase where the debris-covers are sparse or almost absent. This statement is already justified as Benn and Evans (2013) states that the thickness of debris-cover parts are what controls the melt rate and therefore also the thinning rate. They state that where the debris-covers are sparse is where the albedo[7] effect has the strongest influence on the ablation rate. The fluctuation in the surface

[7] Albedo = a term used in glaciology to explain the amount of solar radiation that is reflected on a surface. On debris-covered surfaces this term would be explained as having a low albedo effect, as debris-covered surfaces absorb more incoming solar radiation than e.g. clean ice or snow (Benn and Evans, 2013).

elevation values are probably caused by the supraglacial lakes that have been observed over glacier G090157E28136N and should not take accounted to when one is observing the thinning rate.

Clean ice surfaces, such as the Shimo glacier, have a different form of thinning rate. According to **Fig. 5.4** the Shimo glacier had a faster surface melt at the lower elevation parts but seemed to be reducing as the elevation increased. The same goes for other glacier that consist of solely clean ice, e.g. Luggye glacier 1 and Raphstreng glacier both experience the same form of thinning rate. The surface melt seemed to be uniformly the same as for the debris-covered glaciers and clean ice but are experienced at different levels of elevations. This statement was also found true by Maurer, et al. (2019) in their paper on increased mass loss over the Himalaya. However, one clean ice surface seems to be behaving a bit differently. According to **Fig. 6.3** the surface melt over Zeng glacier behaves quite the same as it would over a debris-covered surface. Where the highest amount of surface melt is on the mid part of the glacier and not the lower part. Based on observing the results this glacier seems to be the only clean ice glacier that has this sort of thinning rate. The Zeng glacier will therefore not be sufficient to discuss, as one glacier cannot overdue the results of several other uniform glaciers.

6.4.1 Glacier change and climate change:

According to **table 5.1**, most of the glaciers had a larger reduction in area size after the 2000, and **Fig. 5.5** shows that the surface elevation change shows the very same trend. This increase in glacier melt and area reduction could be an indication to a local climate change increase after the 2000. Even though table 5.4 & 5.5 present a different result they are both limited by the stereo data outlines. This study where only able to get some high-resolution imagery that covered only a part of the Lunana glacier system, and therefore the 2000-2018/9 and the total results between 1976 and 2018/9 for the geodetic mass balance and surface elevation change do not support enough information to value if there were a higher loss of glacier before or after the 2000.

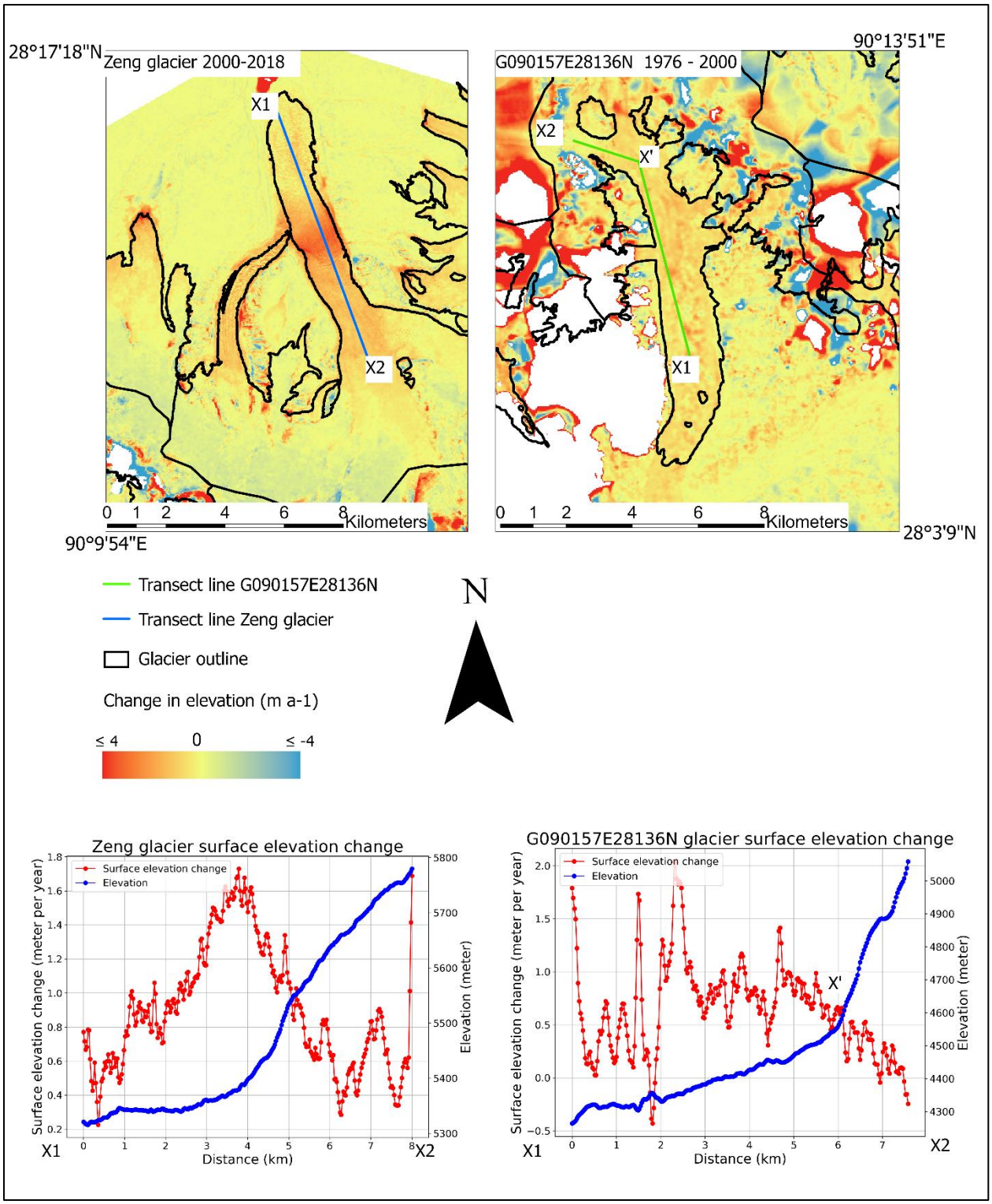

Fig. 6.3: Shows how the surface elevation change is differentiating between clean ice (Zeng glacier) and debris-covered ice (G090157E28136N). The measurements are between 2000-2018/9 for the Zeng glacier, and between 1976-2000 for glacier G090157E28136N. The graphs are generated from the two transect lines in the images, green (G090157E28136N) and blue (Zeng glacier).

6.4.2 Velocity over debris-covered and clean ice surfaces

Based on the result there seems to be almost no velocity on certain debris-covered glacial surfaces. Glacier G090157E28136N had almost no displacement on the debris-covered surfaces with low elevations (**Fig. 6.4**) but increased when the elevation increased to the higher parts where the transition between clean ice and debris-covered ice where. The fluctuation of velocity change over G090157E28136N is most likely caused by the supraglacial lakes located on the debris-covered tongue, as they might give a higher or lower for of displacement then the glacier itself. The same goes for other debris-covered glaciers, e.g. Bechung glacier and Luggye glacier 2, where the velocity is barely picked up in the debris-covered parts but are higher registered in the clean ice parts. The lack of velocity over some surfaces can indicate that the glacier is stagnant ice. This can be compared with a totally debris free glacier, like Zeng glacier, which was calculated to have an average velocity of 0.012 ± 0.002 m d^{-1} which is almost twice as fast as glacier G090157E28136N which had an average glacier velocity of 0.007 ± 0.002 m d^{-1}. Based on **Fig. 6.4** the Zeng glacier flowed the fastest on the mid part region of the glacier tongue. This gradient of the velocity is not visible on the debris-covered glacier G090157E28136N and based on these results it would seem that the debris-covered surfaces limit the movement of the glacier at low elevations.

Comparing it to other work, Sam, et al. (2016) presented with similar observations in their paper. They presented a COSI-Corr correlation of the displacements between Landsat 8 images, to figure out the yearly velocity of debris-covered glacial surfaces in India. The figures presented in the paper showed similar effects of the glacier velocities over low elevation glacial surfaces. The glacier velocities where slow over low elevation glacial surfaces, where most of the debris-covered surfaces where located and would start to increase as the elevation got higher and the surface transgressed to clean ice surfaces. There where however some debris-covered surfaces that showed an increase in velocity as the elevation and slope got higher. Sam, et al. (2016) study used a COSI-corr correlation to show a yearly displacement change over time, which is different from this study which are using offset tracking to show a daily displacement between 22 days. The range between this study and the study by Sam, et al. (2016) is therefore limited by the temporal visualization of the glacier velocity change over debris-covered surfaces and to get a better comparison the area should be calculated with similar methods as the one Sam, et al. (2016) is using. This would lead to a better understanding on how the glacier flow works over the debris-covered surfaces in Lunana, Bhutan.

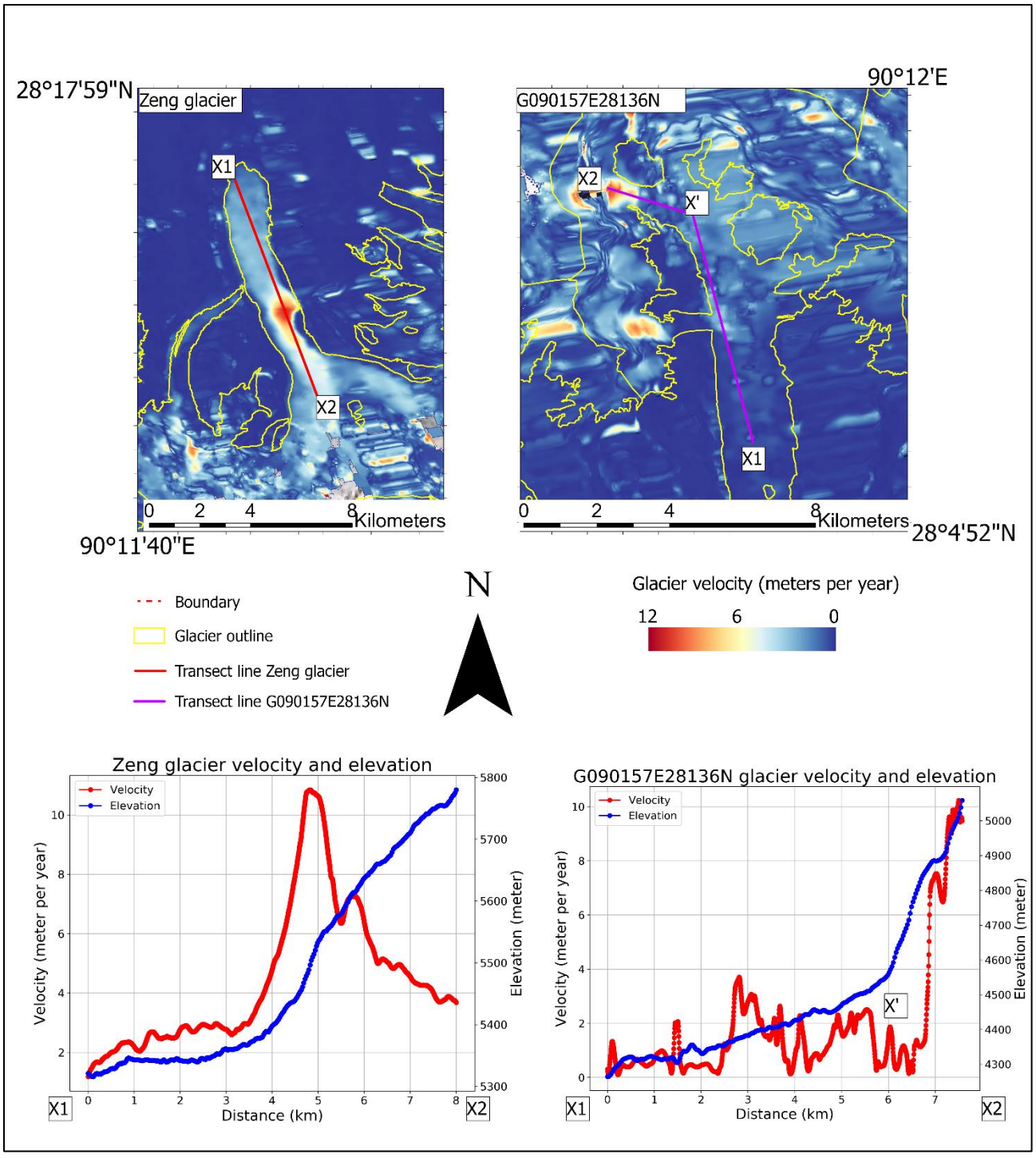

Fig. 6.4: A velocity and elevation change measurements are computed into two individual graphs, displaying the measurements for the clean ice Zeng glacier and the debris covered G090157E28136N glacier. The transect lines over the Zeng glacier (red) and G090157E28136N glacier (purple) are indicate on the two maps. The X' marks the transition between debris-covered surface to clean ice.

6.5 Glacier flow against glacier mass loss

The glacier flow over the Lunana glacier system was defined for the temporal period of Nov/Dec 2016 and will be compared to the glacier mass loss that was calculated for the temporal period between 1976 and 2019.

One of the objectives for this paper was to study the compatibility between glacier velocity and the glacier volume change and see if a loss of glacier mass responses with an increase glacier flow. There seems to be a link between the temporal window and how the glacier flows. Based on the results, the glacier with the highest loss of mass was the Zeng glacier with a 1.17 ± 0.06 m w.e. a^{-1} mass balance reduction between 1976 and 2019. However, if one is looking at the temporal period between 2000 and 2019, Luggye glacier 2 had a 0.74 ± 0.17 m w.e. a^{-1} mass balance reduction and the Zeng glacier was one of the lowest with a 0.28 ± 0.1 m w.e. a^{-1} mass balance reduction. Luggye glacier 2 was classified to consist of both debris-covered glacier parts as well as clean ice parts and Zeng glacier is solely consisting of clean ice. Looking at **table 5.6** the average glacier velocity on Zeng glacier was 0.012 ± 0.002 m d^{-1} while on Luggye glacier 2 the velocity was 0.006 ± 0.002 m d^{-1} about half as fast as the Zeng glacier. As discussed in the last subject, the velocity flow of a glacier seems to be faster in clean ice parts than in the debris-covered parts. This will compute a theory that a glacier consisting of clean ice will flow faster than if it contained debris-covered parts.

The melt rate of a debris-covered glacier decreases with the thickness of the debris layer (Östrem 1959: p. 228 - 230), where the debris layer is at its thinnest, the rate of melting is at its highest, and if the debris cover is thicker than 2 cm the melting rate decreases exponentially. The rate of ice melting inflicts the overall mass balance of a glacier, as glacier melting controls the ablation rate which is used to calculate the glacier mass balance. Based on this, the ticker the layer of the debris, the lower the melting rate and therefore a more positive glacier mass balance. Based on the results of the glacier mass balance, the Zeng glacier had a glacier mass balance reduction (1.17 ± 0.06 m w.e. a^{-1}) that was almost twice as big as glacier G090157E28136N (0.65 ± 0.04 m w.e. a^{-1}), and as mentioned before, glacier G090157E28136N was calculated to have a glacier velocity which was almost twice as slow as the Zeng glacier.

Given that glacier G090157E28136N was classified with debris-covered parts and the Zeng glacier was classified as just clean ice, there could be a connection between glacier melt within debris-covered glaciers and how fast these glacier flows. Based on this, it seems that clean ice flow faster and melt faster than what debris-covered glaciers does. Hence, glacier

melt over clean ice can supplement more meltwater than what debris-covered glaciers can, as clean ice are more active. Emmer (2017) explained that active glaciers supplement meltwater that leads to expansion and/or production of glacial lakes, which in the end can lead to cause of impact to glacial hazards, e.g. GLOF event. It should therefore be taking accountant to what type of glacier is supplementing what glacial lake. If the lake is rated as a potential dangerous glacial lake (PDGL) and it is supplemented by a clean ice glacier, then there should be high glacial hazard risk.

6.5.1 Surface elevation change and velocity

Based on the last chapter there seems to be a correlation between glacier mass balance and glacier velocity. However, based on looking at the results there seems to be a connection between surface elevation change and glacier velocity as well. **Fig. 6.3** revealed that the Zeng glacier had an increased surface melt in the mid part region of the glacier. This uniform flux of change can be observed on **Fig. 6.4** where the same glacier had a similar increase in velocity over the same region. However, the Zeng glacier was the only clean ice glacier that showed this type of thinning rate, every other clean ice glacier was observed to have a different, but uniform, thinning rate.

Assessment of the glacier movement and the change of the glacier surfaces are important regarding debris-covered glaciers. Bolch, et al. (2012) stated that if a debris-covered glacier is stagnating and experiencing surface loss the glacier is in fact producing supraglacial ponds. Supraglacial ponds are already observed on debris-covered glaciers such as glacier G090157E28136N and the graphs in **Fig. 6.3** & **6.4** confirms these observation, as the debris-covered glacier is experiencing very low glacier velocity, and is therefore considered as stagnate ice, and high amounts of surface loss. These ponds can lead to hazardous implications in the future as they increase the local ablation by transmitting stored thermal energy down to the underlying glaciers (Benn, et al. 2012), growing them into larger supraglacial lakes. Based on this it seems to be a certain connection between the glacier flow and how the glacier melts.

6.6 Coherence data and classification of debris-covered glaciers

The glacier classification from this study did it able to classify and compute an estimation on the glacier area change of the Lunana glacier system. The debris-covered glaciers where classified by using coherence data as one of the main threshold inputs. The classification had an accuracy of 97% based on the GLIMS glacier outline polygons. Based on previous studies that have used coherence data as a threshold input for classifying debris-covered glacier, they concluded that by using coherence data one could easily identify moving debris covered tongues (Frey, et al. 2012; Robson, et al. 2015). It was especially effective and precise when they were mapping large valley glaciers that where consisting of extensive debris covers (Frey, et al. 2012). Robson, et al. (2015) noted that their OBIA classification of the glacier system failed to identify some debris-covered parts, because of the threshold set for the slope values. The classification fully classified step tributary of clean ice that flow down towards the glacier, as they had a steepness between 25-50°, when they had set a threshold between 14-16°. In this study there where similar problems. There were certain debris-covered glaciers that where not classified due to slope of these glaciers being either to low or too big for the threshold. This study had a 14-19° slope threshold and would often fail to identify certain glacier parts that where not within the threshold and would have to be corrected by a visual editing. **Fig. 6.5** shows this classification error, where the two separated glacier tongues (X & Y) where failed to identify as debris-covered glaciers. Both glaciers where estimated to have a slope value (ca. 12°) under the threshold, and they had a high coherence value based on the coherence image **B** in **Fig. 2.2**, thus excluding them from the classification. Trying to change the threshold to accommodate these types of glacier parts, resulted in the classification including non-glacial debris parts that where surrounding the glacier tongues. High coherence values indicate no movements and the two debris-covered glacier tongues could be assumed to be stagnant ice and not active ice. It is therefore important to know that by using coherence data, you will not be able to classify stagnant debris-covered glaciers.

The GLIMS glacier inventory outlines seem to have similar issues when it comes to classifying every parts of the glacier system (**Fig. 6.5**). According to GLIMS glacier inventory website, the delineation of the glacier outlines where gathered from Nuimura, et al. (2015) the creator of the “Glacier Area Mapping for Discharge from the Asian Mountains” (GAMDAM). The GAMDAM was manually delineated from 356 Landsat ETM+ scenes from the period 1999-2003, and by using DEM and high-resolution Google Earth. The glacier outlines are regularly updated and was last updated in 2018, according to the metadata from GLIMS data

files. As mentioned before, studies prove that manual delineation is a time consuming and ineffective way to classify debris-covered glacier parts (Bhambri, et al. 2011; Bolch, et al. 2008; Paul, et al. 2013; Robson, et al. 2015). Nuimura, et al. (2015) generate debris-cover outlines by identifying it using contour lines at 20 m intervals and thermal band imagery, and as a last resort thermokarst features. Thermal band imagery can identify thin debris-covers, which has relative low surface temperature (Reznichenko, et al. 2010), and by using high resolution images to identify thermokarst features, one can use these rugged surfaces to identify exposed ice cliffs located on debris-covered glaciers (Nuimura, et al. 2015). In the end, Nuimura, et al. (2015) was able to identify more debris-covered glaciers than the OBIA classification, before the manual correction, from this study. It can be smart to consider the usage of some of the methods used by Nuimura, et al. (2015), e.g. thermal bands, to use as a input threshold for the classification, but that is important to take notice of the thickness of the debris-covers, as anything more than 130 mm would show no thermal activity (Reznichenko, et al. 2010).

The OBIA classification was successful in classifying the large debris-covered glaciers like the Lianggang glacier and G090157E28136N, where there where several shifts in lithology and vegetation, as well as the transition from debris-covered ice to clean ice. However, based on the results, there were some misclassification and overestimations of the glacier outline, with debris masses being classified as debris-covered ice (**Fig. 6.6**). The very same glacier overestimation where a problem in the OBIA classification from the study of Robson, et al. (2015), where debris mass flow where classified as debris-covered ice due to the spectral similarity of the two. This comes to show that automatic classifications like the OBIA cannot solely relay on inputted data and thresholds to get the most accurate results but use them as a guide for large scale classifications and use manual editing to perfect the result.

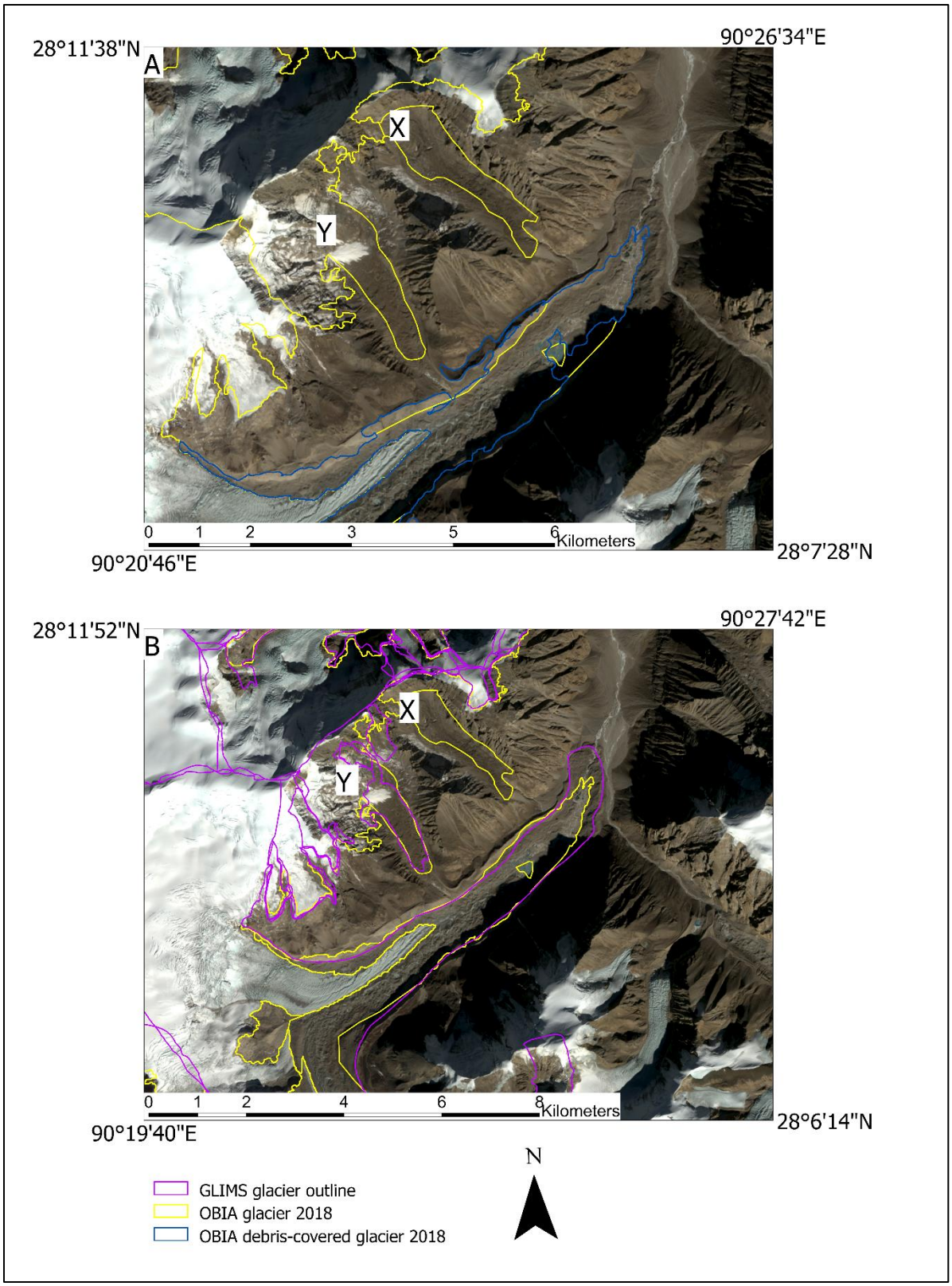

Fig. 6.5: Figure showing how the OBIA classification struggles to classify certain debris-covered glacier tongues. **(A)** shows this identification issue and displays the two glacier tongues as **X** and **Y**. While the OBIA classification struggles to classify all the glacier parts, the GLIMS inventory seems to have a similar issue (B). Glacier part **X** is not identified by the GLIMS outline. Background image: c

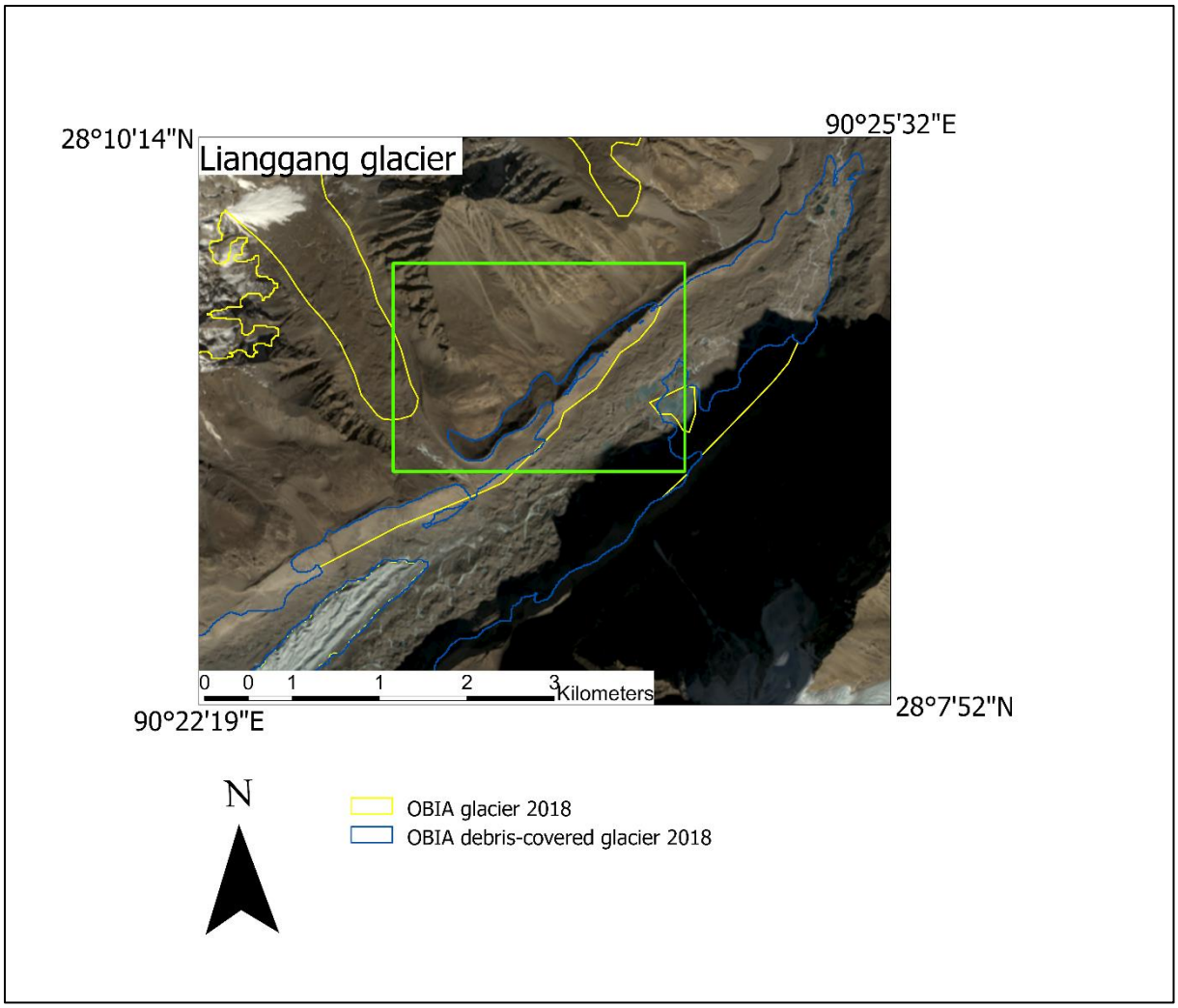

Fig. 6.6: An example of debris masses (green square) on the Lianggang glacier. Due to spectral similarity between the debris masses and the debris-covered glacier, as well as loss of coherence, they have been misclassified as debris-covered ice. Background image: SPOT data (16.12.2018).

6.7 Comparison with other glacier classifications

Other studies have proven the efficiency of using remote sensing to classify glacier changes. Nuimura, et al. (2015) contributed to the GLIMS databases with their manual delineated glacier outlines over high mountain Asia and identified over 87 000 glaciers covering a total area of 91 263 ± 13 689 km^2. Compared to this study, which covers just over 1000 km^2 and about 125 glaciers, Nuimura, et al. (2015) covers a vastly bigger area. However, it seems that the overall area of the glacier outlines is not so accurate even though they use manual delineation to identify them. The GLIMS outlines seems to have overestimated some of their glacier outlines. **Fig. 6.7** displays the outline of the glacier done by the OBIA classification from this study and the GLIMS glacier outline. The GLIMS outline do not seem to take account for high altitude high slope areas, as the nunataq on the Shimo glacier was classified as glacier, and the high slope terrain on glacier G090157E28136N was also classified as glacier. According to Nuimura, et al. (2015) they had excluded steep headwalls (>40°) for the classification as they don't experience any change in surface elevation and therefore has no input for the glacier mass balance change. This study tried to replicate the same threshold maximum for slope based on the literature as (Nuimura, et al. 2015; Paul, et al. 2013; Robson, et al. 2015), but the OBIA classification ended up excluding glacier areas that where snow covered and therefor important for the classification. The result threshold for the slope where sett to 75°. Nuimura, et al. (2015) were following GLIMS outline protocol, where all perennial snow masses had to be classified as glaciers, and that only exposed ground could be excluded from the outlines (Raup and Khalsa 2007), but they were also using both summer and winter Landsat scenes to avoid seasonal snow cover, which this study did as well. The inclusion of snow covers was to take account for avalanches, as they are important sources of glacier nourishment (Nuimura, et al. 2015).

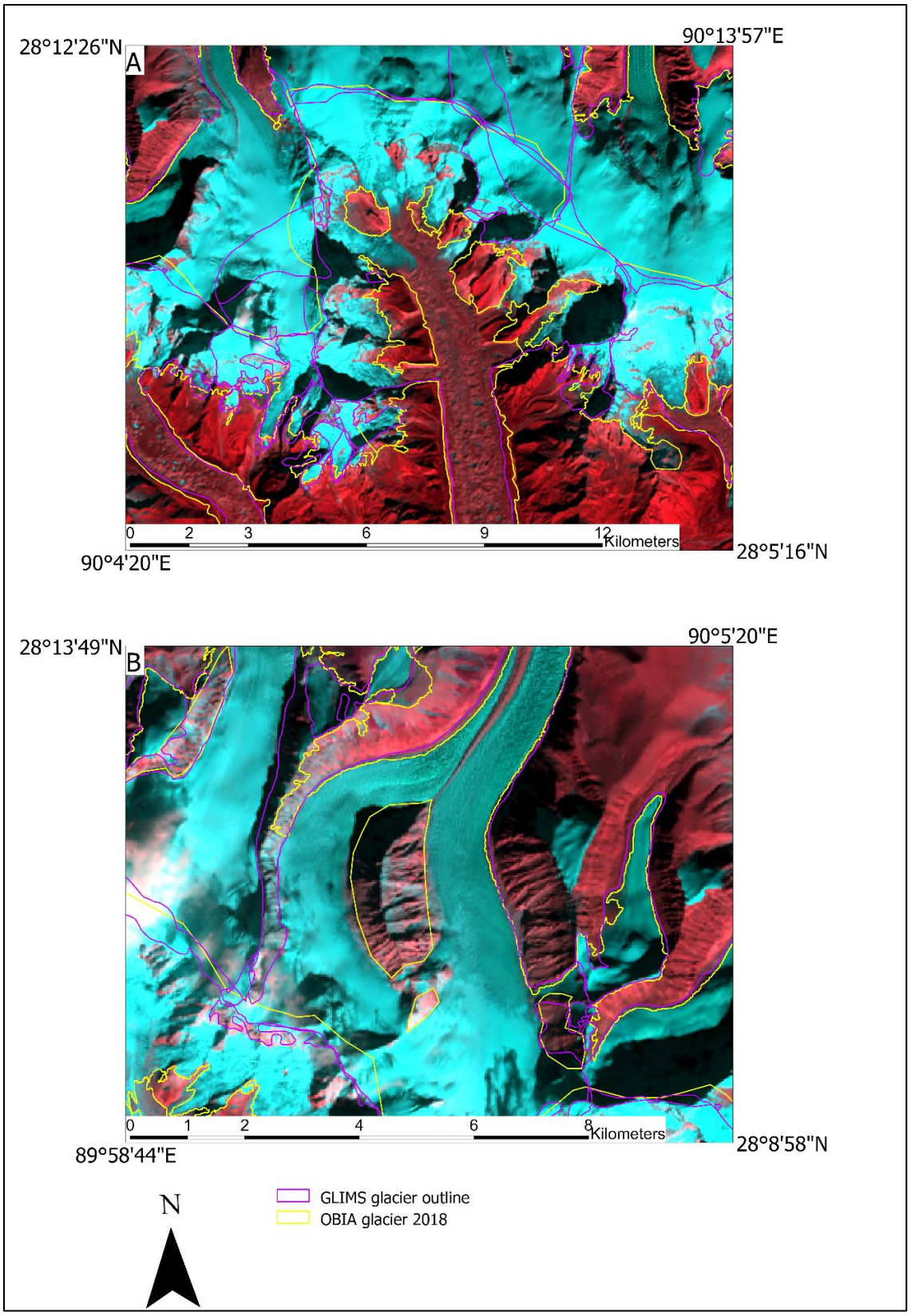

Fig. 6.7: Shows the outlines of both the OBIA classification (2018) as well as the GLIMS glacier inventory outlines (2018). Notice the overestimation on glacier outlines from the GLIMS glacier inventory on both glacier G090157E28136N **(A)** and the Shimo glacier **(B)**. Background image: Landsat 8 false color composite (13.12.2018).

Chapter 7: Conclusion

This study has been using different methods of automatic classifications and manual delineation as well as offset tracking and DEM co-registration, to create a glacier inventory of the Lunana glacier system. It has provided a large-scale time series for the two potential dangerous glacial lakes, Luggye Tsho and Raphstreng Tsho, to enlighten their outburst risk in the future. The Luggye Tsho glacial possesses a dangerous outcome if it were to outburst again, as it has greatly been increasing in size since the 1994 GLOF event, from 0.93 km^2 in 1994 to 1.41 km^2 in 2018, due to increase in glacier retreat and production of meltwater. The geodetic mass balance provided information on the surface elevation and volume change for the Lunana glacier system. The reduction in mass balance of Luggye glacier 1, 1.01 ± 0.069 m w.e. a^{-1} (1976-2019), shows to why the Luggye Tsho glacial lake has had an increase in size over the past 25 years. The Raphstreng Tsho possesses a similar risk, as its areal size of 1.31 km^2, and its location makes it a potential outburst threat. If the supraglacial lakes on Thorthormi glacier or if Luggye Tsho where to outburst and flow down towards Raphstreng Tsho, the hydrostatic pressure from the outburst could result in a massive GLOF event.

The OBIA classification of the Lunana glacier system provided an accurate glacier outline inventory consisting of both debris-covered glaciers and clean ice. The OBIA classification had some restriction when it came to classify stagnant debris-covered ice and of non-glacial debris surfaces. Nevertheless, the classification proved a 97% accuracy and was able to account for every active debris-covered glacier in the study area, with just a small need for post-processing and editing. This study has been investigating how debris-covered surfaces affect the glacier changes and revealed that the glacier velocity is lower over supraglacial debris as to oppose to debris-free ice. For example, G090157E28136N had an average of 2.56 ± 0.73 m a^{-1} glacier velocity over the debris-covered tongue, while the Zeng glacier had an average of 4.4 ± 0.73 m a^{-1} at a maximum of 10± 0.73 m a^{-1} (**Fig. 6.4**).

Between 1976 and 2018/9 the Lunana glacier system had a large reduction in area of 12.7% and a reduction in surface elevation of 0.48 ± 0.08 m a^{-1}, which calculates to a -0.41 ± 0.068 m w.e. a^{-1} in mass balance, and the rate of change is becoming more negative over the last decade. The glacier velocity was only studied on a local scale, divided up between nine glaciers, and the results showed some individual debris-covered glaciers to be stagnant. These debris-covered glaciers showed also high increase in surface elevation change which could indicate production of supraglacial ponds (Emmer 2017). E.g. G090157E28136N where the surface melt was between 1.5 and 2 m a^{-1} (see **Fig. 6.3**) over several locations on the debris

tongue. The increase in production of supraglacial ponds is an indication of surface melt and results in large supraglacial lakes, which can eventually turn into GLOF hazards.

As a continuation from this study there are some recommendations for future studies and improvements:

- To conduct a Normalized Cross Correlation with optical data of the Lunana glacier system to extend the temporal scale for the glacier velocity, as this would further investigate the glacier movement paradox for the debris-covered glaciers.
- Use automatic classification to identify several more glacier outlines of the Lunana glacier system, between 1976 and 2019. To provide a more accurate time series of the glacier changes to further investigate how the glacier area has changed during the last few decades.
- Generate an informetric SAR (InSAR) mapping over the PDGLs, Raphstreng and Luggye Tsho, to monitor and study if the ice-moraine dams are degrading and if so, how much. This will provide a further assessment to the GLOF risk that these two PDGLs contains and provide better learning on how to prevent certain outbursts.
- Study the evolution of the supraglacial lakes on Thorthormi glacier and classify their surface area. As the supraglacial lakes seems to have a high impact on the GLOF risk of Raphstreng Tsho.

Chapter 8: Attachments

I. Surface_elevation_change_2000_1976

II. Surface_elevation_change_2018_9_1976

III. Surface_eleavtion_change_2018_9_2000

IV. Volume_change_2000_1976

V. Volume_change_2018_9_1976

VI. Volume_change_2018_9_2000

VII. Table_mean_glacier_velocity

Chapter 9: References

Ahmed, I., Maund, K. and Gajendran, T. 2020 *Disaster Resilience in South Asia: Tackling the Odds in the Sub-Continental Fringes*: Taylor & Francis.

Ashraf, A., Roohi, R., Naz, R. and Mustafa, N. 2010 'IDENTIFICATION OF GLACIAL FLOOD HAZARDS IN KARAKORAM RANGE USING REMOTE SENSING TECHNIQUE AND RISK ANALYSIS'.

Baatz, M., Benz, U. C., Dehghani, S., Heynen, M., Höltje, A., Hofmann, P., Lingen-fleder, I., Mimler, M., Solbach, M., Weber, M. and G., W. 2005 'Definiens Imaging—eCognition User Guide 4', *Eds., München*.

Baatz, M. and Schäpe, A. 2000 'Multiresolution Segmentation : an optimization approach for high quality multi-scale image segmentation '.

Bajracharya, Sr., Maharjan, S. B. and Shrestha, F. 2014 'The status and decadal change of glaciers in Bhutan from the 1980s to 2010 based on satellite data', *Ann. Glaciol.* 55(66): 159-166.

Belgiu, M. and Dr Guţ, L. 2014 'Comparing supervised and unsupervised multiresolution segmentation approaches for extracting buildings from very high resolution imagery', *ISPRS journal of photogrammetry and remote sensing : official publication of the International Society for Photogrammetry and Remote Sensing (ISPRS)* 96: 67.

Benn, D. and Evans, D. J. A. 2013 'Glaciers and glaciation', 2nd ed. Edition, Oxfordshire, England ;,New York, New York: Routledge.

Benn, D. I., Bolch, T., Hands, K., Gulley, J., Luckman, A., Nicholson, L. I., Quincey, D., Thompson, S., Toumi, R. and Wiseman, S. 2012 'Response of debris-covered glaciers in the Mount Everest region to recent warming, and implications for outburst flood hazards', *Earth-Science Reviews* 114(1-2): 156-174.

Berthier, E., Arnaud, Y., Kumar, R., Ahmad, S., Wagnon, P. and Chevallier, P. 2007 'Remote sensing estimates of glacier mass balances in the Himachal Pradesh (Western Himalaya, India)', *Remote Sensing of Environment* 108(3): 327-338.

Bhambri, R., Bolch, T., Chaujar, R. K. and Kulshreshtha, S. C. 2011 'Glacier changes in the Garhwal Himalaya, India, from 1968 to 2006 based on remote sensing', *Journal of Glaciology* 57(203): 543-556.

Bishop, M. P., Shroder, J. F., Hickman, B. L. and Copland, L. 1998 'Scale-dependent analysis of satellite imagery for characterization of glacier surfaces in the Karakoram Himalaya', *Geomorphology* 21(3): 217-232.

Blaschke, T. 2010 'Object based image analysis for remote sensing', *ISPRS Journal of Photogrammetry and Remote Sensing* 65(1): 2-16.

Blaschke, T. and Strobl, J. 2001 'What's wrong with pixels? Some recent developments interfacing remote sensing and GIS', *GIS – Zeitschrift für Geoinformationssysteme* 14: 12-17.

Bohner, J. 2006 'General climatic controls and topoclimatic variations in Central and High Asia', *Boreas* 35(2): 279-295.

Bolch, T., Buchroithner, M., Pieczonka, T. and Kunert, A. 2008 'Planimetric and volumetric glacier changes in the Khumbu Himal, Nepal, since 1962 using Corona, Landsat TM and ASTER data', *Journal of Glaciology* 54(187): 592-600.

Bolch, T., Kulkarni, A., Kaab, A., Huggel, C., Paul, F., Cogley, J., Frey, H., Kargel, J., Fujita, K., Scheel, M., Bajracharya, S. and Stoffel, M. 2012 'The State and Fate of Himalayan Glaciers', *Science* 336(6079): 310-314.

Braithwaite, R. J. 2002 'Glacier mass balance: the first 50 years of international monitoring', *Progress in Physical Geography* 26(1): 76-95.

Brauner, M., Leber, D., Häusler, H., Payer, T. and Agner, P. 2003 'Glacier Lake Outburst Flood (GLOF) Mitigation Project, Lunana, Bhutan: Technical Mitigation Measures, Thorthormi Outlet', Vienna: University of Vienna.

Carrivick, J. L. and Tweed, F. S. 2016 'A global assessment of the societal impacts of glacier outburst floods', *Global and Planetary Change* 144(C): 1-16.

Casey, K. A., xE, xE, b, A. and Benn, D. I. 2012 'Geochemical characterization of supraglacial debris via in situ and optical remote sensing methods: a case study in Khumbu Himalaya, Nepal.(Case study)', *The Cryosphere* 6(1): 85.
Chandler, B. M. P. and Evans, D. J. A. 2019 'Glacial Processes and Sediments' *Reference Module in Earth Systems and Environmental Sciences*: Elsevier.
Chen, Y., Zhang, G., Ding, X. and Li, Z. 1999 'Monitoring Earth Surface Deformations with InSAR Technology: Principle and Some critical Issues', *Journal of Geospatial Engineering* 2.
Clark, C. 2001 'Introductory Remote Sensing: Principles and concepts', Vol. 86, Sheffield: Geographical Association.
Coenraads, R., Koivula, J. I., Doig, F., Stenløkk, J. and Myhr, E. 2008 *Geologica : den store boken om jorden : klima, vulkaner, elver, dyreliv, planter, fjorder, ørkener, fjell*, Oslo: Spektrum.
Daisuke, Higaki, Go and Satô 2012 'Erosion and Sedimentation Caused by Glacial Lake Outburst Floods in the Nepal and Bhutan Himalayas

'.
Dehecq, A., Gourmelen, N. and Trouve, E. 2015 'Deriving large-scale glacier velocities from a complete satellite archive: Application to the Pamir–Karakoram–Himalaya', *Remote Sensing of Environment* 162(C): 55-66.
Deo Raj, G., Narendra Raj, K., Samjwal Ratna, B., Karma, T., Sharad, J., Phuntsho, T., Lalit Kumar, C., Yeshey, L. and Tashi, P. 2017 'Lemthang Tsho glacial Lake outburst flood (GLOF) in Bhutan: cause and impact', *Geoenvironmental Disasters* 4(1): 1-13.
Dorji, U., Olesen, J. E., Bocher, P. K. and Seidenkrantz, M. S. 2016 'Spatial Variation of Temperature and Precipitation in Bhutan and Links to Vegetation and Land Cover', *Mountain Research and Development* 36(1): 66-79.
Dyurgerov, M. and Meier, M. 2005 'Glaciers and the changing Earth system: a 2004 snapshot', Boulder, CO: Insitute of Arctic and Alpine Research.
Emmer, A. 2017 'Glacier Retreat and Glacial Lake Outburst Floods (GLOFs) ', Vol. 2018, Oxford Research Encyclopedia of Natural Hazard Science.
Fischer, A. 2011 'Comparison of direct and geodetic mass balances on a multi-annual time scale', *The Cryosphere* 5(1): 107.
Floricioiu, D., Eineder, M., Rott, H., Yague-Martinez, N. and Nagler, T. 2009 'Surface velocity and variations of outlet glaciers of the Patagonia Icefields by means of TerraSAR-X', Vol. 2.
Fountain, A., Raymond, C. F., Nakao, M., Snow, I. C. o. and Ice 2000 *Debris-covered Glaciers: Proceedings of an International Workshop Held at the University of Washington in Seattle, Washington, USA, 13-15 September 2000*: IAHS.
Fountain, A. G. and Tangborn, W. V. 1985 'The Effect of Glaciers on Streamflow Variations', *Water Resources Research* v. 21: p. 579 - 586.
Frey, H., Paul, F. and Strozzi, T. 2012 'Compilation of a glacier inventory for the western Himalayas from satellite data: methods, challenges, and results', *Remote Sensing of Environment* 124(C): 832-843.
Fujii, Y. and Higuchi, K. 1977 'Statistical Analyses of the Forms of the Glaciers in the Khumbu Himal

Glaciological Expedition of Nepal, Contribution No. 31', *Journal of the Japanese Society of Snow and Ice* 39(Special): 7-14.
Fujita, K. 2008 'Effect of precipitation seasonality on climatic sensitivity of glacier mass balance', *Earth and Planetary Science Letters* 276(1): 14-19.
Gardelle, J., Arnaud, Y. and Berthier, E. 2011 'Contrasted evolution of glacial lakes along the Hindu Kush Himalaya mountain range between 1990 and 2009', *Global and Planetary Change* 75(1-2): 47-55.
Gardelle, J., Berthier, E., Arnaud, Y. and Kääb, A. 2013 'Region-wide glacier mass balances over the Pamir-Karakoram-Himalaya during 1999-2011', *The Cryosphere* 7(4): 1263.

Gill, A. E. and Niller, P. P. 1973 'The theory of the seasonal variability in the ocean', *Deep-Sea Research and Oceanographic Abstracts* 20(2): 141-177.
Govindha Raj, B. K., Kumar, V. K. and S.N, R. 2013 'Remote sensing-based inventory of glacial lakes in Sikkim Himalaya: semi-automated approach using satellite data', *Geomatics, Natural Hazards and Risk* 4(3): 241-253.
Govindha Raj K, B. 2009 'Remote Sensing based hazard assessment of glacial lakes - A case study from Kumaon Himalaya' 2: 31-39.
Gratton, D. J., Howarth, P. J. and Marceau, D. J. 1990 'Combining DEM Parameters With Landsat MSS And TM Imagery In A GIS For Mountain Glacier Characterization', *IEEE Transactions on Geoscience and Remote Sensing* 28(4): 766-769.
Gupta, R. P., Haritashya, U. K. and Singh, P. 2005 'Mapping dry/wet snow cover in the Indian Himalayas using IRS multispectral imagery', *Remote Sensing of Environment* 97(4): 458-469.
Hall, D. K., Riggs, G. A. and Salomonson, V. V. 1995 'Development of methods for mapping global snow cover using moderate resolution imaging spectroradiometer data', *Remote Sensing of Environment* 54(2): 127-140.
Hubbard, A., Willis, I., Sharp, M., Mair, D., Nienow, P., Hubbard, B. and Blatter, H. 2000 'Glacier mass-balance determination by remote sensing and high-resolution modelling', *Journal of Glaciology* 46(154): 491-498.
Huggel, C., Kaab, A., Haeberli, W., Teysseire, P. and Paul, F. 2002 'Remote sensing based assessment of hazards from glacier lake outbursts: a case study in the Swiss Alps', *Canadian Geotechnical Journal* 39(2): 316-330.
Huss, M. 2013 'Density assumptions for converting geodetic glacier volume change to mass change', *The Cryosphere* 7(3): 877.
IHA 2016 'Bhutan', https://www.hydropower.org/country-profiles/bhutan: IHA - International hydropower association.
Ives, J. D., Shrestha, R. B. and Mool, P. K. 2010 'Formation of Glacial Lakes in the Hindu Kush-Himalayas and GLOF Risk Assessment'.
Joughin, I., Smith, B. E. and Abdalati, W. 2010 'Glaciological advances made with interferometric synthetic aperture radar', *Journal of Glaciology* 56(200): 1026-1042.
Kääb, A., Berthier, E., Nuth, C., Gardelle, J. and Arnaud, Y. 2012 'Contrasting patterns of early twenty-first-century glacier mass change in the Himalayas', *Nature* 488(7412): 495.
Karimi, N., Farokhnia, A., Shishangosht, S., Elmi, M., Eftekhari, M. and Ghalkhani, H. 2012 'Elevation changes of Alamkouh glacier in Iran since 1955, based on remote sensing data', *International Journal of Applied Earth Observations and Geoinformation* 19(1): 45-58.
Karpilo, R. D., Jr.,, Young, R. and Norby, L. 2009 'Glacier monitoring techniques', *Geological Monitoring: Boulder, Colorado, Geological Society of America*.
King, O., Bhattacharya, A., Bhambri, R. and Bolch, T. 2019 'Glacial lakes exacerbate Himalayan glacier mass loss', *Scientific Reports* 9(1): 1-9.
Korup, O. and Tweed, F. 2007 'Ice, moraine, and landslide dams in mountainous terrain', *Quaternary Science Reviews* 26(25-28): 3406-3422.
Kuensel 1994a 'Experts recommend flood-prevention measures '((48)): p. 1-2.
— 1994b 'His Majesty commands special *Kidu* for flood victims.'(40): p. 12.
Kuensel 2011 'Battle Done, War Not Ove' *Kuensel*, Online.
— 2012 'Glacial Districts in Bhutan' *Kuensel*, Online.
Kuhn, M., Dreiseitl, E., Hofinger, S., Markl, G., Span, N. and Kaser, G. 1999 'Measurements and models of the mass balance of hintereisferner', *Geografiska Annaler: Series A, Physical Geography* 81(4): 659-670.
Kulkarni, A. and Bahuguna, I. 2002 'Glacial retreat in the Baspa basin, Himalaya, monitored with satellite stereo data', *J. Glaciol.* 48(160): 171-172.
Lawrence, E. N. 2012 'The Titanic disaster — a meteorologist's perspective', *Weather RMetS* v. 55(3): p. 66-78.

Li, A., Deng, W. and Zhao, W. 2017 *Land Cover Change and Its Eco-environmental Responses in Nepal*, Singapore: Singapore: Springer Singapore.
Lillesand, T. M., Kiefer, R. W. and Chipman, J. W. 2004 *Remote sensing and image interpretation*, 5th ed. Edition, Hoboken, N.J: Wiley.
— 2015 *Remote sensing and image interpretation*, 7th ed. Edition, Hoboken, N.J: Wiley.
Lu J., V. L. 2016 'Sentinel-1 Toolbox' *Offset Tracking Tutorial*, Array Systems Computing Inc.
Maurer, J. M., Schaefer, J. M., Rupper, S. and Corley, A. 2019 'Acceleration of ice loss across the Himalayas over the past 40 years', *Science advances* 5(6): eaav7266.
McFeeters, S. K. 1996 'The use of the Normalized Difference Water Index (NDWI) in the delineation of open water features', *International Journal of Remote Sensing* 17(7): 1425-1432.
Mei, L., Ningsheng, C., Yong, Z. and Mingfeng, D. 2020 'Glacial Lake Inventory and Lake Outburst Flood/Debris Flow Hazard Assessment after the Gorkha Earthquake in the Bhote Koshi Basin', *Water* 12(2): 464.
Mool, K. P., Wangda, D., Bajracharya, S. R., Kunzang, K., Gurung, D. R. and & Joshi, S. P. 2001 *Inventory of glaciers, glacial lakes and glacial lake outburst floods. Monitoring and early warning systems in the Hindu Kush-Himalayan Region: Bhutan*.
Nuimura, T., Sakai, A., Taniguchi, K., Nagai, H., Lamsal, D., Tsutaki, S., Kozawa, A., Hoshina, Y., Takenaka, S., Omiya, S., Tsunematsu, K., Tshering, P. and Fujita, K. 2015 'The GAMDAM glacier inventory: a quality-controlled inventory of Asian glaciers', *The Cryosphere* 9(3): 849-864.
Nuth, C. and Kääb, A. 2011 'Co-registration and bias corrections of satellite elevation data sets for quantifying glacier thickness change', *The Cryosphere* 5(1): 271.
Östrem, G. 1959 'Ice Melting under a Thin Layer of Moraine, and the Existence of Ice Cores in Moraine Ridges', *Geografiska Annaler* 41(4): 228-230.
Paul, F., Barrand N, E., Berthier, E., Bolch, T., Others and Berthier, E. 2013 'On the accuracy of glacier outlines derived from remote sensing data', *Annals of Glaciology* 54(63): 171-182.
Paul, F., Huggel, C. and Kääb, A. 2004 'Combining satellite multispectral image data and a digital elevation model for mapping debris-covered glaciers', *Remote Sensing of Environment* 89(4): 510-518.
Paul, F., Kääb, A., Maisch, M., Kellenberger, T. and Haeberli, W. 2002 'The new remote-sensing-derived Swiss glacier inventory: I. Methods'.
Rastner, P., Bolch, T., Notarnicola, C. and Paul, F. 2014 'A Comparison of Pixel- and Object-Based Glacier Classification With Optical Satellite Images', *IEEE Journal of Selected Topics in Applied Earth Observations and Remote Sensing* 7(3): 853-862.
Raup, B. and Khalsa, S. 2007 'GLIMS analysis tutorial, Boulder, CO,University of Colorado, National Snow and Ice Data Cen-ter', http://www.glims.org/MapsAndDocs/guides.html: GLIMS.
Reznichenko, N., Davies, T., Shulmeister, J. and McSaveney, M. 2010 'Effects of debris on ice-surface melting rates: an experimental study', *Journal of Glaciology* 56(197): 384-394.
Richards, J. A. 1993 'Remote Sensing Digital Image Analysis. An Introduction'.
Richardson, S. D. and Reynolds, J. M. 2000 'An overview of glacial hazards in the Himalayas', *Quaternary International* 65-66(C): 31-47.
Rignot, E., Echelmeyer, K., and Krabill, W. 2001 'Penetration depth of interferometric synthetic-aperture radar signals in snow and ice', *Geophysical Research Letters* 28(18): 3501-3504.
Robson, B. A., Nuth, C., Dahl, S. O., Hölbling, D., Strozzi, T. and Nielsen, P. R. 2015 'Automated classification of debris-covered glaciers combining optical, SAR and topographic data in an object-based environment', *Remote Sensing of Environment* 170(C): 372-387.
Robson, B. A., Nuth, C., Nielsen, P. R., Girod, L., Hendrickx, M. and Dahl, S. O. 2018 'Spatial Variability in Patterns of Glacier Change across the Manaslu Range, Central Himalaya', *Frontiers in Earth Science* 6.
Sakai, A., Takeuchi, N., Fujita, K. and Nakawo, M. 2000 'Role of supraglacial ponds in the ablation process of a debris-covered glacier in the Nepal Himalayas ', Seattle, Washington, USA.
Sam, L., Bhardwaj, A., Singh, S. and Kumar, R. 2016 'Remote sensing flow velocity of debris-covered glaciers using Landsat 8 data', *Progress in Physical Geography: Earth and Environment* 40(2): 305-321.

Sammut, C. and Webb, G. I. 2010 *Encyclopedia of Machine Learning*, Boston, MA: Boston, MA: Springer US.
Schellenberger, T., Dunse, T., xE, xE, b, A., Kohler, J. and Reijmer, C. H. 2015 'Surface speed and frontal ablation of Kronebreen and Kongsbreen, NW Svalbard, from SAR offset tracking', *The Cryosphere* 9(6): 2339.
Shukla, A., Arora, M. K. and Gupta, R. P. 2010 'Synergistic approach for mapping debris-covered glaciers using optical–thermal remote sensing data with inputs from geomorphometric parameters', *Remote Sensing of Environment* 114(7): 1378-1387.
Singh, S. M. 2009 'The Cost of Climate Change the Story of Thorthormi Glacial Lake in Bhutan', Thimphu: World Wide Fund for Nature (WWF).
Varugu, B., Rao, Y. and Singh, M. 2015 *Glacier velocity estimation using high resolution SAR images – Application to Gangotri glacier in Himalayas*.
Vuichard, D. and Zimmermann, M. 1987 'The 1985 catastrophic drainage of a moraine-dammed lake, Khumbu Himal, Nepal: cause and consequences', *The 1985 catastrophic drainage of a moraine-dammed lake, Khumbu Himal, Nepal: cause and consequences*(2): 91-110.
Wangchuk, S., Bolch, T. and Zawadzki, J. 2019 'Towards automated mapping and monitoring of potentially dangerous glacial lakes in Bhutan Himalaya using Sentinel-1 Synthetic Aperture Radar data', *International Journal of Remote Sensing* 40(12): 4642-4667.
Watanbe, T. and Rothacher, D. 1996 'The 1994 Lugge Tsho Glacial Lake Outburst Flood, Bhutan Himalaya', *Mountain Research and Development* 16(1): 77-81.
Wessels, R. L., Kargel, J. S. and Kieffer, H. H. 2002 'ASTER measurement of supraglacial lakes in the Mount Everest region of the Himalaya', *Annals of Glaciology, Vol 34, 2002* 34: 399-408.
Williams, M. W., Wilson, A., Tshering, D., Thapa, P. and Kayastha, R. B. 2016 'Using geochemical and isotopic chemistry to evaluate glacier melt contributions to the Chamkar Chhu (river), Bhutan', *Annals of Glaciology* 57(71): 339-348.
WWF 2009 'The cost of climate change: The story of Thorthormi glacial Lake in Bhutan rep', *WWF*.
Yuanfang, C., Yu, H., Gelder, P. H. A. J. M. and Zhigui, S. 2002 'The Extremes of the Extremes: Extraordinary Floods (Proceedings of a symposium held at Reykjavik, Iceland'.
Zebker, H. and Goldstein, R. 1986 'Topographic Mapping from SAR Observation', *Journal of Geophysical Research* Vol. 911: pp. 4993 - 4999.
Zongli, J., Shiyin, L., Xin, W., Jian, L. and Sichun, L. 2011 'Applying SAR interferometric coherence to outline debris-covered glacier'.